# Syndepositional tectonics and mass-transport deposits control channelized, bathymetrically complex deep-water systems (Aínsa depocenter, Spain)

Daniel Eray Tek*[1], Miquel Poyatos-Moré[2], Marco Patacci[1], Adam Daniel McArthur[1], Luca Colombera[1], Timothy Martin Cullen[1], and William Dale McCaffrey[1].

*1. School of Earth and Environment, University of Leeds, Leeds, LS2 9JT, United Kingdom*

*2. Department of Geosciences, University of Oslo, Oslo, 0371, Norway*

***) E-mail:** ee11dt@leeds.ac.uk

**Keywords:** Turbidites, Channels, Mass transport, Tectonics, Pyrenees

## ABSTRACT

The inception and evolution of channels in deep-water systems is controlled by the axial gradient and lateral confinement experienced by their formative flows. These parameters are often shaped by the action of tectonic structures and/or the emplacement of mass-transport deposits (MTDs). The Arro turbidite system (Aínsa depocenter, Spanish Pyrenees) is an ancient example of a deep-water channelized system from a bathymetrically complex basin, deposited in an active tectonic setting. Sedimentologic fieldwork and geologic mapping of the Arro system has been undertaken to provide context for a detailed study of three of the best-exposed outcrops: Sierra de Soto Gully, Barranco de la Caxigosa, and Muro de Bellos. These locations exemplify the role of confinement in controlling the facies and architecture in the system. Sedimentologic characterization of the deposits has allowed the identification of fourteen facies and eight facies associations; these form a continuum and are non-unique to any depositional environment. However, architectural characterization allowed the grouping of facies associations into four depositional elements: (i) weakly confined, increasing-to-decreasing energy deposits; (ii) progradational, weakly confined to overbank deposits; (iii) alternations of MTDs and turbidites; (iv) channel fills. Different styles of channel architecture are observed. In Barranco de la Caxigosa, a master surface which was cut and subsequently filled hosts three channel stories with erosional bases; channelization was enhanced by quasi-instantaneous imposition of lateral confinement by the emplacement of MTDs. In Muro de Bellos, the inception of partially levee-confined channel stories was enhanced by progressive narrowing of the depositional fairway by tectonic structures, which also controlled their migration. Results of this study suggest that deep-water channelization in active tectonic settings may be enhanced or hindered due to: (1) flow interaction with MTD-margin topography or; (2) MTD-top topography; (3) differential compaction of MTDs and/or sediment being loaded into MTDs; (4) formation of megascours by erosive MTDs; (5) basin-floor topography being reset by MTDs. Therefore, the Arro system can be used as an analog for ancient subsurface or outcropping channelized deposits in bathymetrically complex basins, or as an ancient record of deposits left by flow types observed in modern confined systems.

## INTRODUCTION

Deep-water depositional elements are the product of flows that erode, bypass, and deposit along the constituent parts of a deep-water sedimentary system (Kneller, 2003; Stevenson et al., 2013). The architecture (geometry, distribution, and size) of these elements can be captured in seismic data (e.g, Mayall and Stewart, 2000; Posamentier, 2003; Posamentier and Kolla, 2003; Prather, 2003; Schwenk et al., 2005; Mayall et al., 2006; Wynn et al., 2007; Deptuck et al., 2003, 2007, 2008; Marsset et al., 2009); however, a flow-scale understanding of their constructional mechanisms is essential to inform generic models of their evolution (Peakall and Sumner, 2015). Despite recent advancements in experimental (De Leeuw et al., 2016) and numerical (Dorrell et al., 2018) modelling, direct flow monitoring (Xu et al., 2013; Clare et al., 2016; Hughes Clarke, 2016; Azpiroz-Zabala et al., 2017; Paull et al., 2018; Maier et al., 2019), flow reconstruction (Talling et al., 2007; Stevenson et al., 2013, 2018; Mountjoy et al., 2018), and repeat bathymetry surveying (Hizzett et al., 2018; Vendettuoli et al., 2019), process-informed outcrop studies still provide the most detailed account of system evolution over geologic timescales.

A central parameter of the erosion-deposition threshold of suspended sediment in turbidity currents is velocity (Kuenen and Sengupta, 1970; Kneller, 2003; Stevenson et al., 2015; Dorrell et al., 2013, 2018). Substrate morphology is among the most significant factors which control flow velocity. Kneller (1995) provided a summary overview of topographic effects on flow velocity (Fig. 1A), whereby a flow may change its velocity along a downstream transect due to a change in its down-flow gradient or lateral flow constriction (Fig. 1). However, the complexity of turbidity current "run-up" (Kneller and McCaffrey, 1999) and interaction with asymmetrical (Bell et al., 2018a) and oblique (McCaffrey and Kneller, 2001) obstacles must be acknowledged.

Frontal confinement is defined as a reversal in the dip direction of the down-flow gradient along a longitudinal transect of a basin or flow pathway (Fig. 1A). Flow-scale frontal confinement can cause sufficient velocity reduction to initiate deposition and promote channel backfilling (Pickering et al., 2001). Where deceleration is rapid, it may generate hydraulic jumps (commonly at the ends of channels; Mutti and Normark, 1987, 1991; Hofstra et al., 2018) or cause the formation of hybrid event beds (Haughton et al., 2009). At larger (architectural) scales, down-flow gradient is considered a primary variable in studies of slope grading (Prather et al., 1998, 2017) and submarine channel equilibrium profiles (Kneller, 2003; McHargue et al., 2011; Georgiopoulou and

Cartwright, 2013). Lateral confinement occurs due to the presence of two elongate surfaces situated at both lateral edges of a basin or flow pathway, each orientated quasi-parallel to input flow or regional paleocurrent (Fig. 1B). The architectural effect of lateral confinement is manifested at multiple scales. A flow may be partially or fully confined by prominent basin-floor topography, or by a channel wall composed of incised substrate or overspill deposits. These overspill deposits (commonly referred to as terraces or internal levees; Hansen et al., 2015) may themselves be confined within larger external levees (Kane and Hodgson, 2011), a canyon wall (Kane et al., 2009a), or by confining structures (Casciano et al., 2019). At flow scale, substrate erosion (Eggenhuisen et al., 2011), construction of depositional topography (e.g., levees) from preceding flows (De Leeuw et al., 2016), or both (Hodgson et al., 2016), can progressively generate lateral confinement, increasing the velocity, and hence bypass potential of subsequent flows (Fig. 1B). Continued flow input may trigger a positive feedback mechanism (a "channelization feedback" *sensu* Eggenhuisen et al., 2011; De Leeuw et al., 2016), whereby elevated flow velocities lead to increased basal erosion and lateral overspill, hence imposing greater lateral confinement leading to channelization. The onset of this feedback mechanism occurs as a "channelization threshold" is crossed (*sensu* Eggenhuisen et al., 2011; De Leeuw et al., 2016). Understanding what controls this threshold, when it is crossed, and whether imposition of externally derived lateral confinement may influence this, is crucial to understanding deep-water channel inception.

The processes of deep-water channel initiation and infill have a varied architectural expression (Clark and Pickering, 1996; Deptuck et al., 2003; Macauley and Hubbard, 2013), and a large range of potential autogenic and allogenic controlling factors (Pickering and Corregidor, 2005; Clark and Cartwright, 2011; Flint et al., 2011; Jobe et al., 2015; Gong et al., 2016). In structurally active settings, the influence of protruding structures and mass-transport deposits (hereinafter MTDs) is particularly prevalent.

Channels can be blocked or diverted by a growing structure, or incise through it, depending on: (i) rate of relative sedimentation to structural growth, (ii) timing of structuration, and (iii) geometry and interaction of different structures (Gee and Gawthorpe, 2006; Mayall et al., 2010; Clark and Cartwright, 2011; Jolly et al., 2016). The growth of synsedimentary fault-derived folds may also result in paleoflow directions to be oriented parallel to the structures; in such cases, progressive lateral confinement may be generated by the development of these structures (Clark and Cartwright, 2011).

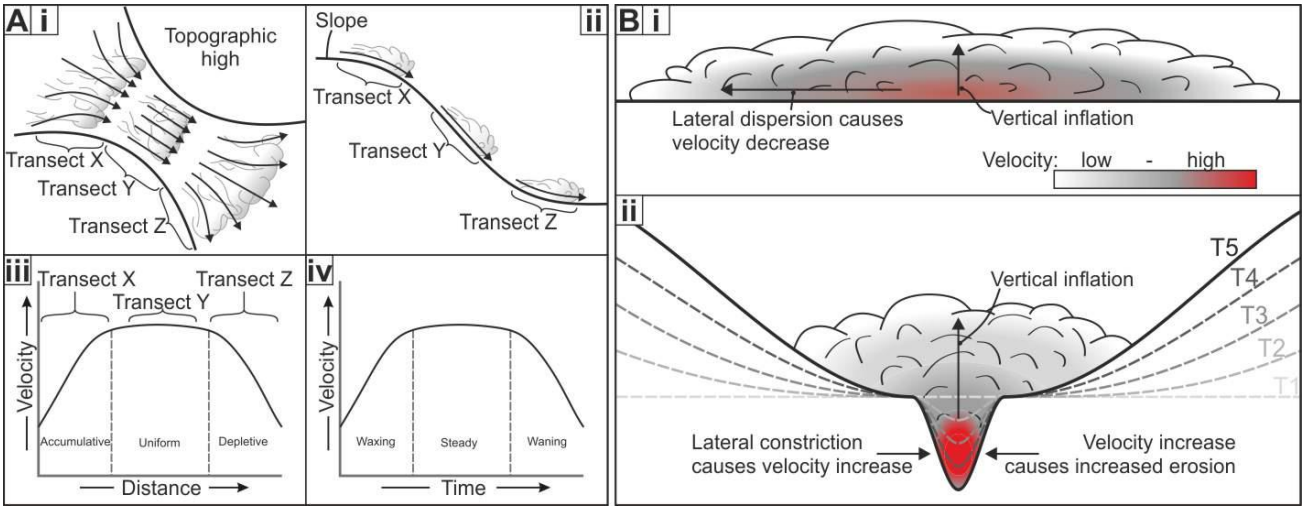


**Figure 1** – Schematic diagrams showing the effect of axial gradient and lateral confinement on flow velocity. Ai) Lateral constriction and release of a flow, or (ii) increasing and decreasing the axial flow gradient can (iii) increase or decrease flow velocity over a longitudinal transect of a flow, or (iv) temporally at the base of a passing flow (modified from Kneller, 1995). B) Velocity response of an unconfined flow (i) as it undergoes progressive lateral confinement (ii).

Herein, MTD is used as a term to describe any of the products of *en masse* transport and deposition (Nelson et al., 2011; Kneller et al., 2016). The term encompasses a continuum of deposits, distinguished by the degree of internal deformation or disaggregation (Moscardelli and Wood, 2008; Bull et al., 2009; Ogata et al., 2012), and named in accordance with their deformational processes: slides (least internal deformation), slumps, and debris flows (most internal deformation). In tectonically active basins, longitudinally emplaced MTDs (see Kremer et al., 2018 for definition) may be sourced from the headwall or sidewalls of a feeding canyon (Nelson et al., 2011) or from a proximal shelf or slope failure (Ortiz-Karpf et al., 2017); transversely emplaced MTDs may be sourced from the local collapse of channel walls (Hansen et al., 2015) or from a laterally confining slope (Arbués et al., 2007a). MTDs can have a profound influence on the evolution and architecture of submarine channels through: (i) quasi-instantaneous imposition of lateral confinement by MTD-top or -margin topography (Schultz et al., 2005; Hansen et al., 2013; Kneller et al., 2016; Masalimova et al., 2016; Kremer et al., 2018; Ward et al., 2018) and/or the development of evacuation scars (Dakin et al., 2013; Hodgson et al., 2016; Qin et al., 2017) leading to channelization; (ii) the perturbation of flows leading to backfilling (Posamentier and Kolla, 2003; Nelson et al., 2009; Bernhardt et al., 2012; Corella et al., 2016); (iii) thalweg plugging, facilitating lateral channel

migration (Kremer et al., 2018), diversion (Nelson et al., 2011; Kneller et al., 2016), or avulsion (Ortiz-Karpf et al., 2015); (iv) affecting channel sinuosity (Deptuck et al., 2007).

To help bridge the resolution gap between event-bed and seismic scale, outcrops from ancient structurally complex basins are commonly used as analogs (e.g., McCaffrey et al., 2002; Brunt et al., 2007; Leren et al., 2007; Janbu et al., 2007; Hubbard et al., 2008; Bernhardt et al., 2011, 2012; Casciano et al., 2019; McArthur and McCaffrey, 2019). One such "natural laboratory" is the Eocene Hecho Group, in the Aínsa depocenter (South Pyrenean Foreland Basin, Spain), where the effect of structures and mass-transport deposits on deep-water channels has been well documented (Pickering and Corregidor, 2005; Arbués et al., 2007a, 2007b; Pickering and Bayliss, 2009; Dakin et al., 2013; Bayliss and Pickering, 2015). This study provides a sedimentologic and architectural characterization of the Arro turbidite system, in the Hecho Group (see Scotchman et al., 2015 for definitions; Fig 2), describing, for the first time, its distal expression in the Aínsa depocenter. The study is used to investigate the extent to which mass-transport- and thrust-related structures influence the establishment, evolution, and infill of axial submarine channels, and the scales at which this control is exerted. A particular line of enquiry is whether the channelization process may be enhanced or hindered by the imposition of frontal or lateral confinement during the emplacement or growth of these features. Investigating the sedimentologic and architectural response to evolving basin-floor topography in channelized deep-water systems is important for elucidating how channels are initiated and what controls their presence and distribution. The findings herein may therefore be used to inform studies in other ancient and modern confined basins.

## GEOLOGIC SETTING

The Lower Eocene stratigraphy of the Aínsa depocenter is part of the fill of the South Pyrenean Foreland Basin, formed on the southern margin of the doubly verging Pyrenean Orogen (Fig. 2; Séguret, 1972; Cámara and Klimowitz, 1985; Puigdefàbregas and Souquet, 1986; Muñoz, 1992; Bentham and Burbank, 1996; Barnolas and Gil-Peña, 2001; Fernández et al., 2004; Arbués et al., 2011). The South Pyrenean Foreland Basin comprises three parts: the terrestrial-to-shallow-marine "Tremp-Graus depocenter"; the channelized deep-water "Aínsa depocenter"; the unconfined, deep-water "Jaca depocenter". The Aínsa depocenter is located in an oblique transfer zone between the Montsec-Peña Montañesa and Cotiella thrust units (Fernández et al., 2004, 2012;

Muñoz et al., 2013). This “relay” forms a wider zone of smaller-wavelength thrust-related SE-NW structures propagating through Cretaceous-Neogene carbonate and clastic sedimentary rocks from a Triassic decollement (Séguret, 1972; Cámara and Klimowitz, 1985; Choukroune, 1992; Muñoz, 1992; Clark et al., 2017).

During the Ypresian, channelized deep-water deposits in the Aínsa depocenter were connected to unconfined deposits in the downstream Jaca depocenter (Fig. 2), hence their collective name: the Hecho Group (Mutti, 1984). Here, the scheme presented by Clark et al. (2017) is followed, wherein the Hecho Group is divided into seven turbidite systems (Fig. 2C). However, nomenclatural inconsistency is common in the description of the deep-water Aínsa depocenter fill (cf. Mutti, 1985; Fernández et al., 2004; Pickering and Corregidor, 2005; Arbués et al., 2007a; Das Gupta and Pickering, 2008; Heard and Pickering, 2008; Pickering and Bayliss, 2009; Muñoz et al., 2013; Heard et al., 2014; Pickering and Cantalejo, 2015; Scotchman et al., 2015; Cornard and Pickering, 2019).

Sediment in the turbidite systems of the Hecho Group was derived predominantly from the fluvio-deltaic environments in the Tremp-Graus depocenter to the east, entering the Aínsa depocenter through a series of submarine canyon systems to the southeast (Fig. 2B). Shelfal deposits of the Castigaleu Group are incised by the Atiart surface, a large submarine unconformity, which is filled by deep-water sediments of the Castissent Group (time equivalent to the Fosado and Arro systems) (Soler-Sampere and Garrido-Megías, 1970; Puigdefàbregas and Souquet, 1986; Mutti et al., 1988; Muñoz et al., 1994; Scotchmann et al., 2015; Chanvry et al., 2018). The Arro system, which was active during the Ypresian (Fig. 2C), was fed through the Pocino surface, a subtle canyon first recognized by Mutti et al. (1988, see also Sgavetti, 1991; Millington and Clark 1995a, 1995b) which was in turn incised by the Lascorz surface (the feeder of the overlying Gerbe system) (Muñoz et al., 1994; Payros et al., 2009; Poyatos-Moré, 2014; Castelltort et al., 2017).

To date, detailed sedimentologic and stratigraphic analysis has been conducted only on the most proximal Arro outcrops, i.e., those of Charo (exposing part of the Arro’s feeder canyon fill), Rio de la Nata, Los Molinos Road, and Santa Catalina (Millington and Clark, 1995a, 1995b; Arbués et al., 2007a, 2007b) (Fig. 3). The Los Molinos Road has commonly been used as the “type locality” for the Arro system (Das Gupta and Pickering, 2008; Caja et al., 2010). Van Lunsen (1970) and Castelltort et al. (2017) present data from more distal outcrops, but the

sedimentology and stratigraphy remain undescribed. This study is focused on the sedimentologic characterization of the more distal parts of the Arro system in the Aínsa depocenter (Fig. 3).

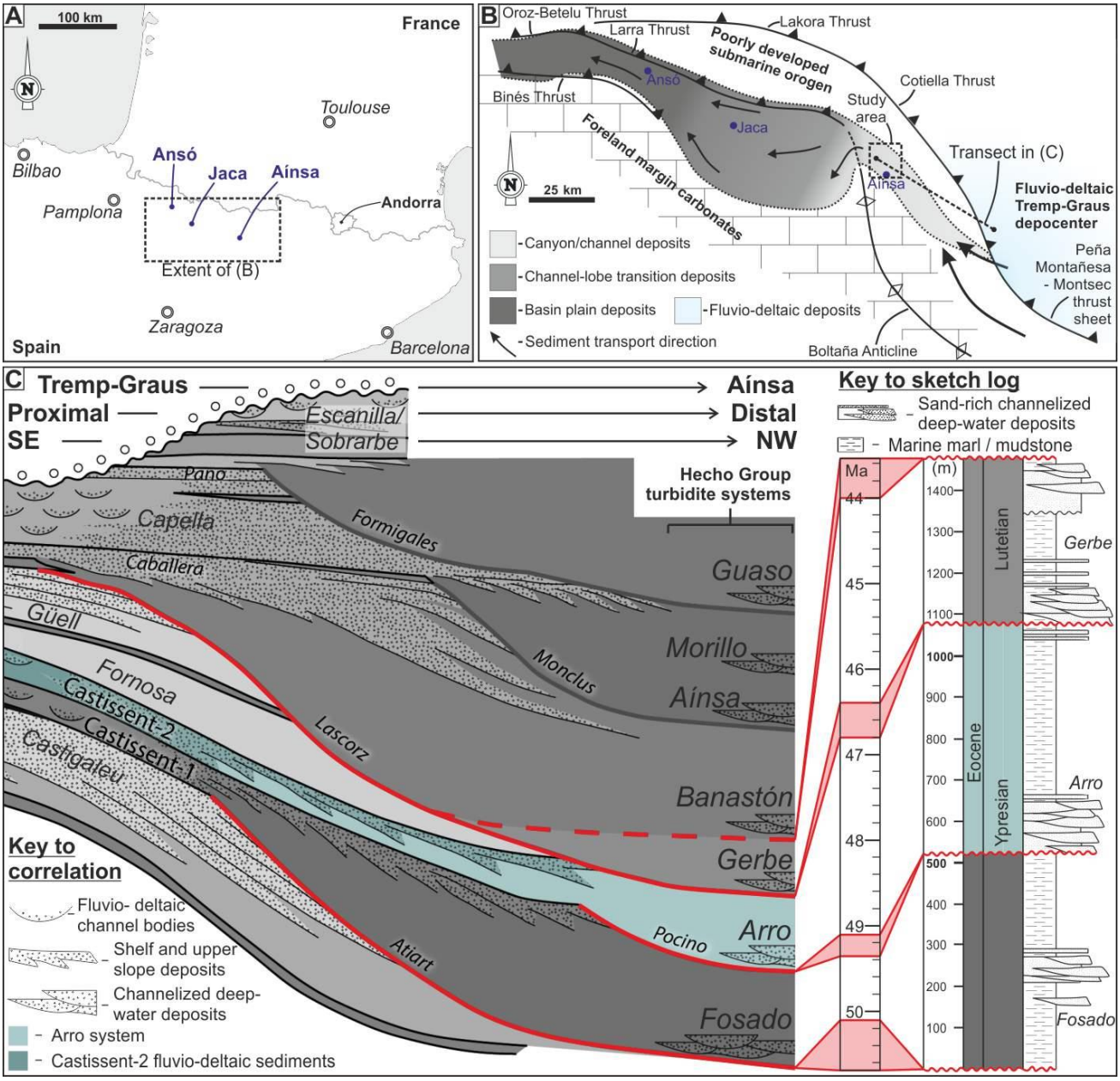


**Figure 2** – A) Map showing broad location of the South Pyrenean Foreland Basin in northern Spain. B) Schematic map showing the sediment routing system from Tremp-Graus (east) to Jaca depocenter (west) in the Eocene, modified from Remacha and Fernández (2003) and Caja et al (2010). C) Depositional dip section showing the correlation of fluvio-deltaic units in the distal part of the Tremp-Graus depocenter to their contemporaneous deep-water units in the Aínsa depocenter, with inset showing the chronostratigraphy of the Fosado, Arro and Gerbe systems (modified from Clark et al., 2017).

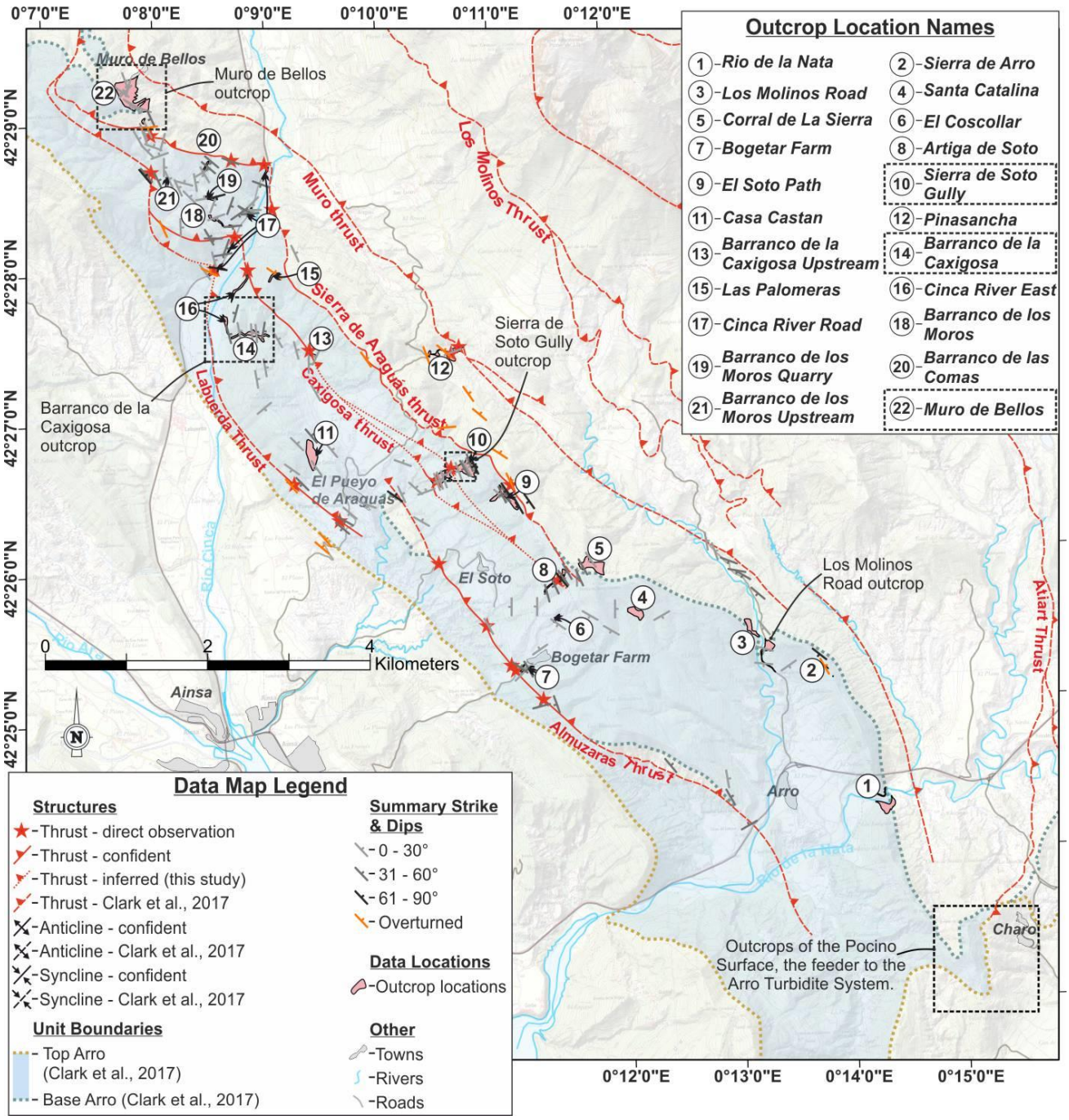


**Figure 3** – Map of the Arro turbidite system modified from Clark et al. (2017) with data from this study, showing locations and names of major tectonic structures, the top and base of the Arro turbidite system, some summary structural data, and the twenty-two locations used to inform this study with Sierra de Soto Gully, Barranco de la Caxigosa, and Muro de Bellos highlighted. Grid is in degrees, minutes, and seconds, georeferenced in European Datum 1950 UTM zone 30N. Basemap at 1:25,000 scale courtesy of Instituto Geográfico Nacional, available from: http://centrodedescargas.cnig.es/CentroDescargas/locale?request_locale=en.

## DATA AND METHODS

The field area, located N-NE of the town of Aínsa, covers approximately 40 $km^2$ (Fig. 3) along an ~ 13-km-long transect oriented SE-NW (parallel to regional paleocurrent). A revised version of a geologic map by Clark et al. (2017) is used; structural amendments are informed by 448 strike and dip measurements of bedding (Fig. 4C) and the tracing of some of the larger, depocenter-scale structures (Fig. 3). Detailed sedimentologic analysis of twenty-two outcrops was undertaken using traditional field methods, augmented by study of aerial photographs acquired using an unmanned aerial vehicle. A total of 230 paleocurrent measurements were taken from flute casts, and ripple and cross-bed foresets (Fig. 4). Fifty-six logs totalling 1,088 m of stratigraphy were measured with centimeter resolution and drawn at 1:10 to 1:50 scale to capture vertical facies and grain-size variations at multiple scales; a high-precision Jacob's staff (Patacci, 2016) was used. As the Charo area and the most proximal outcrops (1, 3, and 4 in Fig. 3) have been studied in detail previously (Millington and Clark, 1995a, 1995b; Arbués et al., 2007a, 2007b), this study is focused primarily on three outcrops in the more distal part of the Arro system in the Aínsa depocenter: Sierra de Soto Gully, Barranco de la Caxigosa, and Muro de Bellos (Fig. 3; outcrops 10, 14, and 22 respectively). At these locations, multiple laterally offset logs, field sketches, and interpreted photomosaics (from ground and aerial photographs) have been used to generate architectural panels.

### *Large-Scale Trends*

The trend of paleocurrents for the Arro system is dominantly to the NW (Fig. 4), which is consistent with the findings of Millington and Clark (1995a, 1995b) and Arbués et al. (2007a, 2007b), who present data from the proximal localities and feeder system. The regional trend of strike orientation of thrusts and related folding within the area is also NW-SE, which is consistent with the trend of the larger, depocenter-bounding structures, such as the Mediano, Anisclo, and Boltaña anticlines (Millington and Clark, 1995a, 1995b; Arbués et al., 2007a; Muñoz et al., 2013). It is possible that these structures have undergone clockwise rotation along with the regional structures (Muñoz et al., 2013). Regardless, the correspondence of the regional paleocurrents (from flutes, ripples, and cross beds; Fig. 4B) and the structural trend (Fig. 4C) allow the Arro system to be classified as an axial deep-water system.

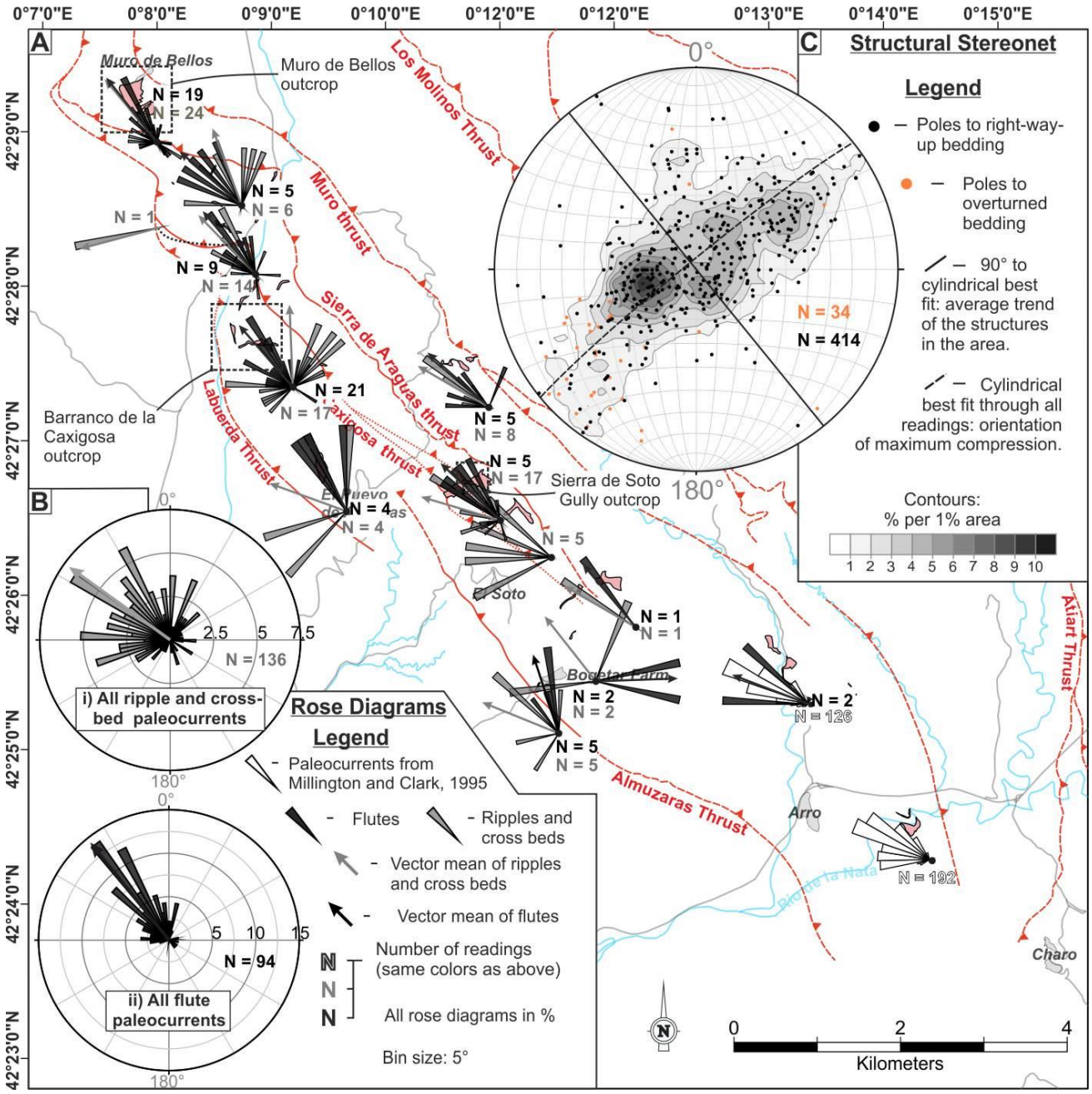


**Figure 4** – A) Map presenting paleocurrent data from fourteen of the visited locations illustrating their relationship with the basinal structures. B) Regional paleocurrent data measured from (i) ripples and cross beds, and (ii) flute casts. C) All strike and dip measurements of bedding, indicating the average structural trend.

| LITHOFACIES | LITHOLOGY | DESCRIPTION | THICKNESS | PROCESS INTERPRETATION | PHOTO |
|---|---|---|---|---|---|
| Lf1 – Structureless mudstone | Carbonate mudstone containing silt. | No obvious grading or structure, weathers with a texture comprising loose spheroids < 10 cm long. Concretionary horizons occur with variable spacing (0.5-10 m). | No clear bedding or lamination | Hemipelagic suspension fallout. | Fig. 5A |
| Lf2 – Graded siltstone | Sometimes graded from very fine-grained sand to mud, typically silt to mud. | Usually structureless, however parallel lamination and starved ripples are sometimes present. | 0.1-4 cm | Fine-grained, dilute-gravity-current deposits, equivalent to a coarse $T_e$ division of Bouma (1962) or a $T_6$ division of Stow and Shanmugam (1980). | Fig. 5B |
| Lf3 – Lenticular sandstone | Very fine- to medium-grained sandstone, occasionally coarse silt or coarse sandstone. | Lenses of sandstone typically 3-7 cm wide, separated laterally by 0.1-10 cm. Lenses are aligned along bedding-conformable horizons which can usually be traced laterally for over 10 m and often over 20 m. | 0.1-1.5 cm | Deposition from a dilute, dominantly bypassing turbidity current. | Fig. 5C |
| Lf4a – Rippled sandstone | Very fine- to coarse-grained sandstone. | Unless they are eroded, rippled bed tops are usually preserved, commonly with internal ripple cross lamination observed, both of which may be disturbed by dewatering effects. Where Lf4a occurs as isolated beds, bases are usually flat but some exhibit basal scouring, making the beds pinch and swell. Ripple heights (crest to trough) typically range from 1.5-5 cm. Ripple lengths (trough to trough) typically range from 7 to 30 cm. In the thinnest intervals the facies nears a lenticular geometry. | 1.5-10 cm | Deposition and tractional reworking by dilute, low-density gravity current (Allen, 1973, 1982). | Fig. 5D |
| Lf4b – Hummocky- | Very fine- to medium-grained sandstone. | Characterized by undulating laminae with wavelengths ranging from 5 to 25 cm and amplitudes ranging from 0.5 to 5 cm, comprising internal lamination truncations and dip changes. Bed | 2-6 cm | Deposition and reworking from reflected or deflected dilute flows, typically in the bypassing part of a | Fig. 5E |

| | | | | | |
|---|---|---|---|---|---|
| cross-stratified sandstone | | tops display 3D bedforms with no dominant inferred paleocurrent direction. Always located at the tops of sandstone beds, sometimes overlying ungraded, cross-stratified (< 7-cm-thick foresets, typically pervasive through an event bed or scour fill), cross-laminated (> 7-cm-thick foresets) or parallel-laminated sandstones. | | bipartite flow (Mutti, 1992; Mulder et al., 2009; Muzzi Magalhaes and Tinterri, 2011; Bell et al., 2018a). | |
| Lf4c – Planar-cross-stratified sandstone | Fine- to medium-grained sandstone. | Foreset heights range from 7 to 50 cm, commonly infilling concave-convex scoured surfaces, sometimes exhibiting positive depositional relief, and sometimes both. Foreset angles vary significantly from ~ 10˚ to ~ 40˚. Fluted bases and rippled tops are also seen. Cross stratification can be pervasive throughout isolated beds or occur above ungraded structureless sandstones. | 7-50 cm | (1) Dunes or mega ripples formed by traction and fallout from a dilute flow (Tinterri, 2011); (2) 'pseudo dunes' formed from scour derived instabilities in a unidirectional flow (Arnott and Al-Mufti, 2017). | Fig. 5F |
| Lf5 – Parallel-laminated sandstone | Very fine- to coarse-grained sandstone. | Parallel laminae spaced 0.1-1 cm apart which may underlie or overlie any other sandstone-rich facies. Can be disturbed or convoluted in parts due to bioturbation and dewatering. | 5-50 cm | Traction carpets from upper-stage plane beds or lower-stage plane beds (Talling et al., 2012). | Fig. 5G |
| Lf6a – Graded, structureless sandstone | Large grain-size range with some beds fining from granules to very fine sand. Typically coarse or medium or medium to fine sand. | Bedded, internally structureless sandstone except for dish structures. Some beds are capped with siltstone, whereas others are bounded by amalgamation surfaces. At amalgamation surfaces and bedding boundaries, load balls and flame structures are seen; flutes, some of which loaded, are common on bed bases, but grooves are rare. | 0.1-2.75 m | Bouma (1962) sequence $T_a$ division deposited from a depositional, and potentially erosional, high-density turbidity current (Lowe, 1982), often with subsequent dewatering. | Fig. 5H |
| Lf6b – Ungraded, structureless sandstone | Fine to coarse-grained sandstone. | Lack of grading characterizes this facies. Flames, load balls, and flutes are found on many bed bases. Amalgamation surfaces and intense internal deformation relating to dewatering are common. | 0.04-1.25 m | Bouma (1962) sequence $T_a$ division deposited from a depositional, and potentially erosional, high-density turbidity current (Lowe, 1982). | Fig. 5I |

| | | | | | |
|---|---|---|---|---|---|
| Lf6c – Sandstone with mudclasts | Fine to coarse sandstone. | Bedded sandstone similar to Lf6a and Lf6b, but containing up to 40% rounded to subangular mudclasts, sometimes armored with sand and granules. Mudclasts may be concentrated at bed bases, tops, or distributed throughout. Amalgamation surfaces exhibiting scouring geometries are sometimes lined with mudclasts. In some cases mudclasts are concentrated on distinct planar, inclined horizons within beds, potentially highlighting cross strata. | 0.2-4 m (upper limit possibly a series of amalgamated beds) | Erosional and depositional high-density turbidity current (Lowe, 1982) carrying "rip-up clasts" (Mutti and Nilsen, 1981; Mutti, 1992). | Fig. 5J |
| Lf7a – Extraclast conglomerate | Granule- to cobble-size extraclasts and bioclasts supported by very poorly sorted, polymictic, argillaceous usually coarse-grained sandstone. | Characterized by the presence, and dominance, of rounded to subangular extrabasinal lithic fragments composed of limestone, quartzite, or other mineral aggregates. The silt and clay content of the matrix varies significantly between and within (laterally and vertically) individual beds. Mudclasts, rounded clasts of sandstone and local heterolithics, and bioclasts such as *Nummulites* and shell fragments (of oysters, other bivalves, and brachiopods) are common yet not in dominant quantities. Extraclasts are almost always matrix supported but may be locally clast supported. | 8-70 cm | Deposition from the traction carpet of dominantly bypassing flow(s) (Mayall et al., 2006; Stevenson et al., 2015) due to frictional freezing (Mutti et al., 2000). | Fig. 5K |
| Lf7b – Mudclast conglomerate | Pebble-size mudclasts supported by sandy matrix of varying texture and grain size. | Size (0.5-20 cm long axis), rounding (rounded to subangular), and proportion (typically > 75% of clasts) of mudclasts varies between and within (laterally and vertically) beds; some mudclasts are armored with coarse sand. Extraclasts and bioclasts are often present. The matrix composition ranges from well-sorted medium and coarse sandstone to poorly sorted, clay- and silt-rich sandstone. | 5-30 cm | A high-energy erosional and dominantly bypassing flow containing abundant "rip-up clasts" (Mutti and Nilsen, 1981; Mutti, 1992) deposited as a lag (Mayall et al., 2006; Stevenson et al., 2015); type A1 and B1 of Johanssen and Stow (1995). | Fig. 5L |

| | | | | | |
|---|---|---|---|---|---|
| Lf8a – Chaotic mudstone | Chaotic mud-rich deposit supporting rafts of heterolithic stratigraphy, blocks of sandstone, extraclasts, and bioclasts | A clay-rich matrix with variable silt and sand content contain: deformed, disaggregated blocks (up to 5 m long axis) of fine-grained heterolithic sediment which exhibit internal structure similar to stratigraphy found elsewhere in the basin; bioclasts such as *Nummulites* and shell fragments; 5-20 cm rounded to subrounded blocks of coarse sandstone, sometimes nummulite and shell rich, similar to that seen in the proximal (shelfal) Castissent Formation; 3-40 cm rounded to subrounded clasts of well-sorted fine to coarse sandstone resembling Lf4-6; and granule- to pebble-size extrabasinal lithic fragments (see Lf7a). The presence and relative proportions of these components is highly variable between deposits. | 0.2-20 m | *En masse* deposition from debris flows and highly disaggregated slumps (termed "blocky beds" by Ogata et al., 2012). The formative material was sourced from: local stratigraphy, possibly due to a growing basin-floor structure (Arbués et al., 2007a, 2007b) or channel-bank collapse (Barton et al., 2010); or from the proximal fluvio-deltaic and shelf deposits of the Castissent Formation (Nijman and Puigdefabregas, 1977; Mutti et al., 1996, 2000; Nijman, 1998). | Fig. 5M |
| Lf8b – Deformed heterolithics | Deformed, not disaggregated local heterolithic stratigraphy. | Folded heterolithic packages with wavelengths between 0.1 and 3 m, sometimes overlying a heavily deformed basal surface. The constituent stratigraphy can be easily matched to the adjacent or underlying stratigraphy and is therefore generally devoid of shelf material. | 0.5-6 m | Slumped local stratigraphy. A continuum exists between these and Lf8a distinguished by the degree of disaggregation (Posamentier and Martinsen, 2011; Ogata et al., 2012). | Fig. 5N |
| Lf9 – Polymictic, bioclastic sandstone | Ranging from very poorly sorted polymictic coarse- to very coarse-grained (average) sandstone with abundant bioclasts. | This bedded facies can exhibit normal grading and scouring bases, sometimes with flutes and sometimes overlying amalgamation surfaces. *Nummulites* (0.2-2.5 cm diameter) are the dominant bioclast with fragmented oyster shells (0.2-4 cm long axis) also abundant; gastropods are rarely found. Relative and absolute bioclast proportions vary between beds and (vertically and laterally) within beds, sometimes over < 5 cm. In | 0.03-1m | Sandstones and bioclasts introduced by density currents, sourced from the Castissent shelf (Marzo et al., 1988; Nijman, 1998). | Fig. 5O |

| | | | | | |
|---|---|---|---|---|---|
| | | some cases bioclasts occur in such abundance that this facies can be classed as a carbonate packstone. | | | |

**Table 1** – Descriptions of the fifteen facies and sub-facies recognized in the stratigraphy of the Arro system, including their lithologies, typical thicknesses and interpretations of their depositional processes.

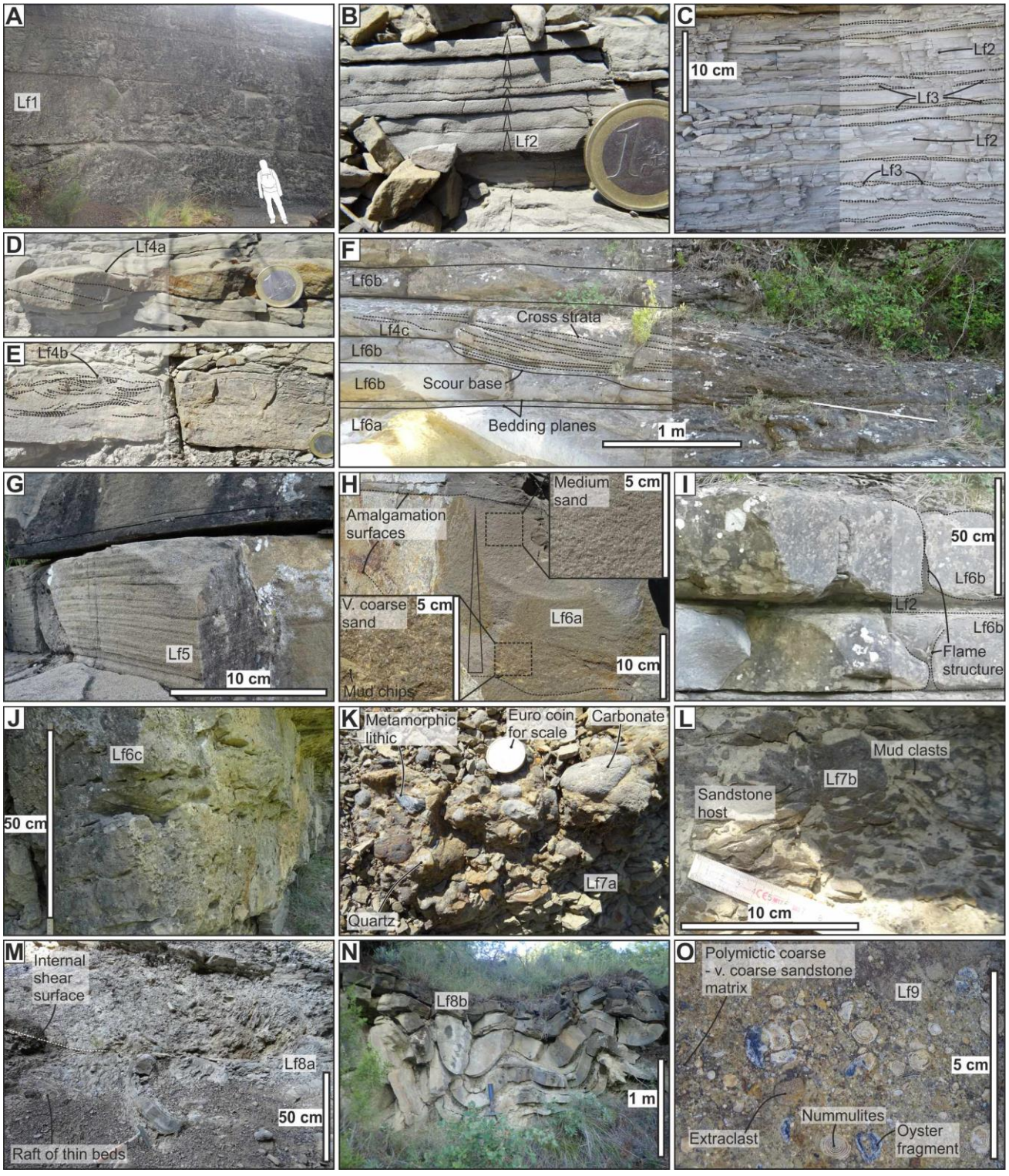


**Figure 5** – Photographs of all fifteen facies and sub-facies which constitute the stratigraphy of the Arro system; descriptions are provided in table 1. A) Lf1 - structureless mudstone; B) Lf2 - graded siltstone; C) Lf3 - lenticular siltstone; D) Lf4a - rippled sandstone; E) Lf4b – hummocky-cross-stratified sandstone; F) Lf4c – planar-cross-stratified sandstone; G) Lf5 – parallel-laminated sandstone; H) Lf6a - graded, structureless sandstone; I) Lf6b - ungraded, structureless sandstone; J) Lf6c - sandstone with mudclasts; K)

Lf7a - extraclast conglomerate; L) Lf7b - mudclast conglomerate; M) Lf8a - chaotic mudstone; N) Lf8b - deformed heterolithics; O) Lf9 - polymictic, bioclastic sandstone.

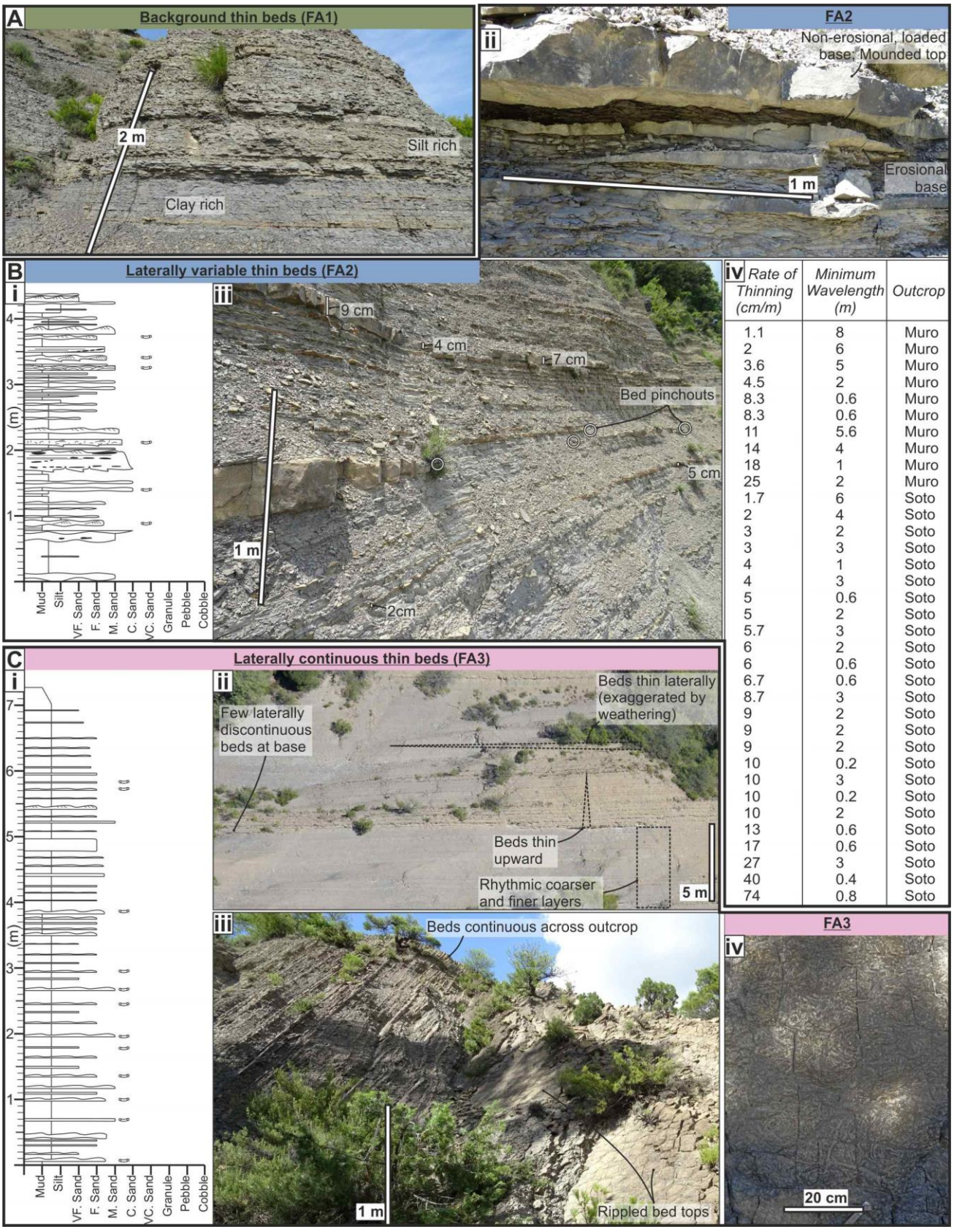

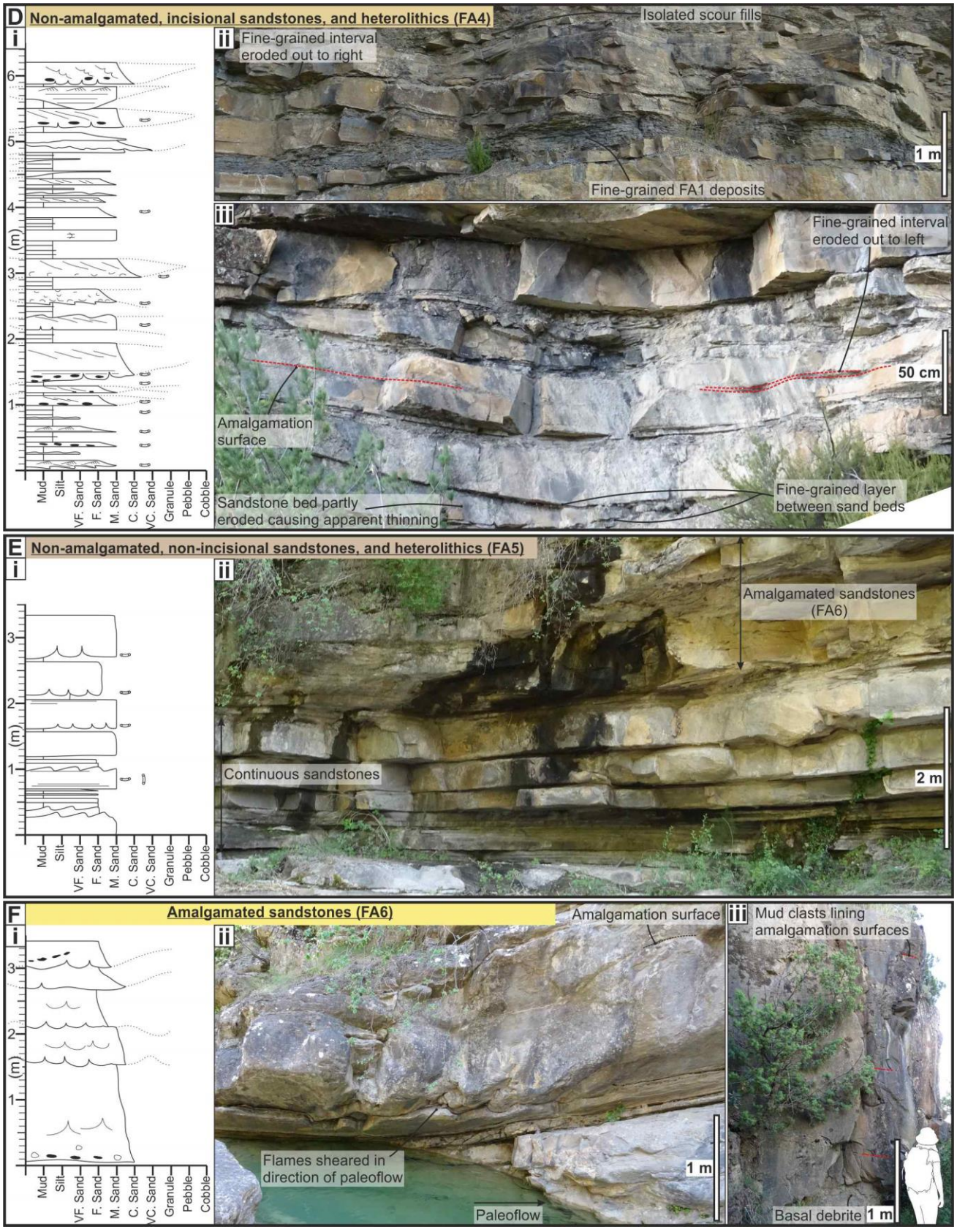
D
Non-amalgamated, incisional sandstones, and heterolithics (FA4)
i
ii
iii
Isolated scour fills
Fine-grained interval eroded out to right
Fine-grained FA1 deposits
1 m
Fine-grained interval eroded out to left
50 cm
Amalgamation surface
Sandstone bed partly eroded causing apparent thinning
Fine-grained layer between sand beds
(m)
Mud
Silt
VF. Sand
F. Sand
M. Sand
C. Sand
VC. Sand
Granule
Pebble
Cobble
E
Non-amalgamated, non-incisional sandstones, and heterolithics (FA5)
Amalgamated sandstones (FA6)
Continuous sandstones
2 m
F
Amalgamated sandstones (FA6)
Amalgamation surface
Mud clasts lining amalgamation surfaces
Flames sheared in direction of paleoflow
Paleoflow
Basal debrite

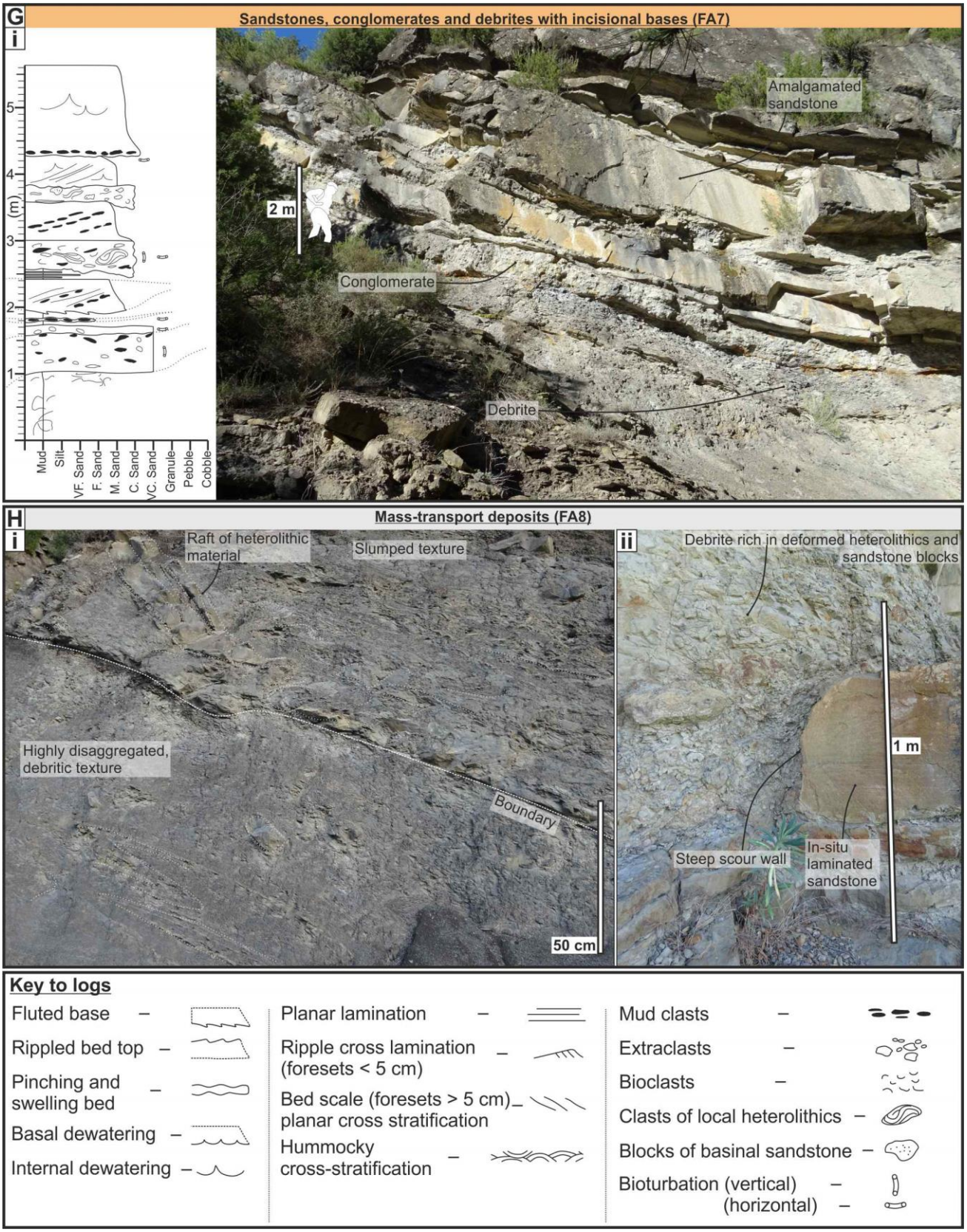


**Figure 6** – A – H) Typical nature of facies associations 1 to 8 (FA1 – FA8) respectively. A, Bii-iii, Cii-iii, Dii-iii, Eii, Fii-iii, Gii and Hi) Representative photographs of all eight facies associations; Bi, Ci, Di, Ei, Fi and Gi) representative logs through idealized sections of FA2 – FA7 respectively; Biv) thinning rates and

wavelengths of pinching and swelling beds in FA2; Ci) bed top in FA3 covered by *Scolicia*; Hi) debritic mass-transport deposit of FA7 forming a steep-walled scour surface into an underlying sandstone bed.

## FACIES ANALYSIS

The fifteen facies and sub-facies defined in the Arro turbidite system are described in Table 1, with photographs presented in Figure 5. These facies and sub-facies are defined according to lithology, grain size, and composition, the presence and type of sedimentary structures, and grading.

The facies are grouped together to form eight facies associations (FA1-8) that can be widely recognized in the Arro system (Fig. 6). These facies associations are not unique to a single depositional environment and often exhibit gradational transitions between one another; the observed continuum prevented any meaningful quantitative facies-association definition based upon facies proportions. The logs displayed in Figure 6 are from representative sections. The interpretation of depositional elements (DE1-4) was therefore based on the combination of facies association occurrence and the presence of key bounding surfaces (see "depositional elements" section).

Turbidite and MTD character is a record of the velocity, concentration, magnitude, and grain size (and modality thereof) of flows traversing the depocenter. As the specific role of each of these parameters is generally indiscernible, the term "energy" will be used such that high-energy flows are those of high velocity, concentration, and magnitude, and coarse grain size (and vice versa for low-energy flows).

### *Facies Association 1 (FA1) – Background Thin Beds*

**Description.---** Constituting most of the depocenter fill, this facies association contains very thin (typically < 3 cm, average thickness ~ 1 cm) very fine- to medium-grained beds of lenticular (Lf3), rippled (Lf4a), and ungraded, structureless (Lf6b) sandstone, which alternate with finer-grained siltstone and mudstone facies of structureless mudstone (Lf1) and graded siltstone (Lf2) (Table 1); Lf2 is dominant. The thickness of mudstone and siltstone layers in FA1 varies from 3 to 25 cm (average: 7 cm), with variable proportions of clay and silt (Fig. 6A). Bedding-concordant packages (a few decimeters to ten meters thick) of alternating grain size can be traced for tens to hundreds of meters. In some outcrops, such as Muro de Bellos (Fig. 7), wedging geometries

in these packages are observed. Bioturbation on sandstone bed tops and bases is seldom observed (possibly due to outcrop limitations), but sand-filled burrows are found in finer-grained layers. Distinct beds of fully disaggregated debrites (Lf8a) are rare, but FA1 is often highly deformed because of synsedimentary remobilization or due to later tectonic activity; subtle deformation can be hard to detect at outcrop scale. The two causes are distinguished by the presence of calcite veining along shear horizons (or faults), which are taken as an indicator of tectonic deformation. FA1 can be found as heterolithic packages between incisional and non-incisional sandstone beds of FA4 and FA5. Lateral and vertical transitions into laterally variable (FA2) and laterally continuous (FA3) thin beds are observed; a continuum exists between these three facies associations.

**Interpretation.---** FA1 comprises the deposits of dilute, low-density flows (Mutti, 1977), which experienced periodic variations in silt and sand content, together with hemipelagites. The vertical distribution of FA1 between and within other facies associations (FA4 and FA5) suggests that it represents the dominant background sedimentation, but not necessarily from hemipelagic settling alone, as has also been recognized in the deep-water strata of the Tanqua depocenter, Karoo Basin (Boulesteix et al., 2019). The formative flows may have been derived from: (i) small sediment failures on the shelf, on the upper slope, or in the feeder canyon (Clare et al., 2016); (ii) hyperpycnal flows associated with direct sediment input from a canyon-connected river mouth, whereby variations in grain size may reflect variations in the flux of the feeding river (Mulder et al., 2003; Mutti et al., 2003; Zavala et al., 2011); (iii) the down-slope flow of sediment plumes that build at the mouth of a feeding river and collapse upon attainment of a critical density (Hizzett et al., 2018; Mutti, 2019). The presence of FA1 lateral to, and gradational with, FA2 and FA3 suggests that FA1 may also represent distal-most or lateral-most fan or levee deposits. In periods of contemporaneous fan or levee deposition, laterally or upstream, this facies association may therefore have experienced increased rates of aggradation.

### *Facies Association 2 (FA2) – Laterally Variable Thin Beds*

**Description.---** FA2 is highly variable with respect to its constituent facies, bed thickness, and bed nature. It is composed of mainly fined-grained packages (3-50 cm thick) of Lf1, Lf2, and Lf3, interbedded with sandstone beds (> 1 cm, < 50 cm, typically 3-25 cm thick) comprising: rippled (Lf4a), hummocky (Lf4b), and planar cross-stratified (Lf4c), parallel-laminated (Lf5), graded, structureless, and mudclast-bearing (Lf6a-c) and polymictic, bioclastic sandstone (Lf9) (Table 1). Lf4a and Lf6b (Fig. 5) are the dominant sandstone facies (Fig.

6B); Lf4b is particularly prevalent in Sierra de Soto Gully. Bioclasts in beds of Lf9 are fragmented and do not display organization; *Nummulites* typically exhibit a lower degree of fragmentation than bivalve and gastropod bioclasts. Chaotic mudstone (Lf8a) is very rarely observed and, where present, occurs as < 50 cm beds. *Ophiomorpha*, *Nereites,* and *Scolicia* traces are found on some sandstone bed tops, *Thalassinoides* burrows are found on some sandstone bed tops and bases, and other undifferentiated sand-filled burrows are found in some of the fine-grained intervals; no single trace is dominant.

The characteristic feature of this facies association is the geometry of its constituent sandstone beds. Some beds form isolated lenses, some form lenses that pinch out along distinct horizons, and others subtly pinch and swell without forming lenses (Fig. 6B). Bed thinning rates and minimum pinch-and-swell wavelengths (constrained by bed exposures) have been calculated from thirty-five measured beds (average thinning rate: 11.3 cm/m; average minimum wavelength: 235 cm) from the Muro de Bellos (average thinning rate: 9.6 cm/m; average minimum wavelength: 348 cm; N = 10) and Sierra de Soto Gully (average thinning rate: 12 cm/m; average minimum wavelength 190 cm; N = 25) outcrops. Ripple-scale bed thickness variations (7-30 cm wavelength) are sometimes superimposed onto the aforementioned, larger-wavelength, pinching and swelling trends (see Fig. 6B (iv)); the two are usually distinguishable. Bed bases can be flat, lightly incisional (< 10 cm), or exhibit a concave-up geometry which is non-erosional and concordant with bedding below; bed tops can be mounded or flat.

FA2 occurs in all locations and is observed in every depositional element (DE1-4; see "depositional elements"), forming lateral transitions with non-amalgamated, incisional sandstones, and heterolithics (FA4) and background thin beds (FA1), and a vertical transition with laterally continuous thin beds (FA3). In some locations, gradational lateral transitions from a package of FA2 in the center to FA1 are observed in both directions. The nature of the bed tops and bases may change dependent on the depositional element in which they are found.

**Interpretation.---** The presence and fragmented nature of bioclasts in Lf9 suggests that some of the original sediment was derived from a shallow-marine domain. Hummocky cross stratification (Lf4b), interpreted as the product of combined flow, could indicate current reflection or deflection by the interaction with syndepositional basin-floor topography (Tinterri, 2011). Beds with erosional bases could represent either the tail deposits of a

bypassing turbidity current that deposited coarser-grained material downstream, or the deposit of a lower-energy flow that infilled an erosional surface left by a preceding, higher-energy flow (Kane et al., 2009b). Bedding-concordant (non-erosional) bed bases, still concave-up, are interpreted to have filled some substrate topography formed by local tectonic deformation or slumping. Mounded bed tops suggest a bedform-related origin, particularly in beds containing planar or hummocky cross stratification (Lf4b-c). In beds with concave-up bases these bedforms may have formed in relation to the infilling of depressions (*sensu* Arnott and Al-Mufti, 2017); however, this process does not account for those with flat bed bases. Another possible formative mechanism is deposition and tractional reworking of sediment forming dunes (Mutti, 1977) or megaripples (Tinterri, 2011). Postdepositional loading and deformation may also cause or enhance the lateral thickness variability observed in these beds (e.g., Owen, 2003; Oliveira et al., 2011).

FA2 exhibits multiple modes of occurrence. Lateral and vertical transitions into a range of other associations means a number of formative scenarios are possible; these are presented in the "depositional elements" section.

### *Facies Association 3 (FA3) – Laterally Continuous Thin Beds*

**Description.---** FA3 comprises fine-grained intervals (2-30 cm thick) of structureless mudstone (Lf1), graded siltstone (Lf2), and lenticular sandstone (Lf3) punctuated by beds (typically 2-8 cm thick, average thickness ~ 3 cm) of rippled sandstone (Lf4) which tend to weather proud. Hummocky and planar cross stratified (Lf4b-c), and ungraded, structureless (Lf6b) sandstone beds are also common. Graded (Lf6a) and mudclast-bearing (Lf6c) sandstones are rare. Chaotic mudstone (Lf8a) beds are rare (but more common than in the laterally variable thin beds; FA2) and, where present are < 75 cm thick. Packages of deformed heterolithics (Lf8b), up to 2 m thick, can be found in FA3. Sand-filled burrows are found in the finer-grained intervals, and *Thalassinoides* is occasionally present on sandstone bed bases (< 10% of beds); however *Scolicia* is the dominant trace in FA3. Where bed tops are exposed, they are commonly (> 50% of beds) pervasively bioturbated with *Scolicia* (Fig. 6C).

While the facies assemblage may resemble that of FA2, sandstone beds of FA3 do not pinch and swell, aside from undulations related to their rippled tops (7-30 cm wavelength). Thin (< 8 cm) sandstone beds are largely observed to maintain their thickness laterally over ~ 20 m (Fig. 6C). However, in outcrops with exposures greater than tens of meters, a systematic lateral thinning of these beds is observed. Concomitant with this lateral

thinning, FA3 transitions gradationally into background thin beds (FA1; Fig. 6C). FA3 also grades upwards into FA1.

**Interpretation.---** The regular, thin-bedded nature and systematic thinning of the rippled and structureless sandstone beds is consistent with overbank deposition from dilute turbidity currents which overspill a contemporaneous lateral conduit (Mutti, 1977; Mutti et al., 1988; Millington and Clark, 1995a, 1995b; Bayliss and Pickering, 2015). Susceptibility to slumping and remobilization is common in overbank deposits (Kane and Hodgson, 2011; Hansen et al., 2015), and the intensity of *Scolicia* bioturbation also supports this interpretation (Heard et al., 2014).

### *Facies Association 4 (FA4) – Non-Amalgamated, Incisional Sandstones, and Heterolithics*

**Description.---** In this facies association, heterolithic packages of graded siltstone (Lf2) and thin (< 5 cm) beds of lenticular (Lf3) and rippled (Lf4a) sandstone are interbedded predominantly with thin to thick beds (highly variable from 5 to 100 cm thick, typically 20-50 cm) of: planar-cross-stratified (Lf4c), parallel-laminated (Lf5), structureless (Lf6a-b), mudclast-bearing (Lf6c) and bioclastic (Lf9) sandstone. Beds (< 50 cm) of extraclast (Lf7a) and mudclast (Lf7b) conglomerates, and debrites (Lf8a) are observed less commonly. The relative proportions of sandstone beds and fine-grained intervals vary between outcrops (Fig. 6D).

Lateral variability in sandstone bed thickness is related to the presence of erosional surfaces that incise the tops of underlying sandstone beds and into the fine-grained intervals, and that host thicker sediment accumulations in the loci of maximum incision (Fig. 6D). These surfaces are almost always filled mainly by sandstone beds (Lf4c, Lf5 and Lf6a-c) or debrites (Lf8a), and they are often draped by finer-grained deposits (Lf2, Lf3 and < 5 cm beds of Lf4a and Lf6b) that also thicken towards the locus of maximum incision. On rare occasions, the fine-grained deposits are observed to heal the erosional surface completely. FA4 forms a continuum between laterally variable thin beds (FA2) and amalgamated sandstones (FA6). The tendency for the erosional surfaces to cut one another (and lateral transitions into FA2 and FA6) makes measurements of their width and relief problematic, but bed thinning rates (which can be used as proxies) range from ~ 4 to 20 cm/m. Sand-filled burrows are observed in the finer-grained intervals, and *Ophiomorpha* traces are observed.

**Interpretation.---** The diversity of sandstone facies (similar to that of FA2) and presence of Lf7a, Lf7b, and Lf8a suggests deposition from flows of various concentrations, magnitudes, grain sizes, and velocities. Fine-grained drapes on scoured surfaces likely represent combined accumulation from the fine-grained remnants of bypassing flows (which formed the scour) and possibly subsequent ones (e.g., Mutti and Normark, 1987; Mutti, 1992; Kane et al., 2009b; Stevenson et al., 2015; Bell et al., 2018a), and a temporary return to background sedimentation (respectively the "bypass" and "abandonment" drape of Barton et al., 2010; Alpak et al., 2013). The erosional nature of FA4 was attained either by unconfined to weakly confined scouring flows which were not fully contained by their lateral confinement but were still able to scour and bypass coarse sediment fractions, and/or as the lateral expression of higher-energy channelized deposits.

### *Facies Association 5 (FA5) – Non-Amalgamated, Non-Incisional Sandstones, and Heterolithics*

**Description.---** This facies association consists of medium-bedded (10-100 cm) rippled (Lf4a), parallel-laminated (Lf5), and structureless (graded and ungraded; Lf6a-b) sandstones interbedded with finer-grained heterolithic packages. These packages (typically < 20 cm thick) comprise graded siltstone (Lf2) and thin (< 5 cm) beds of lenticular (Lf3), rippled (Lf4a) and graded, structureless (Lf6a) sandstone. Sandstone beds usually exhibit a sharp basal boundary followed by a thickening-upward and sometimes a coarsening-upward trend (Fig. 6E). Both sandstone beds and fine-grained packages maintain their thickness for up to 40 m laterally, unless incised by an erosional surface underlying another facies association (Fig. 8). FA5 is observed solely in outcrops containing channelized deposits (locations 3, 18 and 22; Fig. 2), wherein it may both overlie and underlie non-amalgamated, incisional sandstones, and heterolithics (FA4) or amalgamated sandstones (FA6) (Figs. 6E, 8).

**Interpretation.---** Laterally continuous, non-erosional sandstone beds associated with channel deposits may form when a channel has filled its confining surface (the "spill" phase; Gardner et al., 2003), or from the deposition of sand "sheets" from flows which were fully laterally confined but possessed insufficient energy to erode (McCaffrey et al., 2002). The latter interpretation is favored due to the sharp base and upward thickening. The presence of a sharp basal contact with underlying FA4 and FA6 (Fig. 8) deposits which, internally, contain more evidence of erosion, is interpreted to be due to a rapid drop in local sedimentation rate, likely due to an upstream blockage, or avulsion causing an abrupt lateral shift in the channel axis. Vertical transitions into

overlying FA4 and FA6 deposits represent a return to high-energy flow conditions, potentially accompanying an increase in local sedimentation rate (McCaffrey et al., 2002).

### *Facies Association 6 (FA6) – Amalgamated Sandstones*

**Description.---** FA6 is composed solely of sandstone facies, comprising rippled (Lf4a), planar-cross-stratified (Lf4c), parallel-laminated (Lf5), structureless (graded and ungraded; Lf6a-b) and mudclast-bearing (Lf6c) sandstones. Among these, Lf6a-c appear dominant, but its common pervasive dewatering may obscure the identification of sedimentary structures (Fig. 6F). Sandstone packages of FA6 can be > 5 m thick, but internal amalgamation surfaces picked out by grain-size breaks or horizons of aligned mudclasts are ubiquitous (Fig. 6F); these erode into and are filled by sandstone beds. Amalgamation surfaces are concave-up and typically exhibit dips of up to 40˚ (corrected for local bedding). In outcrops oriented quasi-perpendicular (60-90˚) to local paleoflow (e.g., locations 3 and 14; Fig. 2), the wavelength of scouring varies from ~ 1.5 m to > 25 m. In such outcrops, the locus of maximum incision of successive scours switches laterally in both directions; however, scour walls dipping towards higher-energy sandstones, conglomerates, and debrites with incisional bases (FA7) are preferentially preserved. In outcrops orientated subparallel (0-30˚) to local paleoflow (e.g., locations 18 and 19; Fig. 2), scour walls exist in the same dip range, but do not have a preferential orientation of preservation. In FA6, packages of Lf6b can be up to 4 m thick without development of any obvious amalgamation surfaces, although dewatering might obscure them. Where dewatering is not present, maximum bed thickness (between amalgamation surfaces) is rarely > 1.2 m, and is never greater than 2 m, in keeping with typical channel bed thicknesses quoted in Fryer and Jobe (2019). This facies association lies in a continuum between non-amalgamated, incisional sandstones, and heterolithics (FA4) and (FA7).

**Interpretation.---** FA6 is the result of deposition from recurrent, sand-rich turbidity currents that locally eroded, bypassed, and deposited. Common amalgamation surfaces may have been filled by their formative flows or represent periods of sustained bypass (e.g., Kane et al., 2009b; Bell et al., 2018a). Surface-lining mudclasts likely represent residual lag deposits (Stevenson et al., 2015), possibly derived externally (from a proximal source), or locally, from the erosion of a fine-grained drape (Mutti, 1992; Kane et al., 2017). The frequency and/or magnitude of events increased towards a depositional low (i.e., channel axis), causing the preferred preservation of axis-dipping scour walls in cross section, but not longitudinal, paleoflow-parallel sections.

### *Facies Association 7 (FA7) – Sandstones, Conglomerates, and Debrites with Incisional Bases*

**Description.---** FA7 comprises rippled (Lf4a), cross-stratified (Lf4c), parallel-laminated (Lf5), structureless (graded and ungraded; Lf6a-b), mudclast-bearing (Lf6c) and bioclastic (Lf9) sandstones, and extraclast and mudclast conglomerates (Lf7a-b), and MTDs (Lf8a-b) (Fig. 6G). MTDs in FA7 are sometimes stacked (Fig. 8). They mostly occur as < 1-m-thick debrites of variable composition, with a silt- and clay-rich matrix containing a combination of: (i) sandstone (< 40 cm long axis) and local heterolithic (< 1 m long axis) blocks; (ii) bioclasts (< 1.5 cm long axis); (iii) extraclasts (< 3 cm long axis, typically comprising lithic fragments and clasts of rounded carbonate). In distinguishing debrites within FA7 from those comprising FA8, their architectural context is used: debrites in package-bounding confining surfaces (such as channel walls; cf. DE3 and DE4; see "depositional elements") are classified as FA7 deposits (Fig. 9).

FA7 displays internal erosion, with bed bases of each lithofacies incising into one another. Bed thicknesses increase towards the maximum depth of the bounding erosional surface (Fig. 9). In longitudinal, paleoflow-parallel sections, some erosional bed bases are asymmetric, steeper upflow (maximum dip ~ 40˚) than downflow (maximum dip ~ 20˚). These surfaces can contain a higher concentration of imbricated mudclasts against the steep side, dipping down-flow; they are interpreted as megaflutes (Elliott, 2000; Kane et al., 2009b). FA7 forms a continuum with amalgamated sandstones (FA6).

**Interpretation.---** Erosional, generally coarse-grained lags and debrites are commonly observed in channel thalwegs (Mayall et al., 2006; Hubbard et al., 2009; Kane et al., 2009a; Bell et al., 2018b). These build incrementally through repeated scouring, bypassing, and deposition from passing, possibly supercritical flows (Froude number > 1, Komar, 1971).

### *Facies Association 8 (FA8) – Mass-Transport Deposits (MTDs)*

**Description.---** FA8 is composed solely of MTDs exhibiting debritic (Lf8a) and slumped (Lf8b) textures, found outside of confining surfaces that bound packages (see FA7 for distinction); they are typically > 1 m thick and sometimes stack up to > 22 m thick (Fig. 6H). The composition of the debrites (Lf8a) is highly variable, with blocks or clasts derived from any of the other lithofacies in the system (see Table 1) hosted within a heterolithic matrix. Blocks of conglomerate (Lf7) and bioclastic, polymict sandstone (Lf9) are observed amongst isolated

extraclasts and bioclasts. Deformed, isolated blocks (a few decimeters to meters) of background (FA1), laterally variable (FA2) and laterally continuous (FA3) thin beds are common in FA8. The composition of Lf8b is almost exclusively fine-grained heterolithic, thin-bedded deposits.

Basal contacts of FA8 packages can incise up to 3 m into underlying deposits, and are sometimes manifested as broad erosional surfaces (Fig. 9) with the MTD thickening towards the maximum incision depth, or as steep (up to 90˚ in some cases) walled scours (Fig. 6H). The tops of FA8 packages are commonly eroded and filled by FA2, FA4, FA6, and FA7 (Fig. 9).

**Interpretation.---** The formative flow type and the resultant depositional character of an MTD depends mainly on the composition (mainly its clay content) and degree of disaggregation (controlled principally by its transport history; Moscardelli and Wood, 2008; Bull et al., 2009; Ogata et al., 2012). Because the MTDs of FA8 are highly variable in their texture and composition, determining transport distance is problematic. Furthermore, compositional indicators often used to determine source, such as dispersed bioclasts and extraclasts, might all be derived from their feeding lithologies or have been incorporated through basal substrate erosion. Isolated extraclasts and bioclasts may have been incorporated from the disaggregation of blocks of Lf7 and Lf8 during transportation.

Arbués et al. (2007a, 2007b) attributed the < 20 m thick, stacked MTDs at Los Molinos Road to failures on a structurally controlled, laterally confining slope. Mutti (1985) and Dakin et al. (2013), however, recognize longitudinally emplaced MTDs in the Aínsa channel systems. The data presented herein do not allow conclusive determination of whether the thick (> 1 m) MTDs of FA8 (Fig. 9) were derived dominantly from transverse sources, such as growing structures (Arbués et al., 2007a) or the collapse of a confining surface (Hansen et al., 2015), or from more proximal sources such as the head or wall of a feeding canyon (Nelson et al., 2011), the shelf or upper slope (Ortiz-Karpf et al., 2017). Furthermore, an MTD that may appear (based on composition and/or degree of disaggregation) to have been emplaced longitudinally may have been derived from a transverse source in a more proximal location, potentially kilometers upstream. Based on the (slumped) character and composition (all apparently derived from local stratigraphy) of the deposits, a transverse source is favored for the emplacement of the MTDs in FA8.

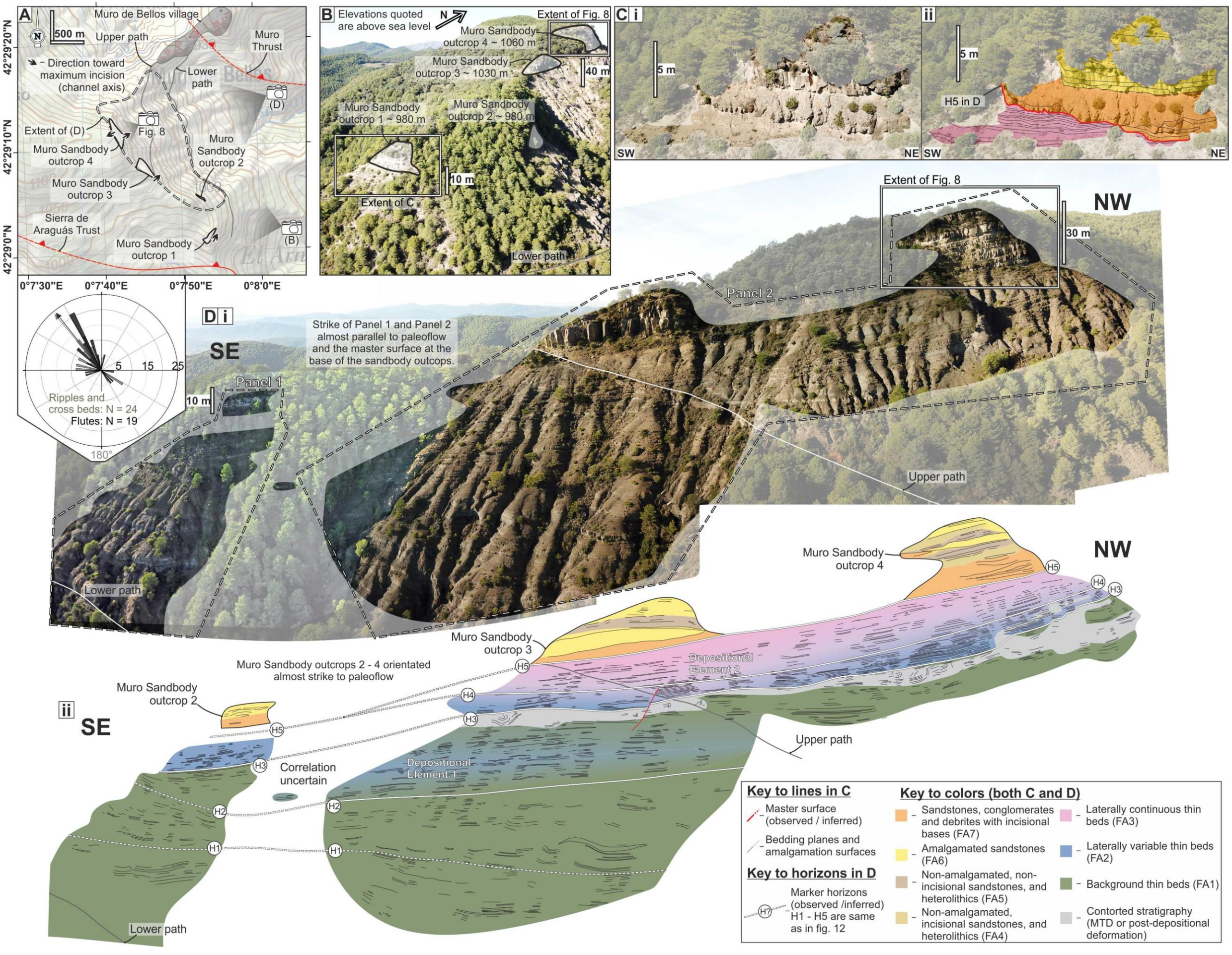


**Figure 7** – Architecture of the Muro de Bellos outcrop. A) Locations of the Muro Sandbody outcrops 1 – 4 and the inferred direction towards their axes, the Muro and Sierra de Araguás thrusts, panels 1 and 2 in part D, and a rose diagram showing all paleocurrents collected from the outcrop (channelized and non-channelized stratigraphy combined). B) Drone photograph from the east showing the relationship between sandbody outcrops 1 – 4 and their respective elevations; C) Raw (i) and interpreted (ii) photograph of Muro Sandbody outcrop 1. Di) Photomosaic showing the location of panels 1 and 2. Dii) Interpretation of the photopanel shown above (panel numbers and marker horizons are the same as in figure 12).

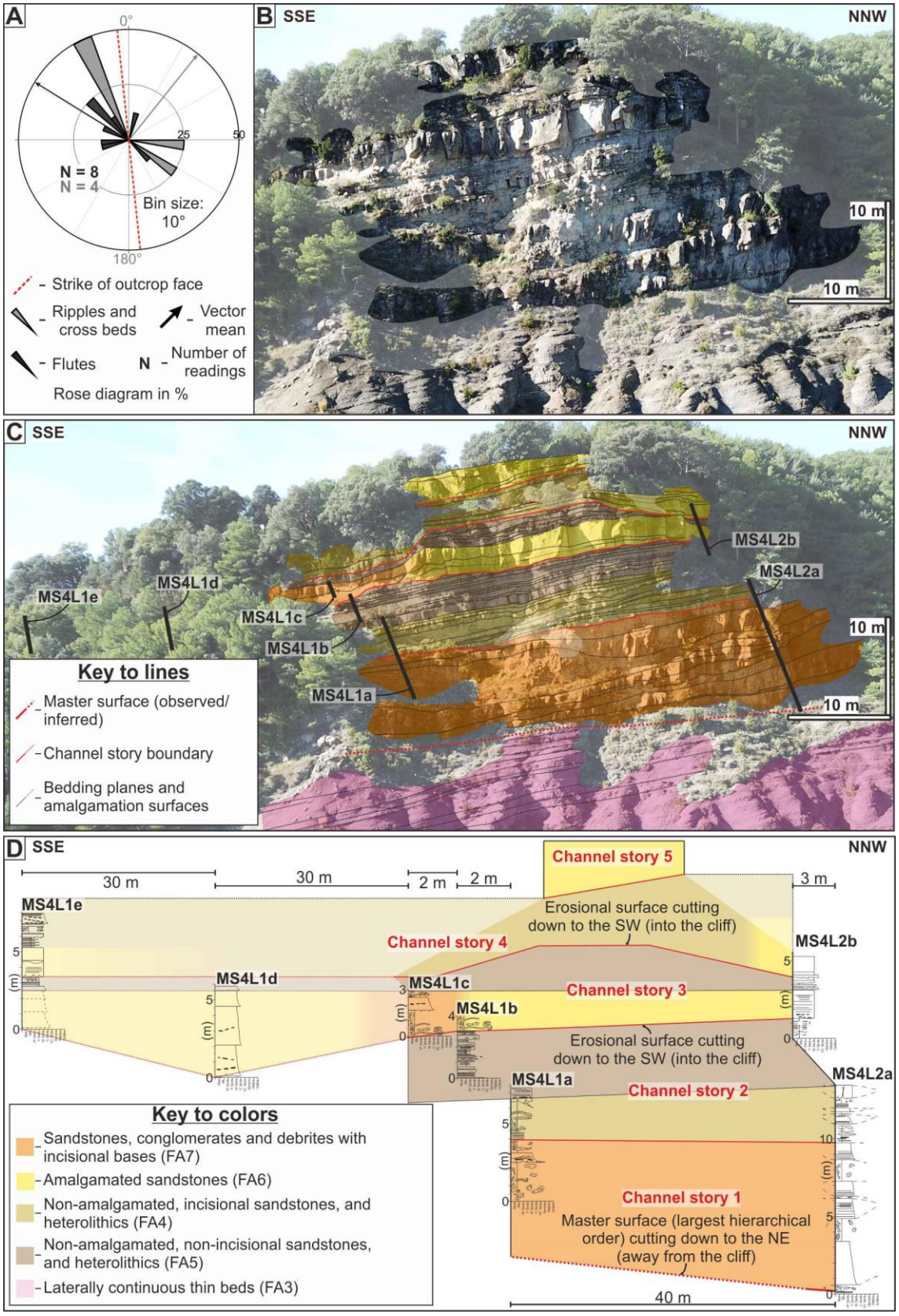


**Figure 8** – A) Rose diagram showing local paleoflow and its relationship with the strike of the outcrop face. B) Drone photograph of the Muro Sandbody outcrop 4. C) Interpretation of photograph in part B, showing bedding planes, facies associations, and log locations. D) Correlation panel built from the logs in part C.

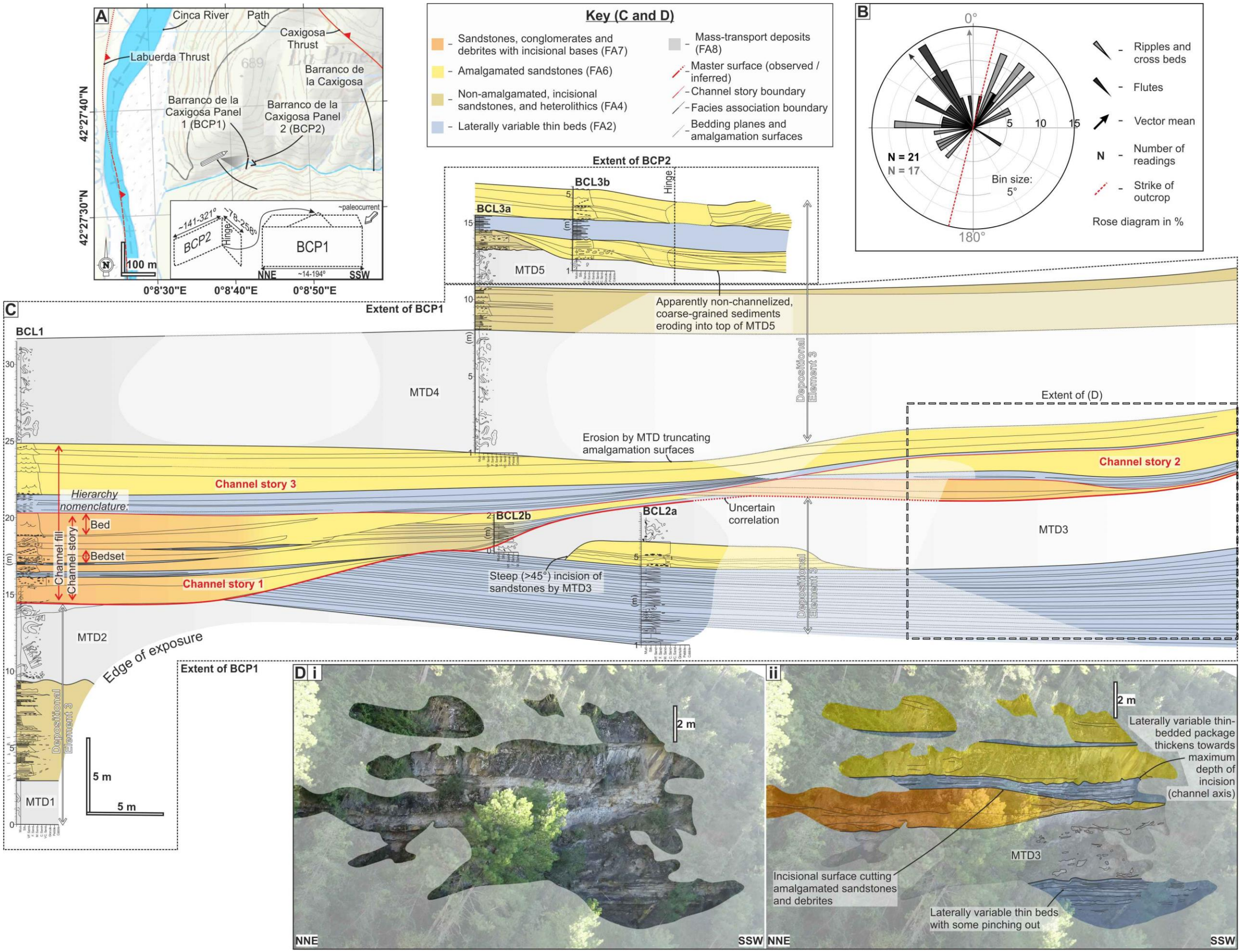


**Figure 9** – Architecture of the Barranco de la Caxigosa outcrop: A) Summary map showing the locations and orientations of the panels in part C, and the Labuerda and Caxigosa thrusts. B) Rose diagram showing local paleoflow and its relationship with the strike of panel BCP1. C) Correlation panel built from logs and interpreted photographs, such as in part D, showing bedding planes, facies associations, and channel stories. D) Raw (i) and interpreted (ii) photograph forming the basis for the correlation in the WSW of panel BCP1.

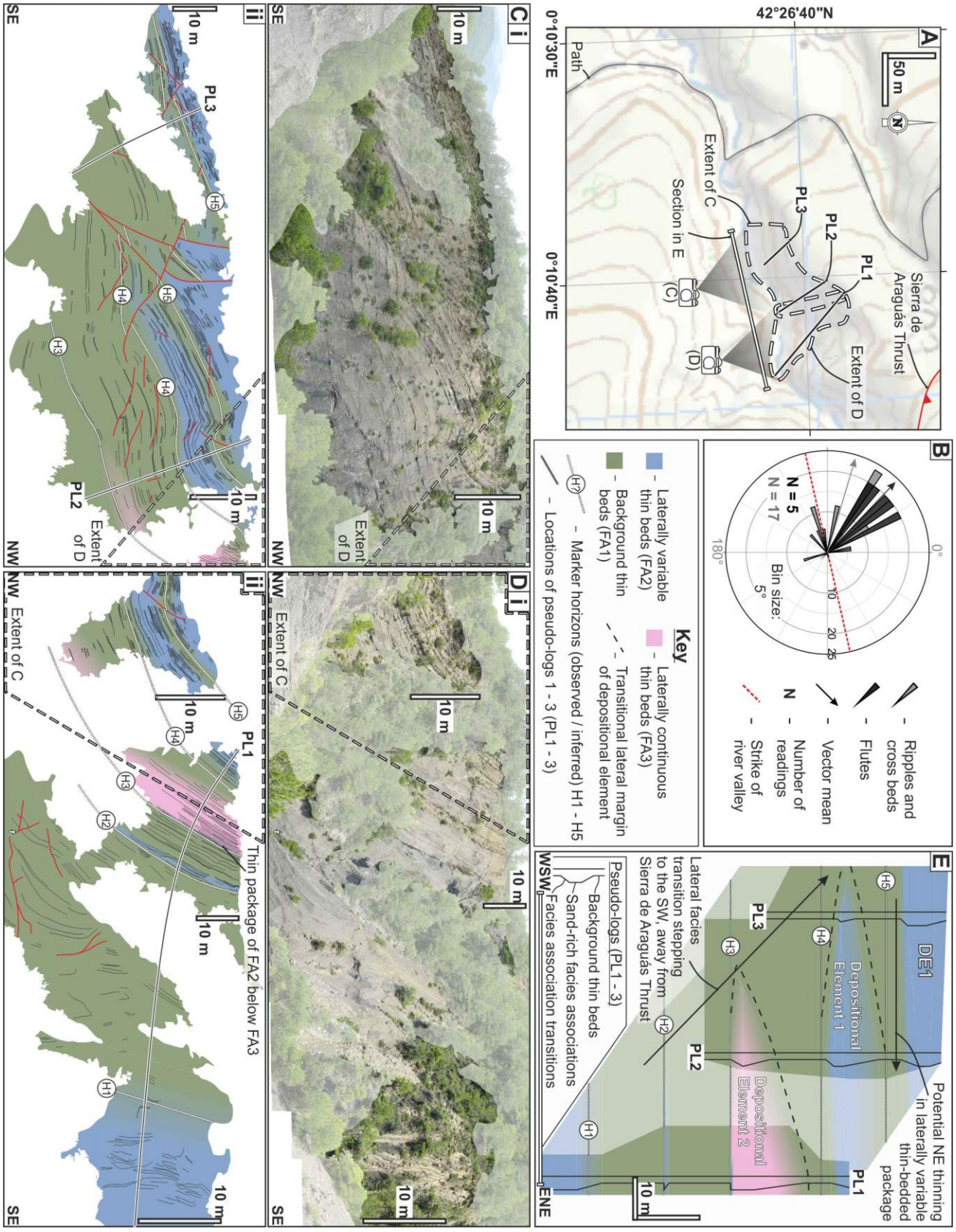


**Figure 10** – Architecture of the Sierra de Soto Gully outcrop: A) Summary map showing the extent of the panels in parts C and D, and the locations of the pseudo-logs in part E and Sierra de Araguás Thrust. B) Rose diagram showing local paleoflow and its relationship with the strike of the gully. C) Photomosaic (i) and

interpreted line drawing (ii) of the western outcrop panel. D) Photomosaic (i) and interpreted line drawing (ii) of the eastern outcrop panel. E) Correlation panel showing DE1 and DE2, and their constituent vertical and lateral facies association transitions, built from pseudo-logs created using outcrop panel interpretations supported by measured log data.

## DEPOSITIONAL ELEMENTS

Classification of depositional elements is useful in systems where facies associations are not unique to a single depositional environment. The following depositional elements are derived from groups of facies associations on the basis of systematically recurring vertical or lateral interrelationships, or of relationships with key bounding surfaces.

### *Depositional Element 1 (DE1) – Weakly Confined, Increasing-to-Decreasing-Energy Deposits*

**Observations.---** The base, top, and lateral edges of DE1 (best observed in Sierra de Soto Gully; between H4 and H5 in Fig. 10) are transitional. Within its basal transition, background thin beds (FA1) grade into laterally variable thin beds (FA2) over 1-4 m. At its top, FA2 grades into FA1 over 2-6 m. Laterally, FA2 transitions into FA1 over tens of meters away from the depositional locus (the location of maximum net sandstone thickness and average sandstone bed thickness). Lateral transitions show a gradual upward increase, followed by a subsequent decrease, in the extent of sandstone beds. While in some outcrops both lateral margins are observed, in most well exposed locations only one margin is preserved. The longitudinal expression of DE1 is poorly constrained, but it is assumed to be elongate in a down-flow orientation. Constituent sandstone beds exhibit all bed geometries recognized in FA2: flat, lightly incisional, or concave-up but non-erosional bases; flat or mounded tops. No common lateral thickening trend is recognized in the sandstone beds, but their average thickness increases towards the depositional locus. From tracing FA2 packages laterally, aggradation in the depositional locus appears to be comparable to that of the margins and surrounding FA1 deposits. Non-amalgamated, incisional sandstones, and heterolithics (FA4) are sometimes present within the depositional locus, transitioning laterally and vertically into FA2.

In Sierra de Soto Gully (Fig. 10), the lateral transition from FA2 to FA1 migrates towards the WSW, away from the Sierra de Araguás thrust; paleoflow directions based on the ripples and cross beds therein also show a western deflection, relative to the flute casts (Fig. 10B). At Muro de Bellos, the same lateral facies transition occurs towards the Muro and Sierra de Araguás Thrusts, which laterally bound the stratigraphy (Fig. 7).

**Interpretation.---** No master confining surface bounds DE1 at the outcrop scale, so the velocity maxima of the formative flows of constituent FA2 deposits were effectively unconfined. However, the constituent sandstones are thinner, laterally more variable, and less amalgamated than those typical of unconfined, sand-rich deposits (cf. Remacha et al., 2005; Liu et al., 2018; Fryer and Jobe, 2019); evidence for compensation is also lacking. The pinching and swelling geometries and bypassing nature of constituent sandstone beds, and the lack of amalgamation and compensation, suggests these are unlike classical "lobes" (Mutti et al., 1994; Prélat et al., 2010). Facies and bed geometries in FA2 deposits show evidence for tractional reworking and scouring (Fig. 6B). However, coarse-grained lag deposits and mud-draped scours indicative of bypassing, high-concentration flows (Barton et al., 2010; Alpak et al., 2013; Stevenson et al., 2015) are largely absent. Therefore, FA2 deposits in DE1 represent low-concentration, generally fine-grained but dominantly bypassing flow deposits.

Observed vertical transitions within DE1 represent increasing and subsequently decreasing flow energy. This motif arises in response to variations in local sediment delivery (Fig. 11), due either to an upstream levee crevasse (formed from a failed avulsion), or driven by basinal supply (Lowe et al., 2019). The relationship with structures suggest that the depositional axes of DE1 coincided with the deepest part of elongate topographic lows, which also controlled the location of lateral facies transitions. Movement (dominantly forward propagation) of fairway-bounding structures is inferred to be responsible for the lateral shifts in the depositional axis and subtle lateral facies association transitions as seen in Sierra de Soto Gully (Fig. 10). Lateral facies transitions are associated with increasing local sand input, as the high-velocity sand-rich part of flows was able to spread over a wider area, whilst still contained within the fairway (Fig. 11b).

Increases in velocity on steep axial gradients may allow a weak flow to exceed its bypass threshold, causing it to erode or bypass, and leaving a thin deposit or no deposit (Stevenson et al., 2015; Dorrell et al., 2018). Elongate sediment pathways provide subtle lateral confinement, which may also cause flow velocity to increase (Fig. 1). At the bases of these weakly confined flows, substrate topography (meters to tens of meters in wavelength)

generated by previous flows, sediment loading or small structures cause localized velocity variability (Eggenhuisen et al., 2010; Dorrell et al., 2019), which leads to the formation of tractional bedforms and scours (Fig. 11). Modern canyons (Paull et al., 2018) and fjord-head delta slopes (Hughes Clarke, 2016) also experience broad lateral confinement (a few kilometers across). Turbidity currents monitored in such settings commonly die out only kilometers from the source (e.g., Paull et al., 2018). DE1 may provide an ancient analog for these weak flows.

### *Depositional Element 2 (DE2) – Progradational, Weakly Confined to Overbank Deposits*

**Observations.---** DE2 is observed in Muro de Bellos (Fig. 7) and Sierra de Soto Gully (Fig. 10). Similarly to the increasing-to-decreasing-energy deposits of DE1, there is a basal vertical transition from background thin beds (FA1) into laterally variable thin beds (FA2) over 1-4 m; the same lateral transition as in DE1 (from FA2 to FA1 over tens of meters away from the depositional locus) is also observed (Fig. 11). Above this, another transition is observed, with a gradual upward decrease in pinching and swelling of beds (of FA2), and a proportional increase in laterally continuous thin beds (FA3). The boundary between the two is arbitrary; however, the FA3 part tends to be thicker (> 20 m) than the FA2 part (> 10 m). FA3 deposits grade vertically into FA1 at the top of DE2. Constituent FA3 deposits can span a wider depositional area than the underlying FA2, leading to some vertical sections showing FA3 grading to FA1 above and below, with an apparently sharp base (see PL1 and PL2, Fig. 10). In Muro de Bellos panel 2 (Fig. 7), DE2 is mostly underlain by a zone of contorted stratigraphy containing folds of meters to tens of meters in wavelength, faults with up to 2 m displacement, and blocks measuring up to several meters. This deformed stratigraphy appears to be composed of, and contained within, FA1 deposits, but locally ramps up and down through the stratigraphy.

**Interpretation.---** DE2 is interpreted to represent the transition from weakly confined deposits (FA2), into overbank deposits (FA3), possibly lateral to the position where a nearby channel was forming (Fig. 11); this is comparable to the transition zone from levee to lobe fringe (Normark et al., 1979; Kane and Hodgson, 2011). With locally increasing sediment delivery, weakly confined deposits will prograde; once flow magnitude in the depositional axis crosses the erosional threshold, a channelization feedback may be initiated (Eggenhuisen et al., 2011; De Leeuw et al., 2016) (Fig. 1B). Accordingly, greater proportions of successive flows will become laterally confined, meaning that progressively lower-energy, finer-grained, and better-sorted flows will deposit

on the margins (Fig. 11). The progressive nature of this process is reflected in the transitional nature of the contact between FA2 and FA3. DE1 and DE2 represent end members of a continuum controlled by channel development. It is unclear whether the disturbed interval beneath DE2 in Muro de Bellos was emplaced as a large MTD, or is a postdepositional product of tectonically or gravitationally driven deformation (Fig. 12). If the former is true, the contorted zone may have influenced progradation and channel inception. However, due to the fact that this contorted zone is not constrained to a stratigraphic interval and ramps into overlying stratigraphy, the deformation is likely postdepositional.

### *Depositional Element 3 (DE3) – Alternating MTDs and Turbidites*

**Observations.---** DE3 comprises packages (1-8 m thick) of turbiditic facies associations (background (FA1) or laterally variable (FA2) thin beds, or non-amalgamated, incisional sandstones, and heterolithics (FA4) between stacked or single MTDs (FA8) (< 20 m)). It is best observed in Barranco de la Caxigosa, where five MTDs (MTD1-MTD5; Fig. 9) are interbedded with ~ 3–10-m-thick, dominantly turbiditic, packages, one of which (between MTD3 and MTD4) is obviously channelized and is not included within DE3 (see DE4). Any of the turbidite packages (FA1, FA2 or FA4), which exist in a continuum with each other, can overlie and underlie sharp basal and top contacts with MTDs of FA8. Lateral transitions exist between FA1 and FA2, and between FA2 and FA4. Where lateral transitions are visible, the higher-energy facies associations overlie the deepest part of the basal contact (MTD top), transitioning laterally into thinner, lower-energy packages. The contacts with the overlying MTDs are commonly erosional. Exposure of MTDs in the Arro system is insufficient to trace their full extent. Millington and Clark (1995a, 1995b) and Arbués et al. (2007a, 2007b) describe DE3 at Los Molinos Road, where the turbidite-prone intervals dominantly thin towards the NE, with one notable exception thinning to the SW.

**Interpretation.---** The nature of DE3 is interpreted to be controlled by the interplay between an underlying MTD and the magnitude, concentration, and grain size of overpassing turbidity currents. The response of turbidity currents to this MTD-top topography is recorded in the overlying turbidite deposits. Depositional lows present on the top of MTDs, or left behind by erosive MTDs, can either generate partial ponding or provide lateral confinement which may enhance channelization (Fig. 11; Schultz et al., 2005; Bull et al., 2009; Hansen et al., 2013; Kneller et al., 2016; Ward et al., 2018). The reason turbidite packages in DE3 may not have crossed

a channelization threshold and formed DE4 may be that the lateral confinement or axial gradient provided by the underlying MTD were insufficient, or the emplacement of a subsequent MTD may have interrupted the process and reset the basin-floor topography (Fig. 11). The interplay of the aforementioned factors means that DE3 can form a continuum with increasing-to-decreasing-energy deposits (DE1), progradational-to-overbank deposits (DE2) and channels (DE4).

Arbués et al. (2007a, 2007b) interpreted deposits of this type at Los Molinos Road as the lateral expression of non-exposed channel bodies to the SW of the outcrop. Therein, FA2 deposits (their "TS" facies association) are interpreted as marginal deposits associated with channel bodies, which are formed in response to the emplacement of MTDs. Definitive distinction of the aforementioned interpretations is not possible based on field data due to limited outcrop exposure in both Los Molinos Road and Barranco de la Caxigosa. However, it is likely that a continuum exists between DE3 and DE4, whereby the early stages of channelization in locations prone to MTD emplacement are similar to those responsible for the deposition of the turbiditic intervals in DE3.

### *Depositional Element 4 (DE4) – Channels*

DE4 comprises sandbodies which are characterized by nested erosional surfaces (see below) and that contain non-amalgamated, incisional sandstones, and heterolithics (FA4), non-amalgamated, non-incisional sandstones, and heterolithics (FA5), amalgamated sandstones (FA6), and sandstones, conglomerates, and debrites with incisional bases (FA7).

Four sandbody exposures crop out at the Muro de Bellos location (Muro Sandbody outcrops 1 – 4; Fig. 7) above a thick (> 150 m) succession of predominantly background thin beds (FA1), but with laterally variable (FA2) and laterally continuous (FA3) thin beds in the upper ~ 30 m (Fig. 7D). While all four outcrops contain DE4 elements, sandbody outcrop 4 exhibits the greatest exposure, therefore allowing the most detailed analysis (Fig. 8). In the Barranco de la Caxigosa outcrop (described above), one of the five turbidite packages (up to 11 m thick) contains FA2, FA4, FA6, and FA7 (Fig. 9) and multiple nested erosional surfaces; this package is therefore classed as DE4.

Because of their characteristic nested erosional surfaces and sandy fill, DE4 deposits are interpreted as the fill of submarine channels. Further description and discussion of these deposits is presented below.

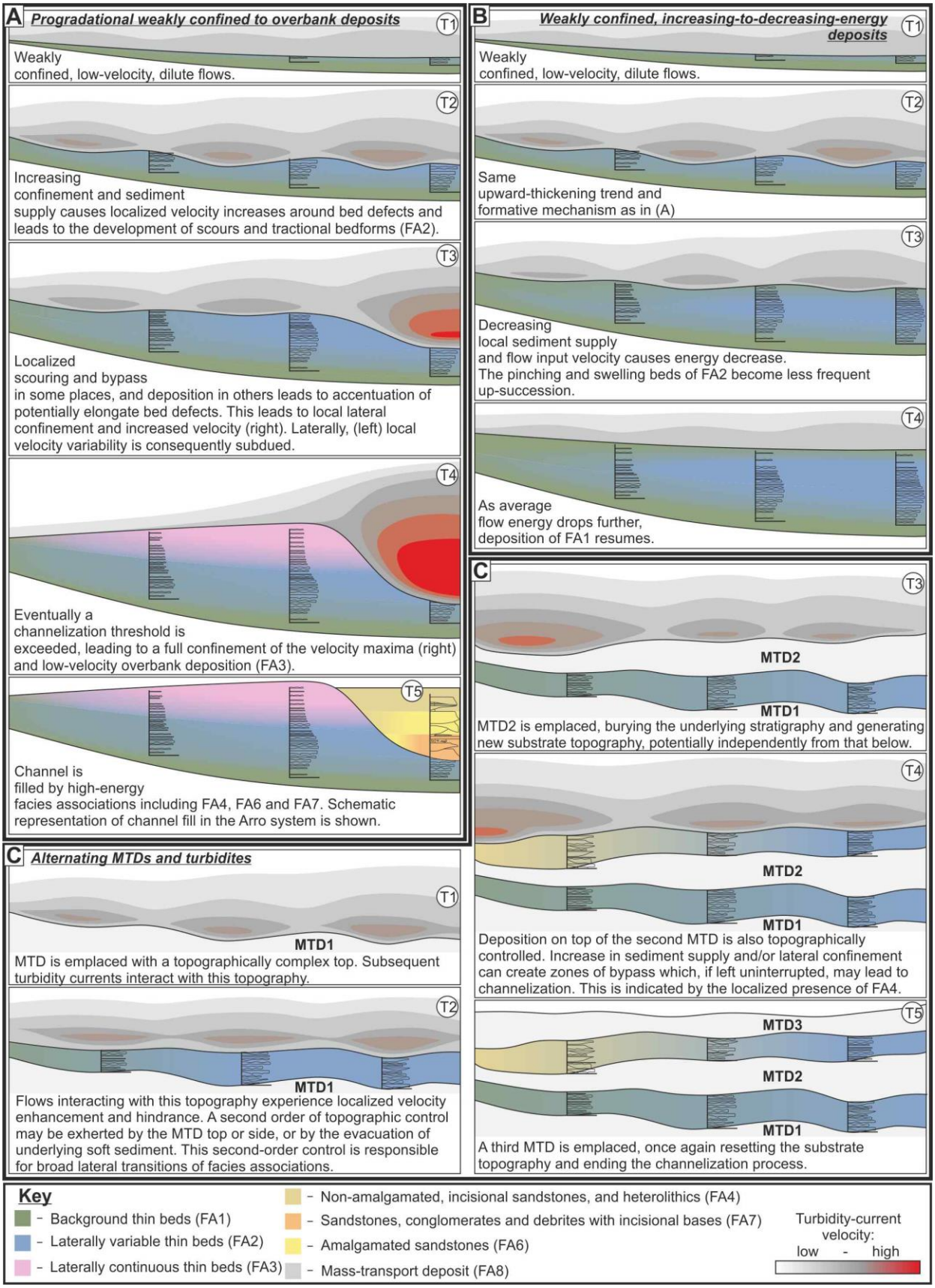


**Figure 11** – Schematic diagrams showing the interpreted formation and evolution of depositional elements 1 – 4: A) DE1; B) DE2 and DE4; C) DE3.

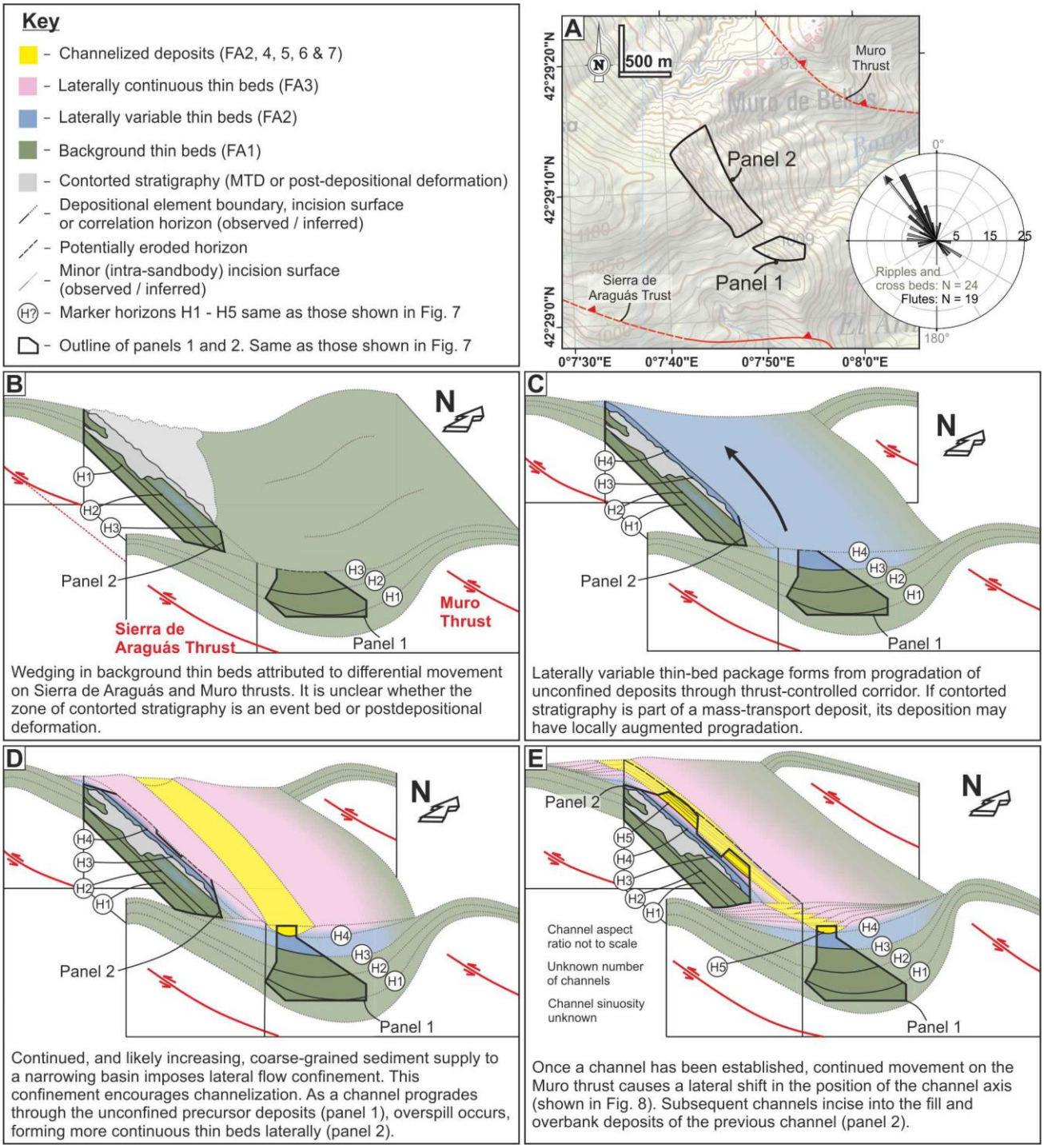


**Figure 12** – A) Map showing the locations of panels 1 and 2, the Sierra de Araguas and Muro thrusts, and local paleocurrent (rose diagram same as in Fig. 7A); B – E) sketch diagrams showing the evolution of the channels in Muro de Bellos through four time steps. Interpreted panels 1 and 2 presented in Fig. 7 have been used to inform the interpretation and are displayed herein.

**Key Surfaces and Hierarchy.---** Channelized deposits are hosted within concave-up surfaces which may be generated by erosion and/or cogenetic thin-bedded turbidites formed from overspill (Hodgson et al., 2011; Brunt et al., 2013). At least three hierarchical orders of confining surface are observed, which are named according to the hierarchical nomenclature scheme of Sprague et al. (2005; Fig. 9). These orders are distinguished based on scale and the recognition of nested surfaces starting at the smallest: bed bases. While key surfaces are used to define each hierarchical order, in areas where bed truncation is not apparent, these surfaces are picked out by major changes in facies associations:

(1) Bed / bedset surfaces (< 3 m deep) with scour-like geometries are observed in paleoflow-parallel and -perpendicular sections (Figs. 8, 9); in sections subparallel to flow (SE-NW; e.g., location 18, Fig. 2) megaflutes can be observed. Scours were cut by the erosive part of an unsteady flow (Kneller, 1995), or by wholly erosive or bypassing flows. They were filled by the depositional part of the scour-forming flow, or by a subsequent depositional flow (e.g., Kane et al., 2009b; Stevenson et al., 2015; Bell et al., 2018a). The process of cut and fill builds stratigraphy incrementally in deep-water channels.

(2) Channel story surfaces (3-10 m deep at axis) are concave-up and elongate (in the direction of local paleoflow), and are best observed at Barranco de la Caxigosa (Fig. 9). These cut through bed and/or bedset fills and exist within larger channel fill surfaces (below). Ranges for the typical depth of incision of bedsets and channel stories overlap, such that these two scales can be difficult to distinguish (Sprague et al., 2005; Cullis et al., 2018). However, at least three channel stories are identified at Barranco de la Caxigosa (Fig. 9), and at least five in Muro Sandbody outcrop 4 (Fig. 8). Sprague et al. (2005) quote typical channel story thicknesses of 3-5 m, meaning that scale overlap with channel fills (10-30 m) is unlikely. However, the basal 10 m of Muro Sandbody outcrop 4 is interpreted to belong to a single channel story. In axial sections, distinguishing bed- or bedset-scale amalgamation within a story from a story bounding surface is difficult. Therefore it is possible that, within this package, more stories are hidden due to the cliff striking at a low angle to local paleoflow, or that an overlap may exist between the channel story scale and the channel fill scale.

(3) Channel-fill surfaces (10-50 m deep at axis). At Barranco de la Caxigosa, vertically and laterally stacked channel stories are confined at both margins by a master basal concave-up surface, and collectively

constitute the channel fill. At Muro de Bellos, the master confining surface may simply be a compound surface resulting from vertical and lateral amalgamation of the bases of channel stories towards the SW. In both cases this master surface also acts as the confining surface to channel stories (Figs. 12, 13).

**Vertical and Lateral Facies Variability.---** Channel story 1 in Barranco de la Caxigosa (Fig. 9) exhibits a lateral facies transition from high-energy deposits of FA7 towards the "axis", through lower-energy "off-axis" deposits of FA4 and FA6, to fine-grained, laterally variable thin-bedded FA2 deposits at its "margin" (*sensu* McHargue et al., 2011; Hubbard et al., 2014). Sandstone beds of marginal FA2 deposits thin towards (and sometimes onlap onto) their confining surface; towards the axis they thicken or are truncated by the incisional bases of overlying beds. The channel margin thin beds in Barranco de la Caxigosa represent the interplay between (i) marginal deposits of dominantly bypassing flows that did not deposit along the paleo-thalweg, (ii) the marginal expression of fully depositional flows which thickened towards the channel axis, where some were subsequently eroded, (iii) deposits left by the tails of bypassing flows, and hosted within scours, and (iv) fine-grained drapes which formed during quiescent periods. Lenses of FA2, independent of the aforementioned margin deposits, exist within the axial fill. These overlie bedset- and channel-story-scale surfaces; they are thickest in the deepest point of the surface and pinch out towards the margin (Fig. 9). Constituent sandstone beds thicken towards the axis of the lens, with thickness variations due to incision at their base. These lenses may represent bypass drapes (Barton et al., 2010; Alpak et al., 2013; Stevenson et al., 2015), whereby sediment from the tail of a dominantly bypassing flow filled topography generated by the flow itself or by a precursor flow. At the base of channel story 1, a single rippled sandstone likely represents reworking during a relatively short bypassing stage, after channel incision (Fig. 9). The bases of channel stories 2 and 3 are overlain by thick (> 1.5 m) bypass drapes that thicken towards the maximum depth of the confining surfaces, partially healing them. These are overlain by amalgamated sandstones (FA6), which are thickest in the axis of the confining surface and gradually thin away from it. Unlike in channel story 1, lateral transitions into marginal FA2 or axial FA7 deposits are not observed; transitions between axis and margin are accommodated by thinning of FA6 deposits and bypass drapes (Fig. 9). The infill of all stories in Barranco de la Caxigosa exhibit vertical trends associated with an upward decrease of energy. In story 1 this is represented by an upward decrease in debritic and conglomeratic facies. In stories 2 and 3 it is marked by the basal bypass drape and gradual fining-up of the

overlying amalgamated sandstones (Fig. 9). In the margin of story 1, however, coarsening- and thickening-up is observed as beds and bedsets become progressively wider up-succession (Fig. 9; Hubbard et al., 2014). An apparent upward increase in the interpreted energy of facies at channel story margins may not be reflective of the nature of the flows that filled it. As a concave-up surface is filled, widening of the conduit causes the margin pinch-out of coarse-grained beds to step away from the channel axis, leading to the superposition of thicker beds onto thinner beds.

In Muro Sandbody outcrop 4 (Fig. 8) FA4, FA6, and FA7 are seen transitioning laterally into one another, and are thought to exhibit a similar axial-to-marginal trend as in Barranco de la Caxigosa, except without laterally variable thin beds (FA2). Fining-up patterns of individual channel stories are also more subtle in Muro de Bellos. At their tops, channel stories 2 and 3 contain > 5 m packages of non-amalgamated sandstones (FA5) which are tabular across the outcrop. These overlie a sharp basal transition and are commonly incised by overlying, higher-energy facies associations (FA4, FA6, and FA7). In Muro Sandbody outcrop 4, the presence of FA5 in channel stories 2 and 3 marks a decrease in average flow energy, possibly due to autogenic processes, in response to a partial upstream blockage (potentially from an MTD) or to an upstream avulsion.

At channel-fill scale, an overall upward decrease in energy is inferred in Muro Sandbody outcrop 4. However, in Barranco de la Caxigosa, vertical facies trends are complex, as they are influenced by the stacking of the constituent channel stories.

**Architecture and Migration Patterns.---** The exposures at Muro de Bellos all strike at a low angle to local paleoflow, making the architecture of the constituent channel stories difficult to ascertain. Therefore, extrapolation of architectures in the Muro de Bellos outcrop has been attempted using geometric relationships between confining surfaces and underlying stratigraphy, and assuming that channel stories exhibit similar axis-to-margin facies-association transitions as in Barranco de la Caxigosa (Fig. 9). Muro Sandbody outcrops 1 and 2 are along strike, at similar elevations (~ 980 m) and can be connected along paleoflow. The master confining surfaces beneath outcrop 1 (Fig. 7C), outcrop 3, and outcrop 4 (Fig. 8) truncate progressively older underlying thin beds towards the NE (Fig. 7A). Muro Sandbody outcrop 3, which comprises dominantly axial FA7 and off-axis FA6 deposits, is laterally (perpendicularly to paleoflow) offset ~ 200 m and vertically offset ~ 50 m (not restored for local tilt of ~ 11 - 16˚) from outcrop 2, which contains axial FA7 deposits. Muro Sandbody outcrop

4 is ~ 50 m laterally (perpendicular to paleoflow) and ~ 30 m vertically offset from sandbody outcrop 3. In sandbody outcrop 4, four incision surfaces are observed, two of which cut progressively older underlying beds to the SW (into the cliff), the direction opposite to the incision at the base of the outcrop (NE); the cutting direction of the other two surfaces is not obvious (Fig. 8). While a general vertical decrease in the energy of the facies associations in Muro Sandbody outcrop 4 (Fig. 8) is interpreted, the base of channel stories 3 and 5 comprise dominantly off-axis FA6 deposits, interpreted as higher energy than the FA4 deposits that constitute the basal part of their underlying channel stories (2 and 4 respectively). This variability may reflect changes in the overall energy of the fill of successive channel stories, or variability of channel story stacking, superimposing more axial onto more marginal facies associations.

McHargue et al. (2011) define two contrasting styles of stacking observed (in plan view) at channel-fill scale (therein "channel elements"): (i) disorganized, whereby successive channels do not resemble each other; (ii) organized, where successive channels modify the course of the previous element. Herein, we apply this terminology to describe the stacking of channel stories. We interpret that the channel stories in Muro Sandbody outcrops 1– 4 stacked vertically and laterally to the southwest, generally in an organized manner (Fig. 12), based principally on the vertical and lateral offset of axial FA7 deposits between outcrops 2, 3, and 4, and the vertical change from the NE truncation of older underlying stratigraphy to SW truncation in outcrop 4. However, the superposition of channel stories containing high-energy FA6 deposits (stories 3 and 5) onto those containing lower-energy FA4 deposits (stories 2 and 5; Fig. 8) suggests that local variability may exist.

Compounded erosion of these channel stories may create a through-going surface on their southwestern side (represented by H5; Fig. 7); the architecture on the northeastern margin cannot be constrained (Fig. 12).

In Barranco de la Caxigosa, channel stories 1 and 2 are offset at least 70 m laterally and 6 m stratigraphically. Stories 2 and 3 are laterally offset by ~ 50 m, and the maximum depth of the confining surface of story 3 is ~ 50 cm stratigraphically lower than that of story 2. Although none of the stories is fully exposed, story 1 appears to have a lower aspect ratio than story 3. The master bounding surface, containing the channel fill, displays a concave-up geometry which then abruptly flattens to the SSW; the concave-up part is ~ 6 m thick. The increase in lateral offset (relative to vertical) of channel story axes, and vertical increase in aspect ratio is concomitant with the widening and flattening of the master bounding surface (Fig. 9).

The channel fill at Barranco de la Caxigosa is situated within an erosional bounding surface (Figs. 9, 13), in which the channel stories are stacked in a disorganized or compensational manner. Changes in lateral stacking and aspect ratio were potentially controlled by a widening of the master confining surface: stories 2 and 3, situated above the wider and shallower part of the master confining surface, experienced greater offset and formed channel deposits of higher aspect ratios, likely because their confinement was not dictated by the presence of a steep channel wall.

## DISCUSSION

### *Timing of Structures in the Arro System*

The western deflection of ripples and cross beds (relative to flutes) and westward stepping of the lateral facies transitions in Sierra de Soto Gully (Figs. 4, 10) suggest that the formative flows interacted with growing seafloor topography to the east, likely caused by growth of the Sierra de Araguás thrust. Wedging geometries of the background thin beds (Fig. 7) and the onset of channelization in Muro de Bellos are attributed to movement on the Muro and Sierra de Araguás thrusts (Fig. 12). Previous works suggest that structures in the most proximal outcrops were active at the time of deposition, with the growth of the Los Molinos Thrust as the cause of MTD emplacement at Los Molinos Road (Millington and Clark, 1995a, 1995b; Arbués et al., 2007a, 2007b). It is therefore also possible that the origin of the MTDs in Barranco de la Caxigosa was linked to the activity of the nearby Caxigosa thrust. Furthermore, cross sections through the Aínsa depocenter fill (e.g., Muñoz et al., 2013; Clark et al., 2017) commonly show a thinning of Arro stratigraphy towards the depocenter-bounding thrust-cored anticlines, suggesting that these structures were growing during deposition.

### *Controls on Variability in Channel-Deposit Architecture*

Multiple autogenic and allogenic controls dictate the architecture and facies distribution of deep-water deposits (Clark and Cartwright, 2011). For example, sequence stratigraphy is built on various scales of external forcing (Vail et al., 1977; Gardner et al., 2003; Flint et al., 2011), whereas other studies focus on the stratigraphic response of autogenic processes (Pirmez et al., 2000; McHargue et al., 2011). Furthermore, studies from modern deep-water channel systems (e.g., Vendettuoli et al., 2019) are beginning to reveal the true complexity of seabed deposition. However, although it can be challenging to discern the extent to which individual factors control the

nature of ancient sedimentary successions, it is possible to assess the relative importance of a suite of controls at various hierarchical scales.

At bed to bedset scale, local scouring and filling builds stratigraphy incrementally in a channel. Scours may be filled by their formative flow or by successive flows (Kane et al., 2009b). The preserved deposit of a flow may be present only in the axis or margin of a channel, or across its entirety (Hubbard et al., 2014). Variations in scour depth and fill between individual beds is likely due to random variations in the type and magnitude of individual flows.

Because there may be scale overlap between bedset and channel story surfaces, the relative likelihood of different factors controlling their inception may also vary, rather than being fixed for each level. Both Muro de Bellos and Barranco de la Caxigosa display incision at the bases of their constituent channel stories, and a general upward decrease in the inferred energy of their constituent facies associations (Figs. 8, 9). Therefore, they are interpreted to result from repeated incision and filling of the surfaces that confine them. Repeated "cut and fill" can be attributed to:

- Increases (cut) and subsequent decreases (fill) in average flow magnitude and erosive potential arising from variations in sediment delivery rate and/or caliber enhanced by relative sea-level changes and/or climatic variations (Gardner et al., 2003; Flint et al., 2011).
- Surfaces being generated by erosive flows trying to maintain equilibrium, potentially after an upstream avulsion (Pirmez et al., 2000). In this case fill is initiated by backfilling due to a downstream blockage (Pickering et al., 2001) or a decrease in flow efficiency (Mutti et al., 1999; Hodgson et al., 2011, 2016), or by aggradation of a below grade channel, seeking its equilibrium profile (Pirmez et al., 2000; Kneller, 2003; Prather, 2003).
- The upstream migration of knickpoints (Heiniö and Davies, 2007; Gales et al., 2019) or other bedforms, as seen in modern submarine channels (Hage et al., 2018; Vendettuoli et al., 2019), may produce an erosional surface. Immediately downstream of knickpoints (commonly the location of hydraulic jumps) flow efficiency is reduced, resulting in deposition of higher-energy sediments from flows which would previously have bypassed (Postma and Cartigny, 2014). As channel-floor topography is healed and the knickpoint or bedform migrates farther upstream, flow efficiency is reattained. This may cause a general

upwards decrease in inferred flow energy as the higher-energy parts of flows bypass with increasing efficiency.

- Quasi-instantaneous erosion by a bypassing MTD (Dakin et al., 2013) or an outsized turbidity current may generate the confining surface. The infill is progressive: as the narrowest and deepest part of a concave-up surface (axis) is filled with high-energy facies, the effective conduit size widens. Lateral confinement is relieved, leading to a decrease in efficiency of the next flow, which may form a feedback mechanism, depositing progressively lower-energy facies.

The relative likelihood of these formative mechanisms can be determined based on the architecture of the channel fill more generally. The architectural interpretation of Muro de Bellos is that of partially overbank-confined channel stories, whose southwestern migration is accommodated by small-scale avulsions (Fig. 12). Therefore, their architectural expression is likely due to (structurally derived) changes in lateral confinement and axial gradient. In contrast, the internal architecture of the channel fill at Barranco de la Caxigosa is less well organized; the bounding surface likely resulted from cut and fill. In this scenario, any of the aforementioned mechanisms may have formed its channel stories. However, the Barranco de la Caxigosa outcrop contains multiple MTDs with incisional bases, interbedded with channelized and non-obviously channelized turbidite deposits. Due to the MTD-prone nature of the deposits, it is possible that the confining surfaces of channel stories 2 and 3 were excavated partially or fully by large, erosive MTDs. The surface originally generated by this large flow may have been partially filled by the deposit of the formative MTD, and is likely to have been modified, progressively, by successive flows that shaped its preserved geometry (Fig. 9). Progressive incision alone, however, cannot be ruled out.

The master confining surface of the channel fill at Muro de Bellos is interpreted to represent a compound surface. This did not exist as a basin-floor feature in its entirety at any point, but instead formed by the lateral and vertical migration (stacking) of its channels stories in response to movement on the Muro thrust (Fig. 12). The basal incision at Barranco de la Caxigosa is interpreted to have formed from the cut and fill of a steep-sided conduit, at channel-story hierarchical order. Once this basal story was filled, channel stories formed within a much larger conduit, potentially derived from structural confinement or a lower order channel surface. The evolution away from flow-scale lateral confinement was responsible for the increase in the ratio of horizontal

to vertical stacking and lower-energy facies in stories 2 and 3 (Fig. 13). At the lowest order, an overall increase then decrease in the rate of delivery of coarse-grained sediment to each location is necessary for the inception, fill, and occlusion of these channels.

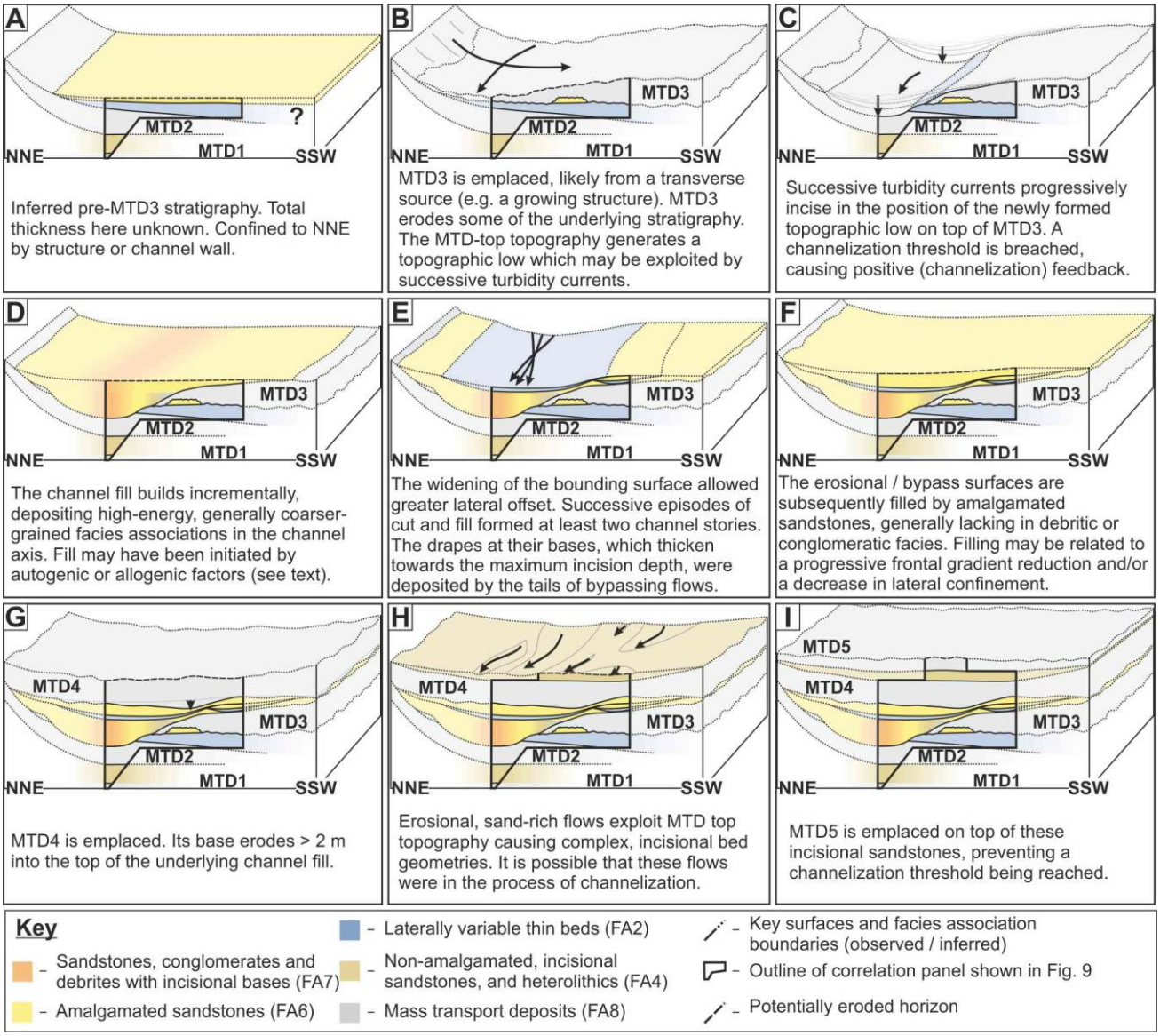


**Figure 13** – Sketch block models showing the evolution of Barranco de la Caxigosa through nine time steps (A – I). Interpretation is informed by panels presented in Fig. 9 and displayed herein.

Observations from outcropping deep-water channel systems such as those in the Laingsburg (Di Celma et al., 2011), Capistrano (Campion et al., 2005) and Tres Pasos (Macauley and Hubbard, 2013) formations has led to the development of predictive models, wherein laterally offset stacking is observed at channel-fill scale, whereas channel stories are assumed to stack vertically with little or no lateral offset (McHargue et al., 2011). In both

Muro de Bellos and Barranco de la Caxigosa, and in other systems of the Aínsa depocenter (Pickering and Cantalejo, 2015), lateral stacking of channel stories is observed. In Barranco de la Caxigosa, disorganized lateral channel-story stacking was driven by the interplay between MTDs and turbidites (Fig. 13); in Muro de Bellos, organized lateral channel-story stacking was driven by thrust-derived shifting of the depositional fairway (Fig. 12). It is possible that, in exceptionally tectonically active and MTD-prone areas like the Aínsa depocenter, the processes which typically affect the lateral stacking of channel fills, such as avulsion, MTDs and tectonic structure, may act at smaller temporal scales. This may result in less predictable channel-story stacking patterns, and may obscure the distinction between channel stories and channel fills, making hierarchy-based comparisons with other systems difficult.

Despite their differences in architecture, vertical sections through the channel fill in Barranco de la Caxigosa and Muro de Bellos (Muro Sandbody outcrop 4) show a similar facies trend: high-energy facies at the base, which gradually decrease upwards, with channel stories providing nested higher-order trends. In Muro de Bellos, this trend arises from the progressive superposition of off-axial deposits on top of axial facies associations. The presence of debritic and conglomeratic material at the base of both Muro Sandbody outcrops 1 and 4 (Fig. 7) suggests that the fill of the successive channel stories was similar. Therefore, observed vertical facies transitions are more likely to reflect the progressive migration of the channel-story axes, than a decrease in input flow energy between successive channel stories (Fig. 12). In Barranco de la Caxigosa, the trend in channel fill is interpreted to be partly due to a marked widening of the master confining surface, leading to a decrease in flow efficiency in the axis. However, this widening allowed subsequent channel stories to stack with greater lateral offset (Fig. 13; Li et al., 2018). Axial deposits of channel stories 2 and 3 were superimposed onto the margin of channel story 1, leading to a local upward increase in inferred flow energy (Figs. 9, 13). The fill of channel story 1 exhibits the same pattern. While a section through the axis of channel story 1 (BCL1 in Fig. 9C) records an upward decrease in inferred flow energy, a section through the margin (in the position of BCL2b in Fig. 9C) records upward bed thickening (Fig. 9). This marginal trend is interpreted to be due to the widening of the depositional fairway as the channel was progressively filled, meaning that the sand-rich part of the flows could deposit over more of the channel floor (Hubbard et al., 2014). The decrease in flow-scale lateral confinement accompanying conduit widening may also have inhibited the bypass potential at the axis of the

channel, causing an autogenic decrease in the inferred energy of channel-axis facies. Therefore, at this scale, vertical facies trends may be more influenced by filling of sea-floor topography rather than records of energy changes. At channel-fill scale (see Fig. 9), one-dimensional facies trends recording an upward decrease in inferred energy may be generated by the vertical and lateral migration of constituent channel stories (Muro de Bellos) (Figs. 7, 8, 12) or by the widening of the master confining surface (Barranco de la Caxigosa) (Figs. 9, 13). Therefore, stacking-pattern analysis is best undertaken at the channel-story scale. However, at channel-story scale, axial facies trends recording upward decreasing flow energies may be associated with marginal facies which record the opposite. Architectural information is therefore required when imposing environmental interpretations onto non-unique facies associations.

### *Influence of MTDs on Channelization and Channel-Deposit Architecture*

Previous studies have focused mainly on the effect of MTDs on established channel forms (e.g., Masalimova et al., 2015; Kremer et al., 2018). Mass-transport deposits can form blockages which may lead to backfilling (Posamentier and Kolla, 2003; Nelson et al., 2009; Bernhardt et al., 2012; Corella et al., 2016) or avulsion (Ortiz-Karpf et al., 2015). Less attention has been given to how MTDs may lead to, or prevent, the formation of channelized flow pathways. In the Arro system, the interplay between sediment supply, axial gradient and lateral confinement may be the principal drivers of channelization at the channel-fill hierarchical scale, whereas MTDs may have a profound influence on the channelization process at the channel-story scale. Five processes are proposed below, to describe the ways MTDs can enhance or hinder channelization (Fig. 14) in elongate confined settings (bounded by a large-scale erosional surface or tectonic structures). Although the origin of the MTDs in the Arro system is unknown, it should be noted that each mechanism can be associated with either longitudinally or transversely emplaced mass-transport deposits. These process may co-occur.

**MTD-Margin Topography.---** Arbués et al. (2007a) propose a model in which relief on the margin of transversely emplaced MTDs provides lateral confinement that is responsible for the formation of channels. A similar model may be invoked in Barranco de la Caxigosa: channel initiation, and formation of the bounding surface for channel story 1 (Fig. 13), likely formed in response to MTD-margin topography (Fig. 14A). In the case of transversely emplaced MTDs, either the margin farthest from the source (e.g., Arbués et al., 2007a) or the near-source margin (e.g., Kremer et al., 2018) can provide this confinement (Fig. 14A). Other studies from

the Austrian Molasse Basin (Bernhardt et al., 2012; Masalimova et al., 2015) show how the lateral edges of longitudinally emplaced MTDs can have the same effect (Fig. 14a). Pickering and Corregidor (2000, 2005) show how the upstream margin of an MTD can frontally confine or reduce the axial gradient of subsequent turbidites, causing a loss of efficiency which may hinder channel development (Fig. 14B).

**MTD-Top Topography.---** The effects of MTD-top and -margin topography are similar. MTDs, particularly large slumps and slides, often exhibit very complex topography on their tops (Armitage et al., 2009; Kneller et al., 2016; Brooks et al., 2018; Ward et al., 2018; Bull et al., 2020). Depressions elongate in the direction of paleoflow provide lateral confinement and are likely to encourage channelization (Fig. 14C). Thickness variations and localized scouring in turbidite deposits that overlie MTDs in Barranco de la Caxigosa (comprising DE3 deposits) are interpreted as the result of interaction with such depressions (Figs. 11, 13). Depressions which have no elongation or are elongate in a paleoflow-perpendicular orientation may provide frontal confinement and therefore hinder channelization (Fig. 14D).

Accentuation or hindrance of channelization can be achieved by either transversely or longitudinally emplaced MTDs. However, the typical distribution and orientation of structures on large MTDs, with secondary ridges striking at a high angle to the emplacement direction (Sharman et al., 2015), means that transversely emplaced MTDs are more likely to encourage channelization, whereas longitudinally emplaced MTDs are likely to hinder it.

**Syndepositional Substrate Deformation and/or Differential Compaction.---** The complexity of the composition of MTDs dictates the spatial distribution of mechanically strong and weak areas. Lithological zones of varying competence and the presence of large mostly undeformed blocks may allow higher compaction rates on top of weak zones (Alves, 2010; Dykstra et al., 2011; Ward et al., 2018). Furthermore, the depositional weakness of mud-rich MTDs may be sufficient for evacuation of substrate material below subsequently deposited turbidites (Kneller et al., 2016). If the initial MTD-top deposits are elongate and aligned with local paleoflow, differential compaction may cause lateral confinement and hence encourage channelization (Fig. 14e). If the deposits and the depression formed by their presence are elongated in a paleoflow-perpendicular orientation or are not elongated, frontal confinement and ponding may arise, inhibiting channel formation (Fig. 14f). Substrate deformation and/or differential compaction is likely responsible for the lateral facies transitions

observed in the turbidite packages which are underlain and overlain by MTDs (DE3) and may have augmented channelization in Barranco de la Caxigosa.

**Megascour Evacuation by Erosive MTDs.---** Dakin et al. (2013) show how longitudinally sourced, erosive-mass-transport deposits in the Upper Hecho Group can create "megascours", which may show cross-sectional profiles similar to submarine channels (see also Moscardelli and Wood, 2008; Brooks et al., 2018 Soutter et al., 2018). The proximal-distal longitudinal section of Dakin et al. (2013) through the Aínsa II fan passes from a fully evacuated elongate megascour on the slope, through a zone filled with chaotic deposits at the base of slope, ending distally in turbidite deposition. These quasi-instantaneously generated pathways can provide sufficient lateral confinement to subsequent turbidity currents for a channelization threshold to be exceeded (Fig. 14g). A similar process has been documented at larger scales, where lateral confinement and a local increase in the axial gradient can be provided by the proximal headwall scar of a large MTD (Qin et al., 2017). The stratigraphic and architectural context of channel stories 2 and 3 in Barranco de la Caxigosa (below erosive MTD4; Fig. 9) suggest that their confining surfaces may have been formed or initiated by mass-transport-derived megascours. These megascours may have been exploited and possibly significantly modified by subsequent bypassing, and potentially erosive, flows, which formed channel-base drapes, and were eventually filled by amalgamated sandstones (Fig. 13E, F). If the axial orientation of the erosional surface is perpendicular to local paleoflow, the downstream wall of the erosional surface may cause a decrease in axial gradient and block, or deviate, successive turbidity currents (Fig. 14H). Commonly, the erosional basal surfaces of MTDs on the lower slope and basin-floor are partially or fully filled by the remnant deposit of their formative flow (e.g. MTD4, Fig. 9; Dakin et al., 2013). The lack of remnant MTD at the base of channel stories 2 and 3 may be because: (i) Barranco de la Caxigosa was sufficiently proximal, or possessed a sufficient axial gradient, for MTDs to have fully evacuated their basal surface (Gomis-Cartesio et al., 2018), (ii) the flows that formed the basal surfaces of channel stories 2 and 3 were abnormally large and were therefore able to erode and bypass for longer distances downstream, or (iii) the remnant MTD has been eroded and replaced by subsequent turbidity currents and their deposits (e.g., Qin et al., 2017).

**Topographic Resetting by MTDs.---** Of the five turbidite packages that separate the MTDs in Barranco de la Caxigosa, only one is obviously channelized. The mechanism invoked to explain the hindrance of

channelization in these nonchannelized intervals (which, together with their associated MTDs, form DE3) is burial by subsequent MTDs. A large depositional MTD may fill the elongate flow pathway, suppressing and effectively resetting the basin-floor topography (Figs. 11C, 14I); the channelization process is thereby halted and must then start again (McArthur and McCaffrey, 2019).

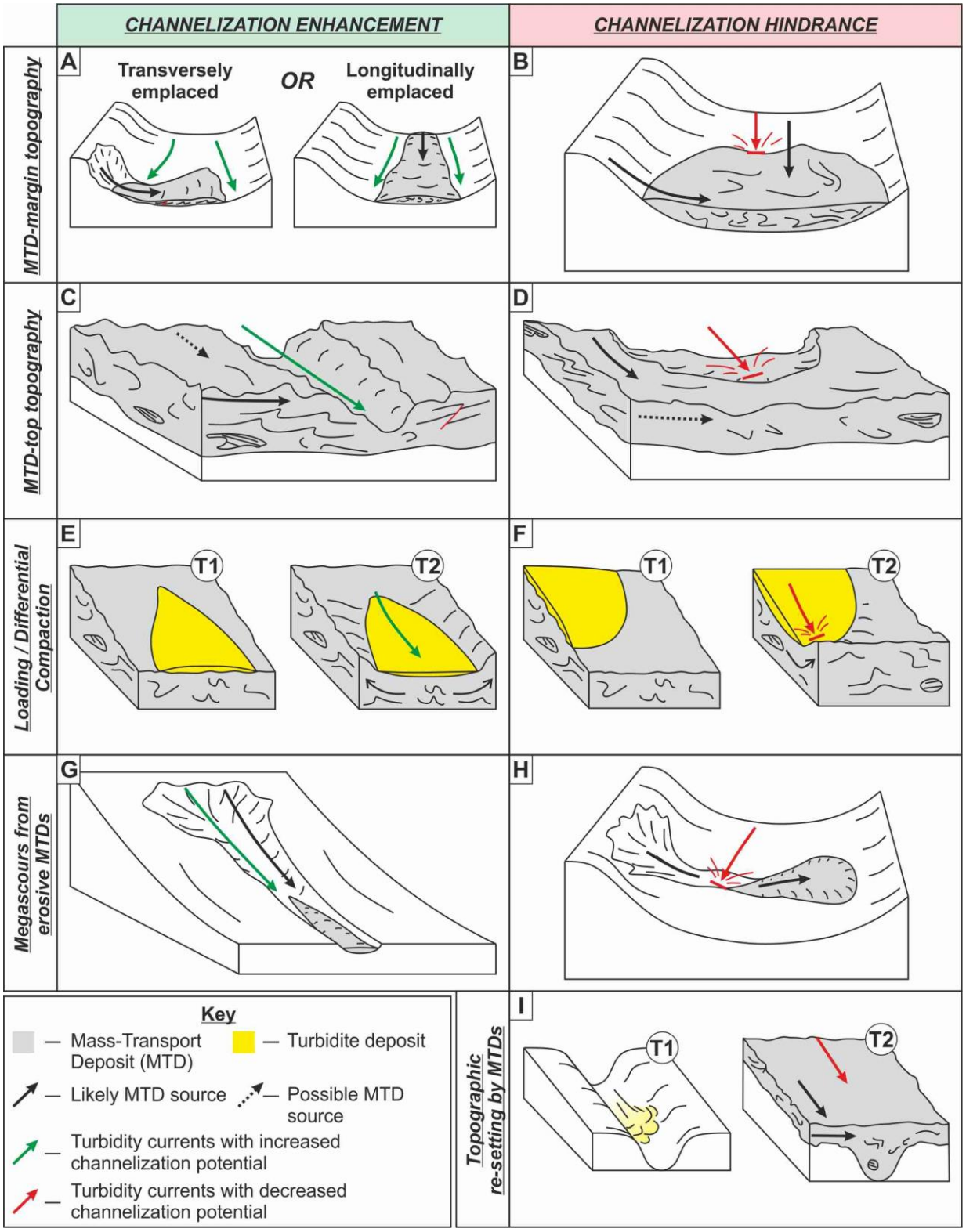

**Figure 14** – Conceptual diagram showing the mechanisms by which MTD emplacement can help (A, C, E, G) or hinder (B, D, F, H, I) channelization: A, B) interaction with MTD-margin topography; C, D) interaction with MTD-top topography; E, F) syndepositional substrate deformation and/or differential compaction; G, H) megascours excavated by erosive MTDs; I) MTDs filling a fully or partially channelized pathway and resetting basin-floor topography.

### *Precursor Deposits and Channel Initiation*

Examples of lobate, unconfined deposits cut by a channel that progrades over them are well documented (e.g., Gardner et al., 2003; Macdonald et al., 2011; Hodgson et al., 2011, 2016). Deposits from the Laingsburg depocenter, Karoo Basin, South Africa, record evidence of channel progradation cutting into unconfined deposits (Hodgson et al., 2011, 2016), and are herein compared with examples from the Arro system (Fig. 15). To first order, for fine-grained background deposits (FA1) to be overlain or incised by coarse-grained channelized deposits requires an increase in local delivery of coarse-grained sediment to the particular outcropping location (not necessarily to the whole basin). Channelization in an unconfined, progradational system will typically be preceded by deposition of lobes (deposited by unconfined flows) followed by progressive channelization, caused by incision and levee construction (Burgreen and Graham, 2014; Hodgson et al., 2016). If assuming time-transgressive flow confinement in submarine channels is the norm, the absence of precursor lobate deposits is enigmatic. Such cases may arise when: (i) a master erosional surface has completely eroded through the axis or the thinner marginal parts of a precursor lobe (more likely where lateral architectural control is limited), (ii) the conduit was formed (and filled) quasi-instantaneously, negating the requisite for frontal lobe development and channel progradation, or (iii) precursor unconfined deposits are absent or are not in the form of classical lobes, potentially because the axial gradient or externally imposed lateral confinement was sufficient to promote bypass.

Muro de Bellos is an example of where lobate precursor deposits are apparently absent. Progradation and channelization are interpreted to have arisen from steadily increasing local delivery of coarse-grained sediment through a corridor confined by the Muro and Sierra de Araguás thrusts, both of which were active at the time of deposition (Fig. 12B). The assumed high axial gradient of the depositional fairway and broad lateral

confinement imposed by these structures is thought to be partially responsible for the bypass-prone nature of the laterally variable thin-bed deposits (FA2) that form part of both increasing-to-decreasing-energy deposits (DE1), and progradational-to-overbank (DE2) deposits. Enhanced velocities related to high axial gradients and lateral confinement likely prevent the formation of thick and continuous lobate deposits (Fig. 12C). Contemporaneous narrowing of this (high gradient) corridor and increasing local delivery of coarse-grained sediment is then thought to have initiated a channelization feedback mechanism and the formation of Muro Sandbody outcrops 1 and 2 (Fig. 12D). Subsequent migration of partially levee-confined channels to the SW arose due to movement of the inboard Muro Thrust (located to the NE) predominating over movement on the outboard Sierra de Arguas thrust (located to the SW) (Fig. 12D). In this example, the lack of well-developed, sand-rich, unconfined precursor deposits is therefore likely due to the elevated bypass potential experienced by the formative flows of turbidites of FA2. By extension, thrust-derived, progressive lateral confinement may have augmented the effects of a high axial gradient in lowering the channelization threshold, allowing channelization to occur earlier, and at lower coarse-grained sediment delivery rates, than in an unconfined setting (Fig. 15). Therefore, less sand is sequestered in the pre-channelization stratigraphy, and more is transported down dip.

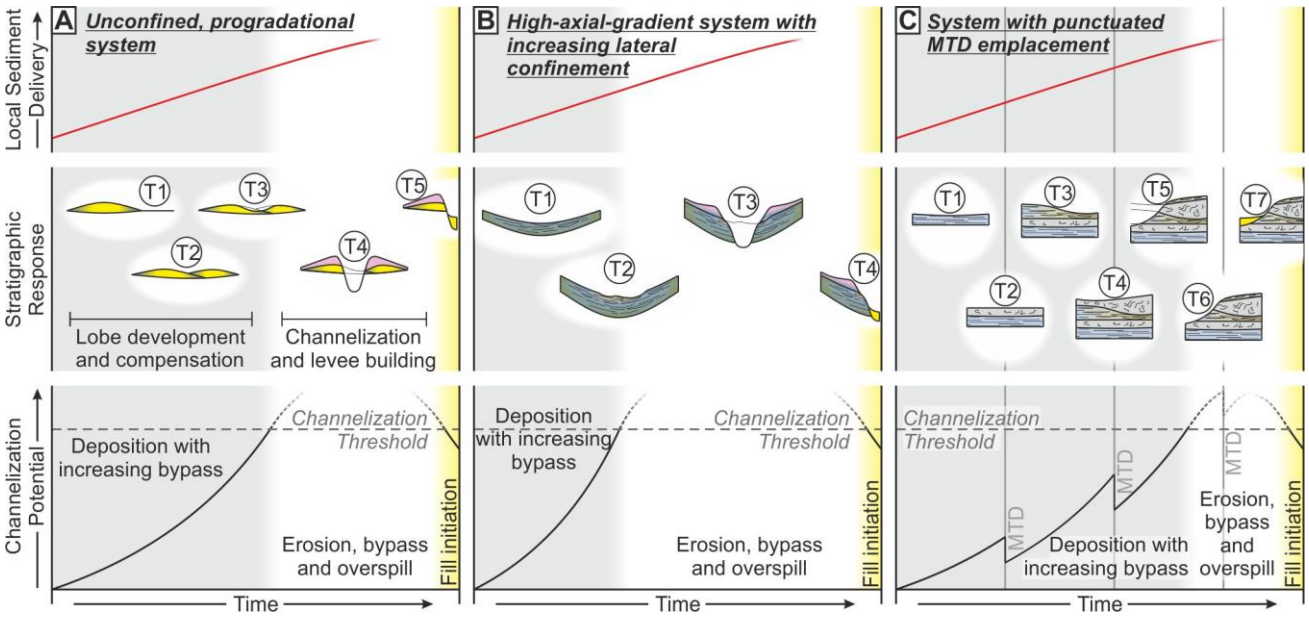


**Figure 15** – Conceptual diagrams showing how progressive, structurally derived lateral confinement, and the punctuated emplacement of MTDs can affect channel inception and resultant sedimentary architecture:

A) in an unconfined, progradational system experiencing increasing local coarse-grained sediment delivery, a channel will incise through unconfined precursor deposits after a channelization threshold is crossed (sketches based on Hodgson et al., 2016); B) imposed lateral confinement from growing tectonic structures allows the channelization threshold to be crossed earlier and at lower rates of delivery of coarse-grained sediment, inhibiting the development of sand-rich unconfined precursor deposits (example from Muro de Bellos); C) regular input of MTDs can interrupt the channelization process by periodically removing the previously formed lateral confinement, which leads to delayed crossing of the channelization threshold and the formation of DE3 deposits in replacement of sand-rich unconfined precursor deposits (example from Barranco de la Caxigosa).

A delay in crossing the channelization threshold can be caused by the regular deposition of MTDs that reset topography (Fig. 14I), because of their effect of removing the lateral confinement developed by preceding flows (Fig. 15). The result of this process is the development of pre-channelization interbedded packages of MTDs and turbidites (DE3), such as those seen in Barranco de la Caxigosa (Fig. 9). These might represent the equivalent deposits in an MTD-prone setting to the pre-channelization precursor lobes deposited in the absence of MTDs (cf. those shown by Hodgson et al., 2016). In areas where MTD and turbidite deposition occur concurrently, decreasing the frequency of MTD input or increasing the frequency or magnitude of turbidity-current input may lead to conditions favorable for channelization.

### *The Arro System as an Analog*

Much of the research on the younger channelized systems in the Aínsa depocenter, principally the Banastón, Aínsa, and Morillo systems, is centered around the role of syndepositional structures (Pickering and Bayliss, 2009; Bayliss and Pickering, 2015) or MTDs (Pickering and Corregidor, 2005; Dakin et al., 2013) in controlling the sedimentology and architecture of turbidite deposits; deposition in the Arro system was influenced by, and records the effects of, both. The processes discussed in this article can be exported to other exhumed topographically complex basins traversed by axial sediment routing systems such as the Magallanes foreland basin (Hubbard et al., 2008; Bernhardt et al., 2011, 2012), the Sinop basin (Leren et al., 2007; Janbu et al., 2007), the Grès du Champsaur (McCaffrey et al., 2002; Brunt et al., 2007), and the Gorgoglione Flysch

(Casciano et al., 2019). Studies concerning interplay between structures, MTDs, and turbidite deposition in the Austrian Molasse basin (Bernhardt et al., 2012; Masalimova et al., 2015; Kremer et al., 2018) may provide a subsurface analog.

The Arro system formed in an elongate corridor with high axial gradients bound by structures or canyon walls, similar to that of the younger Aínsa systems (Cornard and Pickering, 2019). The deposits therein can therefore be compared with those deposited in modern high-gradient confined systems such as large canyons (e.g., the Monterrey Canyon; Paull et al., 2018) or fjord-head delta slopes (e.g., the Bute Inlet, British Columbia; Hughes Clark, 2016). Comparing the results of this study to these modern systems allows (i) evaluation of the possible depositional signature of modern seafloor processes, and (ii) postulation of new mechanisms for the formation of recognized deep-water facies associations that have not hitherto been interpreted or have been attributed to other processes. For example, the dilute flows which form the background thin beds (FA1) of the Arro system have three possible origins, all of which have been monitored directly in fjord-head systems: (a) hyperpycnal flows, (b) small sediment failures on the shelf, upper slope, or in the feeder canyon (Clare et al., 2016), and (c) plume related density currents, which generate so-called “plumites” (Hizzett et al., 2018; Mutti, 2019). Weak, partially bypassing flows are inferred to have created the bedforms in laterally variable thin beds (FA2), specifically in increasing-to-decreasing-energy (DE1) and progradational-to-overbank (DE2) deposits. These may be analogous to some of the short-run-out flows observed by Hughes Clark (2016) and Paull et al. (2018), which do not reach the terminal deposits of the system. Traditionally, models accounting for the formation of channel stories invoke episodic variations in sediment supply and/or equilibrium gradients. Upstream-migrating knickpoints and crescentic bedforms are commonly recognized in modern submarine channels (Heiniö and Davies, 2007; Hughes Clark, 2016; Gales et al., 2019), indicating that more spatio-temporally complex patterns of incision and deposition may be involved in building submarine-channel stratigraphy (Hage et al., 2018; Vendettuoli et al., 2019). In the channelized units (DE4) of the Arro system, cut and fill at channel-story scale may result from the passing of upstream-migrating knickpoints or other bedforms; other causes however, cannot be discounted.

No interpretation is given for the source or triggers of flows that formed the Arro turbidite system because its constituent facies associations (from background thin beds, FA1, to sandstones, conglomerates, and debrites

with incisional bases, FA7) exist as part of a continuum with non-unique representations. If the formative flows were initiated by a single process (e.g., hyperpycnal flows or instability-driven sediment failures) that acted at a large range of magnitudes, a natural lack of distinction between different facies assemblages and bed types might be expected. Alternatively, if flows of overlapping magnitude were initiated by different trigger mechanisms, a range of processes may result in deposits with similar sedimentologic character. Flow genesis cannot, therefore, be differentiated using the methodologies employed here and in the current state of knowledge.

## CONCLUSIONS

The Arro turbidite system is confirmed as a channelized, axial sedimentary system that traversed the SE-NW-oriented Aínsa depocenter during the Eocene (Ypresian). It records a complex interplay between tectonic structuration, emplacement of mass-transport deposits (MTDs), and routing of turbidity currents. The principal findings from this field-based study are that:

- The locations of sandy turbidite and muddy debrite pathways were controlled by the development of tectonic structures that were active at the time of deposition.
- The deposits of the Arro system can be grouped into eight facies associations. These form a continuum of constituent facies and bed geometries attributed principally to variations in the velocity, magnitude, and grain size of their formative flows. In the Arro system, facies associations are non-unique to single depositional elements. Four depositional elements are recognized by the combined observation of groupings of facies associations, their lateral and vertical transitions, and the presence or absence of key surfaces: i) Weakly confined, increasing-to-decreasing-energy deposits (DE1), ii) progradational, weakly confined to overbank deposits (DE2), iii) alternating MTDs and turbidites (DE3), and iv) submarine-channel deposits (DE4). The different styles of observed channel architecture contain at least three orders of hierarchical organization.
- Tectonic structuration and emplacement of MTDs can affect the timing and nature of channel inception, and may inhibit the formation of precursor sand-rich, lobe deposits of the type typically observed in unconfined, progradational systems. Thus 1) high axial gradients and lateral confinement (e.g., due to thrust-related fairway narrowing) can promote higher flow velocities, allowing the onset of

channelization earlier (and at lower rates of local delivery of coarse-grained sediment) than would be expected in an unconfined system, resulting in the development of discontinuous, thin-bedded deposits below the channelized deposits (as seen in the Muro de Bellos outcrop). 2) Extra-channel MTD emplacement may act to delay the onset of channelization due to the punctuated healing of substrate topography and eradication of lateral confinement. The stratigraphic response to this is the presence of alternating MTDs and packages of non-channelized turbidites, below the channelized deposits (as observed in the Barranco de la Caxigosa outcrop).

- Five mechanisms describe how the emplacement of extra-channel MTDs can affect seafloor topography and therefore channelization: (i) flow interaction with MTD-margin topography or; (ii) MTD-top topography; (iii) differential compaction of MTDs and/or synsedimentary loading into them; (iv) formation of megascours by erosive MTDs; or (v) resetting of basin-floor topography by MTDs that occlude fully or partially channelized pathways. Apart from the last, which may only impede it, any of these mechanisms may accelerate or hinder the channelization process.

In this study confinement imposed by tectonic structures and by MTDs is seen to exert significant control on the inception, evolution, and fill of deep-water channels. The controlling processes are likely analogous to those observed or inferred in both modern and ancient confined systems. Therefore, in basins traversed by axial channel systems, the bathymetric expression of tectonic structures and MTDs may dictate the presence, distribution, architecture, and internal sedimentologic character of channelized units and their precursor deposits.

## ACKNOWLEDGMENTS

This work was funded by Turbidites Research Group sponsors: AkerBP, BP, ConocoPhillips, Equinor, Eni, HESS, Murphy, OMV, OXY, and Shell. We thank reviewers Suzanne Bull and Julian Clark for their constructive comments which helped improve the manuscript. We would also like to thank Adriana Crisostomo Figueroa, Alex Burton-Johnson, Ashley Ayckbourne, and Laura Bührig for their assistance in the field. Cai Puigdefàbregas is thanked for discussions which helped improve the manuscript.

## REFERENCES

Allen, J.R.L., 1973, A classification of climbing-ripple cross-lamination: Geological Society of London Journal, v. 129, p. 537–541.

Allen, J.R.L., 1982, Sedimentary Structures: Their Character and Physical Basis: Amsterdam, The Netherlands, Elsevier, 592 p.

Alpak, F.O., Barton, M.D., and Naruk, S.J., 2013, The impact of fine-scale turbidite channel architecture on deep-water reservoir performance: American Association of Petroleum Geologists, Bulletin, v. 97(2), p. 251–284.

Alves, T.M., 2010, 3D Seismic examples of differential compaction in mass-transport deposits and their effect on post-failure strata: Marine Geology, v. 271, p. 212–224

Arbués, P., Mellere, D., Puig, M., and Marzo, M., 2007a, Los Molinos Road, Spain: The Effect of Slumping on Sandstone Distribution in the Arro Turbidites, *in* Nilsen, T.H., Shew, R.D., Steffens, G.S., and Studlick, J.R.J., eds., Atlas of Deep-Water Outcrops: American Association of Petroleum Geologists, Studies in Geology, p. 1–17.

Arbués, P., Mellere, D., Puig, M., and Marzo, M., 2007b, The Effect of Slumping on Sandstone Distribution in the Arro Turbidites, Los Molinos Road, Spain, i*n* Nilsen T.H., Shrew, R.D., Steffens, G.S., and Studlick, J.R.J., eds., Atlas of Deep-Water Outcrops: American Association of Petroleum Geologists, Studies in Geology, p. 333–335.

Arbués, P., Butillé, M., López-Blanco, M., Marzo, M., Monleon, O., Muñoz, J.A., and Serra-Kiel, J., 2011, Exploring the relationships between deepwater and shallow-marine deposits in the Aínsa piggy-back basin fill (Eocene, South-Pyrenean Foreland Basin), *in* Arenas, C., Pomar L., and Colombo, F., eds., Post-Meeting Field Trips Guidebook, 28th International Association of Sedimentologists Meeting, Zaragoza, vol. 8: Zaragoza, Spain: Sociedad Geológica. de España, p. 199–240.

Armitage, D.A., Romans, B.W., Covault, J.A., and Graham, S.A., 2009. The influence of mass-transport-deposit surface topography on the evolution of turbidite architecture: The Sierra Contreras, Tres Pasos Formation (Cretaceous), Southern Chile: Journal of Sedimentary Research, v. 79, p. 287–301

Arnott, R.W.C., and Al-Mufti, O., 2017, Deep-marine pseudo dune cross-stratification—Similar, but completely different: Journal of Sedimentary Research, v. 87(3), p. 312–323.

Azpiroz-Zabala, M., Cartigny, M.J.B., Talling, P.J., Parsons, D.R., Sumner, E.J., Clare, M.A., Simmons, S.M., Cooper, C., and Pope, E.L., 2017, Newly recognized turbidity current structure can explain prolonged flushing of submarine canyons: Science Advances, v. 3(10), p. 1–12.

Barnolas, A., and Gil-Peña, I., 2001, Ejemplos de relleno sedimentario multiepisódico en una cuenca de antepaís fragmentada: La Cuenca Surpirenaica: Boletín Geológico y Minero, v. 112(3), p. 17– 38.

Barton, M., Byrne, C.O., Pirmez, C., Prather, B., Vlugt, F. Van Der, Alpak, F.O., and Sylvester, Z., 2010, Turbidite Channel Architecture: Recognizing and Quantifying the Distribution of Channel-base Drapes Using Core and Dipmeter Data, *in* Pöppelreitem, M., García-Carballido, C., and Kraaijveld, M., eds., Dipmeter and Borehole Image Log Technology: American Association of Petroleum Geologists, Memoir 92, p. 195–210.

Bayliss, N., and Pickering, K.T., 2015, Transition from deep marine lower slope erosional channels to proximal basin floor stacked channel-levee-overbank deposits, and synsedimentary growth structures, middle Eocene Banastón System, Ainsa Basin, Spanish Pyrenees: Earth-Science Reviews, v. 144, p. 23–46.

Bell, D., Stevenson, C.J., Kane, I.A., Hodgson, D.M., and Poyatos-Moré, M., 2018a, Topographic controls on the development of contemporaneous but contrasting basin-floor depositional architectures: Journal of Sedimentary Research, v. 88, p. 1166–1189.

Bell, D., Kane, I.A., Pontén, A.S.M., Flint, S.S., Hodgson, D.M., and Barrett, B.J., 2018b, Spatial variability in depositional reservoir quality of deep-water channel-fill and lobe deposits: Marine and Petroleum Geology, v. 98, p. 97–115.

Bentham, P.A., and Burbank, D.W., 1996, Chronology of Eocene foreland basin evolution along the western oblique margin of the South-Central Pyrenees, *in* Friend, P.F., and Dabrio, C.J., eds., Tertiary Basins of Spain: New York, Cambridge University Press, p. 144–152.

Bernhardt, A., Jobe, Z.R., and Lowe, D.R., 2011, Stratigraphic evolution of a submarine channel-lobe complex system in a narrow fairway within the Magallanes foreland basin, Cerro Toro Formation, southern Chile: Marine and Petroleum Geology, v. 28(3), p. 785–806.

Bernhardt, A., Jobe, Z.R., Grove, M., and Lowe, D.R., 2012, Palaeogeography and diachronous infill of an ancient deep-marine foreland basin, Upper Cretaceous Cerro Toro Formation, Magallanes Basin: Basin Research, v. 24(3), p. 269–294.

Boulesteix, K., Poyatos-Moré, M., Flint, S.S., Taylor, K.G., Hodgson, D.M., and Hasiotis, S.T., 2019, Transport and deposition of mud in deep-water environments: Processes and stratigraphic implications: Sedimentology, v. 66(7), p. 1–32.

Bouma, A.H., 1962, Sedimentology of Some Flysch Deposits: A Graphic Approach to Facies Interpretation: New York, Elsevier, 168 p.

Brooks, H.L., Hodgson, D.M., Brunt, R.L., Peakall, J., and Flint, S.S., 2018, Exhumed lateral margins and increasing flow confinement of a submarine landslide complex: Sedimentology, v. 65(4), p. 1067-1096.

Brunt, R.L., McCaffrey, W.D., and Butler, R.W.H., 2007, Architectural Elements of the Grès du Champsaur: Chaillol Area, Haute Alpes, Southeast France, *in* Nilsen, T.H., Shew, R.D., Steffens, G.S., and Studlick, J.R.J., eds., Atlas of Deep-Water Outcrops: American Association of Petroleum Geologists, Studies in Geology, p. 1–17.

Brunt, R.L., Di Celma, C.N., Hodgson, D.M., Flint, S.S., Kavanagh, J.P., and van der Merwe, W.C., 2013, Driving a channel through a levee when the levee is high: An outcrop example of submarine down-dip entrenchment: Marine and Petroleum Geology, v. 41(1), p. 134–145.

Bull, S., Cartwright, J., and Huuse, M., 2009, A review of kinematic indicators from mass-transport complexes using 3D seismic data: Marine and Petroleum Geology, v. 26(7), p. 1132–1151.

Bull, S., Browne, G.H., Arnot, M.J. and Strachan, L.J., 2020, Influence of Mass Transport Deposit (MTD) surface topography on deep-water deposition: an example from a predominantly fine-grained continental margin, New Zealand: Geological Society of London, Special Publication 500, DOI: https://doi.org/10.1144/SP500-2019-192.

Burgreen, B., and Graham, S., 2014, Evolution of a deep-water lobe system in the Neogene trench-slope setting of the East Coast Basin, New Zealand: Lobe stratigraphy and architecture in a weakly confined basin configuration: Marine and Petroleum Geology, v. 54, p. 1–22.

Caja, M.A., Marfil, R., Garcia, D., Remacha, E., Morad, S., Mansurbeg, H., Amorosi, A., Martínez-Calvo, C., and Lahoz-Beltrá, R., 2010, Provenance of siliciclastic and hybrid turbiditic arenites of the Eocene Hecho Group, Spanish Pyrenees: Implications for the tectonic evolution of a foreland basin: Basin Research, v. 22(2), p. 157–180.

Cámara, P., and Kilmowitz, J., 1985, Interpretación qeodinámica de la vertiente centro-occidental surpirenaica (cuencas de Jaca-Tremp): Estudios Geológicos, v. 41, p. 391–404.

Campion, K.M., Sprague, A.R.G., and Sullivan, M.D., 2005, Architecture and lithofacies of the Capistrano Formation (Miocene–Pliocene), San Clemente, California: Pacific Section, SEPM, Fieldtrip Guidebook, October 29, 2005, 42 p.

Casciano, C.I., Patacci, M., Longhitano, S.G., Tropeano, M., Mccaffrey, W.D., and Celma, C.D.I., 2019, Multi-scale analysis of a migrating submarine channel system in a tectonically-confined basin: The Miocene Gorgoglione Flysch Formation, southern Italy: Sedimentology, v. 66(1), p. 205–240.

Castelltort, S., Honegger, L., Adatte, T., Clark, J.D., Puigdefàbregas, C., Spangenberg, J.E., Dykstra, M.L., and Fildani, A., 2017, Detecting eustatic and tectonic signals with carbon isotopes in deep-marine strata, Eocene Ainsa Basin, Spanish Pyrenees: Geology, v. 45(8), p. 707–710.

Chanvry, E., Deschamps, R., Joseph, P., Puigdefàbregas, C., Poyatos-Moré, M., Serra-Kiel, J., Garcia, D., and Teinturier, S., 2018, Impact of intrabasinal tectonics in the stratigraphic evolution of piggyback basin fills: an example from the Eocene South-Pyrenean Foreland Basin (Spain): Sedimentary Geology, v. 377, p. 34-62.

Choukroune, P., 1992, Tectonic evolution of the Pyrenees: Annual Review of Earth and Planetary Sciences, v. 20, p. 143–158.

Clare, M.A., Hughes Clarke, J.E., Talling, P.J., Cartigny, M.J.B., and Pratomo, D.G., 2016, Preconditioning and triggering of offshore slope failures and turbidity currents revealed by most detailed monitoring yet at a fjord-head delta: Earth and Planetary Science Letters, v. 450, p. 208–220.

Clark, I.R., and Cartwright, J.A., 2011, Key controls on submarine channel development in structurally active settings: Marine and Petroleum Geology, v. 28(7), p. 1333–1349.

Clark, J.D., and Pickering, K.T., 1996, Architectural elements and growth patterns of submarine channels: Applications to hydrocarbon exploration: American Association of Petroleum Geologists, Bulletin, v. 80(2), p. 194–22.

Clark, J., Puigdefàbregas, C., Castelltort, S., and Fildani, A., 2017, Propagation of Environmental Signals within Source-to-Sink Stratigraphy: SEPM Field Trip Guidebook No. 13: Tulsa, Oklahoma, USA, 63 p.

Corella, J.P., Loizeau, J.L., Kremer, K., Hilbe, M., Gerard, J., le Dantec, N., Stark, N., González-Quijano, M., and Girardclos, S., 2016, The role of mass-transport deposits and turbidites in shaping modern lacustrine deepwater channels: Marine and Petroleum Geology, v. 77, p. 515–525.

Cornard, P.H., and Pickering, K.T., 2019, Supercritical-flow deposits and their distribution in a submarine channel system, middle Eocene, Ainsa Basin, Spanish Pyrenees: Journal of Sedimentary Research, v. 89, p. 576–597.

Cullis, S., Colombera, L., Patacci, M., and McCaffrey, W.D., 2018, Hierarchical classifications of the sedimentary architecture of deep-marine depositional systems: Earth-Science Reviews, v. 179, p. 38–71.

Dakin, N., Pickering, K.T., Mohrig, D., and Bayliss, N.J., 2013, Channel-like features created by erosive submarine debris flows: Field evidence from the Middle Eocene Ainsa Basin, Spanish Pyrenees: Marine and Petroleum Geology, v. 41, p. 62–71.

Das Gupta, K., and Pickering, K.T., 2008, Petrography and temporal changes in petrofacies of deep-marine Ainsa – Jaca basin sandstone systems, Early and Middle Eocene, Spanish Pyrenees: Sedimentology, v. 55, p. 1083–1114.

De Leeuw, J., Eggenhuisen, J.T., and Cartigny, M.J.B., 2016, Morphodynamics of submarine channel inception revealed by new experimental approach: Nature Communications, v. 7, p. 1–7.

Deptuck, M.E., Steffens, G.S., Barton, M., and Pirmez, C., 2003, Architecture and evolution of upper fan channel-belts on the Niger Delta slope and in the Arabian Sea: Marine and Petroleum Geology, v. 20(6–8), p. 649–676.

Deptuck, M.E., Sylvester, Z., Pirmez, C., and O'Byrne, C., 2007, Migration-aggradation history and 3-D seismic geomorphology of submarine channels in the Pleistocene Benin-major Canyon, western Niger Delta slope: Marine and Petroleum Geology, v. 24(6–9), p. 406–433.

Deptuck, M.E., Piper, D.J.W., Savoye, B., and Gervais, A., 2008, Dimensions and architecture of late Pleistocene submarine lobes off the northern margin of East Corsica: Sedimentology, v. 55(4), p. 869–898.

Di Celma, C.N., Brunt, R.L., Hodgson, D.M., Flint, S.S., and Kavanagh, J.P., 2011, Spatial and temporal evolution of a Permian submarine slope channel-levee system, Karoo Basin, South Africa: Journal of Sedimentary Research, v. 81(8), p. 579–599.

Dorrell, R.M., Hogg, A.J., and Pritchard, D., 2013, Polydisperse suspensions: Erosion, deposition, and flow capacity: Journal of Geophysical Research: Earth Surface, v. 118(3), p. 1–17.

Dorrell, R.M., Amy, L.A., Peakall, J., and McCaffrey, W.D., 2018, Particle size distribution controls the threshold between net sediment erosion and deposition in suspended load dominated flow: Geophysical Research Letters, v. 45, p. 1443–1452.

Dorrell, R.M., Peakall, J., Darby, S.E., Parsons, D.R., Johnson, J., Sumner, E.J., Wynn, R.B., Özsoy., E. and Tezcan, D., 2019, Self-sharpening induces jet-like structure in seafloor gravity currents: Nature Communications, v. 10(1381), p. 1–10.

Dykstra, M., Garyfalou, K., Kertznus, V., Kneller, B.C., Milana, J.P., Molinaro, M., Szuman, M., and Thompson, P., 2011, Mass transport deposits: combining outcrop studies and seismic forward modeling to understand lithofacies distributions, deformation, and their seismic stratigraphic expression., *in* Shipp, R.C., Weimer, P., and Posamentier, H.W., eds., Mass-Transport Deposits in Deepwater Settings: SEPM (Society for Sedimentary Geology), Special Publication 96, p. 293–310.

Eggenhuisen, J.T., Caffrey, W.D.M.C., Haughton, P.D.W., and Butler, R.W.H., 2010, Small-scale spatial variability in turbidity-current flow controlled by roughness resulting from substrate erosion: field evidence for a feedback mechanism: Journal of Sedimentary Research, v. 80(2), p. 129–136.

Eggenhuisen, J.T., Mccaffrey, W.D., Haughton, P.D.W., and Butler, R.W.H., 2011, Shallow erosion beneath turbidity currents and its impact on the architectural development of turbidite sheet systems: Sedimentology, v. 58(4), p. 936–959.

Elliott, T., 2000, Depositional Architecture of a Sand-Rich, Channelised Turbidite System: The Upper Carboniferous Ross Sandstone Formation, Western Ireland: Gulf Coast Section SEPM Foundation 20th Annual Research Conference, Deep-Water Reservoirs of the World, p. 342–373.

Fernández, O., Muñoz, J.A., Arbués, P., Falivene, O., and Marzo, M., 2004, Three-dimensional reconstruction of geological surfaces: An example of growth strata and turbidite systems from the Ainsa basin (Pyrenees, Spain): American Association of Petroleum Geologists, Bulletin, v. 88(8), p. 1049–1068.

Fernández, O., Muñoz, J.A., Arbués, P., and Falivene, O., 2012, 3D structure and evolution of an oblique system of relaying folds: the Ainsa basin (Spanish Pyrenees): Geological Society of London Journal, v. 169(5), p. 545–559.

Flint, S.S., Hodgson, D.M., Sprague, A.R., Brunt, R.L., Van der Merwe, W.C., Figueiredo, J., Prélat, A., Box, D., Di Celma, C., and Kavanagh, J.P., 2011, Depositional architecture and sequence stratigraphy of the Karoo basin floor to shelf edge succession, Laingsburg depocentre, South Africa: Marine and Petroleum Geology, v. 28(3), p. 658–674.

Fryer, R.C., and Jobe, Z.R., 2019, Quantification of the bed-scale architecture of submarine depositional environments: SEPM, The Depositional Record, v. 5(2), p. 192–211.

Gardner, M.H., Borer, J.M., Melick, J.J., Mavilla, N., Dechesne, M., and Wagerle, R.N., 2003, Stratigraphic process-response model for submarine channels and related features from studies of Permian Brushy Canyon outcrops, West Texas: Marine and Petroleum Geology, v. 20(6–8), p. 757–787.

Gales, J.A., Talling, P.J., Cartigny, M.J.B., Hughes Clarke, J., Lintern, G., Stacey, C., and Clare, M.A., 2019, What controls submarine channel development and the morphology of deltas entering deep-water fjords?: Earth Surface Processes and Landforms, v. 44(2), p. 535–551.

Gee, M.J.R., and Gawthorpe, R.L., 2006, Submarine channels controlled by salt tectonics: Examples from 3D seismic data offshore Angola: Marine and Petroleum Geology, v. 23, p. 443–458.

Georgiopoulou, A., and Cartwright, J.A., 2013, A critical test of the concept of submarine equilibrium profile: Marine and Petroleum Geology, v. 41, p. 35–47.

Gomis-Cartesio, L.E., Poyatos-Moré, M., Hodgson, D.M., and Flint, S.S., 2018, Shelf-margin clinothem progradation, degradation and readjustment: Tanqua depocentre, Karoo Basin (South Africa): Sedimentology, v. 65(3), p.809–841.

Gong, C., Steel, R.J., Wang, Y., Lin, C., and Olariu, C., 2016, Grain size and transport regime at shelf edge as fundamental controls on delivery of shelf-edge sands to deepwater: Earth-Science Reviews, v. 157, p. 32–60.

Hage, S., Cartigny, M.J.B., Clare, M.A., Sumner, E.J., Vendettuoli, D., Clarke, J.E.H., Hubbard, S.M., Talling, P.J., Lintern, D.G., Stacey, C.D., Englert, R.G., Vardy, M.E., Hunt, J.E., Yokokawa, M., Parsons, D.R., Hizzett, J.L., Azpiroz-zabala, M., and Vellinga, A.J., 2018, How to recognize crescentic bedforms formed by supercritical turbidity currents in the geologic record: Insights from active submarine channels: Geology, v. 46(6), p. 563–566.

Hansen, L., L'Heureux, J.S., Sauvin, G., Polom, G., Lecomte, I., Vaneste, M., Longva, O., and Krawczyk, C., 2013, The effect of mass-wasting on the stratigraphic architecture of a fjord-valley fill: correlation of onshore, shear wave seismics and marine seismic data at Trondheim, Norway: Sedimentary Geology, v. 289, p. 1–18.

Hansen, L.A.S., Callow, R.H.T., Kane, I.A., Gamberi, F., Rovere, M., Cronin, B.T., and Kneller, B.C., 2015, Genesis and character of thin-bedded turbidites associated with submarine channels: Marine and Petroleum Geology, v. 67, p. 852–879.

Haughton, P., Davis, C., McCaffrey, W., and Barker, S., 2009, Hybrid sediment gravity flow deposits - Classification, origin and significance: Marine and Petroleum Geology, v. 26(10), p. 1900–1918.

Heard, T.G., and Pickering, K.T., 2008, Trace fossils as diagnostic indicators of deep-marine environments, Middle Eocene Ainsa-Jaca basin, Spanish Pyrenees: Sedimentology, v. 55(4), p. 809–844.

Heard, T.G., Pickering, K.T., and Clark, J.D., 2014, Ichnofabric characterization of a deep-marine clastic system: A subsurface study of the Middle Eocene Ainsa System, Spanish Pyrenees: Sedimentology, v. 61(5), p. 1298–1331.

Heiniö, P., and Davies, R.J., 2007, Knickpoint migration in submarine channels in response to fold growth, western Niger Delta: Marine and Petroleum Geology, v. 24(6–9), p. 434–449.

Hizzett, J.L., Hughes Clarke, J.E., Sumner, E.J., Talling, P.J., and Clare, M.A., 2018, Which Triggers Produce the Most Erosive, Frequent, and Longest Runout Turbidity Currents on Deltas?: Geophysical Research Letters, v. 45, p. 855–863.

Hodgson, D.M., Di Celma, C.N., Brunt, R.L., and Flint, S.S., 2011, Submarine slope degradation and aggradation and the stratigraphic evolution of channel-levee systems: Geological Society of London Journal, v. 168(3), p. 625–628.

Hodgson, D.M., Kane, I.A., Flint, S.S., Brunt, R.L., and Ortiz-Karpf, A., 2016, Time-transgressive confinement on the slope and the progradation of basin-floor fans: Implications for the sequence stratigraphy of deep-water deposits: Journal of Sedimentary Research, v. 86(2), p. 73–86.

Hofstra, M., Peakall, J., Hodgson, D.M., and Stevenson, C.J., 2018, Architecture and morphodynamics of subcritical sediment waves in an ancient channel – lobe transition zone: Sedimentology, v. 65(7), p. 2339–2367.

Hubbard, S.M., Romans, B.W., and Graham, S.A., 2008, Deep-water foreland basin deposits of the Cerro Toro Formation, Magallanes basin, Chile: Architectural elements of a sinuous basin axial channel belt: Sedimentology, v. 55(5), p. 1333–1359.

Hubbard, S.M., De Ruig, M.J., and Graham, S.A., 2009, Confined channel-levee complex development in an elongate depo-center: Deep-water Tertiary strata of the Austrian Molasse basin: Marine and Petroleum Geology, v. 26, p. 85–112.

Hubbard, S.M., Covault, J.A., Fildani, A. and Romans, B.W., 2014, Sediment transfer and deposition in slope channels: Deciphering the record of enigmatic deep-sea processes from outcrop: Geological Society of America, Bulletin, v. 126(5–6), p. 857–871.

Hughes Clarke, J.E., 2016, First wide-angle view of channelized turbidity currents links migrating cyclic steps to flow characteristics: Nature Communications, v. 7(11896), p. 1–13.

Janbu, N.E., Nemec, W., Kirman, E., and Özaksoy, V., 2007, Facies anatomy of a sand-rich channelized turbiditic system: the Eocene Kusuri Formation in the Sinop Basin, north-central Turkey, *in* Nichols, G., Williams, E., and Paola, C., eds., Sedimentary Processes, Environments and Basins: A Tribute to Peter Friend: International Association of Sedimentologists, Special Publication 38, p. 457–517.

Jobe, Z.R., Sylvester, Z., Parker, A.O., Howes, N., Slowey, N., and Pirmez, C., 2015, Rapid adjustment of submarine channel architecture to changes in sediment supply: Journal of Sedimentary Research, v. 85(6), p. 729–753.

Johansson, M. and Stow, D.A.V., 1995, A classification scheme for shale clasts in deep water sandstones, *in* Hartley A.J., and Prosser, D.J., eds., Characterization of Deep Marine Clastic Systems: Geological Society of London, Special Publication 94, p. 221–241.

Jolly, B.A., Lonergan, L., and Whittaker, A.C., 2016, Growth history of fault-related folds and interaction with seabed channels in the toe-thrust region of the deep-water Niger delta: Marine and Petroleum Geology, v. 70, p. 58–76.

Kane, I.A., and Hodgson, D.M., 2011, Sedimentological criteria to differentiate submarine channel levee subenvironments: Exhumed examples from the Rosario Fm. (Upper Cretaceous) of Baja California, Mexico, and the Fort Brown Fm. (Permian), Karoo Basin, S. Africa: Marine and Petroleum Geology, v. 28(3), p. 807–823.

Kane, I.A., Dykstra, M.L., Kneller, B.C., Tremblay, S., and McCaffrey, W.D., 2009a, Architecture of a coarse-grained channel-levée system: The Rosario Formation, Baja California, Mexico: Sedimentology, v. 56(7), p. 2207–2234.

Kane, I.A., McCaffrey, W.D., and Martinsen, O.J., 2009b, Allogenic vs. autogenic controls on megaflute formation: Journal of Sedimentary Research, v. 79(9), p. 643–651.

Kane, I.A., Pontén, A.S.M., Vangdal, B., Eggenhuisen, J.T., Hodgson, D.M., and Spychala, Y.T., 2017, The stratigraphic record and processes of turbidity current transformation across deep-marine lobes: Sedimentology, v. 64(5), p. 1236–1273.

Kneller, B., 1995, Beyond the turbidite paradigm: physical models for deposition of turbidites and their implications for reservoir prediction, *in* Hartley, A. J., and Prosser, D. J., eds., Characterization of Deep Marine Clastic Systems: Geological Society of London, Special Publication 94, p. 31–49.

Kneller, B., 2003, The influence of flow parameters on turbidite slope channel architecture: Marine and Petroleum Geology, v. 20(6–8), p. 901–910.

Kneller, B., and McCaffrey, W.D., 1999, Depositional effects of flow nonuniformity and stratification within turbidity currents approaching a bounding slope: deflection, reflection, and facies variation: Journal of Sedimentary Research, v. 69(5), p. 980–991.

Kneller, B., Dykstra, M., Fairweather, L., and Milana, J.P., 2016, Mass-transport and slope accommodation: Implications for turbidite sandstone reservoirs: American Association of Petroleum Geologists, Bulletin, v. 100(2), p. 213–235.

Komar, P.D., 1971, Hydraulic Jumps in Turbidity Currents: Geological Society of America, Bulletin, 82, p. 1477–1488.

Kremer, C.H., Mchargue, T., Scheucher, L., and Graham, S.A., 2018, Transversely-sourced mass-transport deposits and stratigraphic evolution of a foreland submarine channel system: Deep-water tertiary strata of the Austrian Molasse Basin: Marine and Petroleum Geology, v. 92, p. 1–19.

Kuenen, P.H., and Sengupta, S., 1970, Experimental marine suspension currents, competency and capacity: Geologie en Mijnbouw, v. 49(2), p. 89–118.

Leren, B.L.S., Janbu, N.E., Nemec, W.C.H., Kirman, E., and Ilgar, A., 2007, Late Cretaceous to early Eocene sedimentation in the Sinop – Boyabat Basin, north-central Turkey: a deep-water turbiditic system evolving into

littoral carbonate platform, *in* Nichols, G., Williams E., and Paola, C., eds., Sedimentary Processes, Environments and Basins: A Tribute to Peter Friend: International Association of Sedimentologists, Special Publication 38, p. 401–456.

Li, P., Kneller, B., Thompson, P., Bozetti, G., and dos Santos, T., 2018, Architectural and facies organisation of slope channel fills: Upper Cretaceous Rosario Formation, Baja California, Mexico: Marine and Petroleum Geology, v. 92, p. 632–649.

Liu, Q., Kneller, B., Fallgatter, C., and Valdez Buso, V., 2018, Quantitative comparisons of depositional architectures of unconfined and confined turbidite sheet systems: Sedimentary Geology, v. 376, p. 72–89.

Lowe, D.R., 1982, Sediment gravity flows: II. Depositional models with special reference to the deposits of high-density turbidity currents: Journal of Sedimentary Petrology, v. 52(1), p. 279–297.

Lowe, D.R., Graham, S.A., Malkowski, M.A., and Das, B., 2019, The role of avulsion and splay development in deep-water channel systems: Sedimentology, architecture, and evolution of the deep-water Pliocene Godavari "A" channel complex, India: Marine and Petroleum Geology, v. 105, p. 81–99.

Macauley, R.V., and Hubbard, S.M., 2013, Slope channel sedimentary processes and stratigraphic stacking, Cretaceous Tres Pasos Formation slope system, Chilean Patagonia: Marine and Petroleum Geology, v. 41, p. 146–162.

Macdonald, H.A., Peakall, J., Wignall, P.B., and Best, J.L., 2011, Sedimentation in deep-sea lobe-elements: implications for the origin of thickening-upward sequences: Geological Society of London Journal, v. 168, p. 319–332.

Maier, K.L., Gales, J.A., Paull, C.K., Rosenberger, K., Talling, P.J., Simmons, S.M., Gwiazda, R., Mcgann, M., Cartigny, M.J.B., Lundsten, E., Anderson, K., Clare, M.A., Xu, J., Parsons, D., Barry, J.P., Wolfson-schwehr, M., Nieminski, N.M., and Sumner, E.J., 2019, Linking Direct Measurements of Turbidity Currents to Submarine Canyon-Floor Deposits: Frontiers in Earth Science, v. **7**(144), p. 1–18.

Marsset, T., Droz, L., Dennielou, B., and Pichon, E., 2009, Cycles in the architecture of the Quaternary Zaire turbidite system: A possible link with climate, *in* Kneller, B.C., Martinsen, O.J., and McCaffrey, W.D., eds., External Controls on Deep-Water Depositional Systems: SEPM (Society for Sedimentary Geology), Special Publication 92, p. 89–106.

Marzo, M., Nijman, W., and Puigdefàbregas, C., 1988, Architecture of the Castissent fluvial sheet sandstones, Eocene, South Pyrenees, Spain: Sedimentology, v. 35(5), p. 719–738.

Masalimova, L.U., Lowe, D.R., Mchargue, T., and Derksen, R., 2015, Interplay between an axial channel belt, slope gullies and overbank deposition in the Puchkirchen Formation in the Molasse Basin, Austria: Sedimentology, v. 62(6), p. 1717–1748.

Masalimova, L.U., Lowe, D.R., Sharman, G.R., King, P.R., and Arnot, M.J., 2016, Outcrop characterization of a submarine channel-lobe complex: the lower Mount Messenger Formation, Taranaki Basin, New Zealand: Marine and Petroleum Geology, v. 71, p. 360–390.

Mayall, M., and Stewart, I., 2000, The Architecture of Turbidite Slope Channels: Gulf Coast Section SEPM Foundation, 20th Annual Research Conference, Deep-Water Reservoirs of the World, p. 578–586.

Mayall, M., Jones, E., and Casey, M., 2006, Turbidite channel reservoirs - Key elements in facies prediction and effective development: Marine and Petroleum Geology, v. 23(8), p. 821–841.

Mayall, M., Lonergan, L., Bowman, A., James, S., Mills, K., Primmer, T., Pope, D., Rogers, L., and Skeene, R., 2010, The response of turbidite slope channels to growth-induced seabed topography: American Association of Petroleum Geologists, Bulletin, v. 94(7), p. 1011–1030.

McArthur, A.D., and McCaffrey, W.D., 2019, Sedimentary architecture of detached deep-marine canyon heads: Examples from the East Coast Basin of New Zealand: Sedimentology, v. 66, p. 1067-1101

McCaffrey, W.D., and Kneller, B., 2001, Process controls on the development of stratigraphic trap potential on the margins of confined turbidite systems and aids to reservoir evaluation: American Association of Petroleum Geologists, Bulletin, v. 85(6), p. 971–988.

McCaffrey, W.D., Gupta, S. and Brunt, R., 2002, Repeated cycles of submarine channel incision, infill and transition to sheet sandstone development in the Alpine Foreland Basin, SE France: Sedimentology, v. 49(3), p. 623–635.

McHargue, T., Pyrcz, M.J., Sullivan, M.D., Clark, J.D., Fildani, A., Romans, B.W., Covault, J.A., Levy, M., Posamentier, H.W., and Drinkwater, N.J., 2011, Architecture of turbidite channel systems on the continental slope: Patterns and predictions: Marine and Petroleum Geology, v. 28(3), p. 728–743.

Millington, J., and Clark, J.D., 1995a, The Charo/Arro canyon-mouth sheet system, South-Central Pyrenees, Spain: A structurally influenced zone of sediment dispersal: Journal of Sedimentary Research, v. B65(4), p. 443–454.

Millington, J., and Clark, J.D., 1995b, Submarine canyon and associated base-of-slope sheet system: the Eocene Charo-Arro system, south-central Pyrenees, Spain, *in* Nilsen, T.H., Shew, R.D., Steffens G.S., and Studlick, J.R.J., eds., Atlas of Deep-Water Outcrops: American Association of Petroleum Geologists, Studies in Geology, p. 150–156.

Moscardelli, L., and Wood, L., 2008, New classification system for mass transport complexes in offshore Trinidad: Basin Research, v. 20(1), p. 73–98.

Mountjoy, J.J., Howarth, J.D., Orpin, A.R., Barnes, P.M., Bowden, D.A., Rowden, A.A., Schimel, A.C.G., Holden, C., Horgan, H.J., Nodder, S.D., Patton, J.R., Lamarche, G., Gerstenberger, M., Micallef, A., Pallentin, A., and Kane, T., 2018, Earthquakes drive large-scale submarine canyon development and sediment supply to deep-ocean basins: Science Advances, v. 4(3), p. 1–8.

Mulder, T., Syvitski, J.P.M., Migeon, S., Faugères, J.-C., and Savoye, B., 2003, Marine hyperpycnal flows: initiation, behavior and related deposits. A review: Marine and Petroleum Geology, v. 20, p. 861–882.

Mulder, T., Razin, P., and Faugeres, J., 2009, Hummocky cross-stratification-like structures in deep-sea turbidites: Upper Cretaceous Basque basins (Western Pyrenees, France): Sedimentology, v. 56(4), p. 997–1015.

Muñoz, J.A., 1992, Evolution of a continental collision belt: ECORS-Pyrenees crustal balanced cross-section, *in* McClay, K.R., ed., Thrust Tectonics: London, Chapman and Hall, p. 235–246.

Muñoz, J.A., McClay, K., and Poblet, J., 1994, Synchronous extension and contraction in frontal thrust sheets of the Spanish Pyrenees: Geology, v. 22, p. 921–924.

Muñoz, J.-A., Beamud, E., Fernández, O., Arbués, P., Dinarès-Turell, J., and Poblet, J., 2013, The Ainsa Fold and thrust oblique zone of the central Pyrenees: Kinematics of a curved contractional system from paleomagnetic and structural data: Tectonics, v. 32, p. 1142–1175.

Mutti, E., 1977, Distinctive thin-bedded turbidite facies and related depositional environments in the Eocene Hecho Group (South-central Pyrenees, Spain): Sedimentology, v. 24, p. 107–131.

Mutti, E., 1984, The Hecho Eocene Submarine Fan System, South-Central Pyrenees, Spain: Geo-Marine Letters, v. 3, p. 199–202.

Mutti, E., 1985, Turbidite systems and their relations to depositional sequences, *in* Zuffa, G.G., ed., Provenance of Arenites: Dordrecht, The Netherlands, Reisel Publishing Company, p. 65–93.

Mutti, E., 1992, Turbidite Sandstones. San Donato Milanese: Istituto di Geologia, Università di Parma, 275 p.

Mutti, E., 2019, Thin-bedded plumites: an overlooked deep-water deposit: Journal of Mediterranean Earth Sciences, v. 11, p. 1–20.

Mutti, E., and Nilsen, T.H., 1981, Significance of intraformational rip-up clasts in deep-sea fan deposits: Proceedings of the International Association of Sedimentologists 2nd European Meeting, Bologna, p. 117–119.

Mutti, E., and Normark, W.R., 1987, Comparing Examples of Modern and Ancient Turbidite Systems: Problems and Concepts, *in* Leggett, J.K., and Zuffa, G.G., eds., Marine Clastic Sedimentology: Concepts and Case Studies: London, UK, Graham and Trotman, p. 1–38.

Mutti, E., and Normark, W. R., 1991, An integrated approach to the study of turbidite systems, *in* Weimer, P., and Link, M.H., eds., Seismic Facies and Sedimentary Processes of Submarine Fans and Turbidite Systems: New York, Springer-Verlag, p. 75-106.

Mutti, E., Seguret, M., and Sgavetti, M., 1988, Sedimentation and deformation in the Tertiary Sequences of the Southern Pyrenees: American Association of Petroleum Geologists, Mediterranean Basins Conference Guidebook Field Trip No. 7, p. 1–153.

Mutti, E., Davoli, G., Mora, S., and Papani, L., 1994, Internal Stacking Patterns of Ancient Turbidite Systems from Collisional Basins, *in* Weimer, P., Bouma, A.H., and Perkins, B.F., eds., Gulf Coast Section SEPM Foundation 15th Annual Research Conference, Submarine Fans and Turbidite Systems: Sequence Stratigraphy, Reservoir Architecture and Production Characteristics, Gulf of Mexico and International, p. 257–268.

Mutti, E., Davoli, G., Tinterri, R., and Zavala, C., 1996, The importance of ancient fluvio-deltaic systems dominated by catastrophic flooding in tectonically active basins: Memorie di Scienze Geologiche de Padova, v. 48, p. 233–291.

Mutti, E., Tinterri, R., Remacha, E., Mavilla, N., Angella, S., and Fava, L., 1999, An Introduction To the Analysis of Ancient Turbidite Basins From an Outcrop Perspective: American Association of Petroleum Geologists, Continuing Education Course Notes, Series 39: Tulsa, Oklahoma, USA, 96 p.

Mutti, E., Tinterri, R., di Biase, D., Fava, L., Mavilla, N., Angella, S. and Calabrese, L., 2000, Delta-front facies associations of ancient flood-dominated fluvio-deltaic systems: Sociedad Geológica de España, Revista, v. 13(2), p. 165–190.

Mutti, E., Tinterri, R., Benevelli, G., di Biase, D., and Cavanna, G., 2003, Deltaic, mixed and turbidite sedimentation of ancient foreland basins. Marine and Petroleum Geology, v. 20(6–8), p. 733–755.

Muzzi Magalhaes, P., and Tinterri, R., 2010, Stratigraphy and depositional setting of slurry and contained (reflected) beds in the Marnoso-arenacea Formation (Langhian-Serravallian) Northern Apennines, Italy: Sedimentology, v. 57(7), p. 1685–1720.

Nelson, C.H., Escutia, C., Goldfinger, C., Karabanov, E., Gutierrez-pastor, J., and DeBatist, M., 2009, External Controls on Modern Clastic Turbidite Systems: Three Case Studies, *in* Kneller, B.C., Martinsen, O.J., and McCaffrey, W.D., eds., External Controls on Deep-Water Depositional Systems: SEPM (Society for Sedimentary Geology), Special Publication 96, p. 57–76.

Nelson, C.H., Escutia, C., Damuth, J.E., and Twichell, D.C., 2011, Interplay of Mass-Transport and Turbidite-System Deposits in Different Active Tectonic and Passive Continental Margin Settings: External and Local Controlling Factors, *in* Shipp, R.C., Weimer, P., and Posamentier, H.W., eds., Mass-Transport Deposits in Deepwater Settings: SEPM (Society for Sedimentary Geology), Special Publication 96, p. 39–66.

Nijman, W., 1998, Cyclicity and basin axis shift in a piggyback basin: towards modelling of the Eocene Tremp-Ager Basin, South Pyrenees, Spain, *in* Mascle, A., Puigdefàbregas, C., Luterbacher, H.P., and Fernàndez, M., eds., Cenozoic Foreland Basins of Western Europe: Geological Society of London, Special Publication 134, p. 135–162.

Nijman, W., and Puigdàfabregas, C., 1977, Coarse-grained point bar structure in a molasse-type fluvial system, Eocene Castisent sandstone formation, South Pyrenean Basin: Canadian Society of Petroleum Geologists, Memoir 5, p. 487–510.

Normark, W.R., Piper, D.J.W., and Hess, G.R., 1979, Distributary channels, sand lobes, and mesotopography of Navy Submarine Fan, California Borderland, with applications to ancient fan sediments: Sedimentology, v. 26(6), p. 749-774.

Ogata, K., Mutti, E., Andrea, G., and Tinterri, R., 2012, Mass transport-related stratal disruption within sedimentary mélanges: Examples from the northern Apennines (Italy) and south-central Pyrenees (Spain): Tectonophysics, v. 568–569, p. 185–199.

Oliveira, C.M.M., Hodgson, D.M., and Flint, S.S., 2011, Distribution of soft-sediment deformation structures in clinoform successions of the Permian Ecca Group, Karoo Basin, South Africa: Sedimentary Geology, v. 235(3–4), p. 314–330.

Ortiz-Karpf, A., Hodgson, D.M., and McCaffrey, W.D., 2015, The role of mass-transport complexes in controlling channel avulsion and the subsequent sediment dispersal patterns on an active margin: The Magdalena Fan, offshore Colombia: Marine and Petroleum Geology, v. 64, p. 58–75.

Ortiz-karpf, A., Hodgson, D.M., Jackson, C.A., and McCaffrey, W.D., 2017, Influence of seabed morphology and substrate composition on mass-transport flow processes and pathways: Insights from the Magdalena Fan, offshore Colombia: Journal of Sedimentary Research, v. 87(3), p. 189–209.

Owen, G., 2003., Load structures: Gravity-driven sediment mobilization in the shallow subsurface., *in* Van Rensbergen, P., Hillis, R.R., Maltman, A.J., and Morley, C.K., eds., Subsurface Sediment Mobilization: Geological Society of London, Special Publication 216, p. 21–34.

Patacci, M., 2016, A high-precision Jacob's staff with improved spatial accuracy and laser sighting capability: Sedimentary Geology, v. 335, p. 66–69.

Paull, C.K., Talling, P.J., Maier, K.L., Parsons, D., Xu, J., Caress, D.W., Gwiazda, R., Lundsten, E.M., Anderson, K., Barry, J.P., Chaffey, M., Reilly, T.O., Rosenberger, K.J., Gales, J.A., Kieft, B., McGann, M., Simmons, S.M., McCann, M., Sumner, E.J., Clare, M.A., and Cartigny, M.J., 2018, Powerful turbidity currents driven by dense basal layers: Nature Communications, v. 9(4114), p. 1–9.

Payros, A., Tosquella, J., Bernaola, G., Dinarès-turell, J., Orue-Etxebarria, X., and Pujalte, V., 2009, Filling the North European Early/Middle Eocene (Ypresian / Lutetian) boundary gap: Insights from the Pyrenean continental to deep-marine record: Palaeogeography, Palaeoclimatology, Palaeoecology, v. 280(3–4), p. 313–332.

Peakall, J., and Sumner, E.J., 2015, Submarine channel flow processes and deposits: A process-product perspective: Geomorphology, v. 244, p. 95–120.

Pickering, K.T., and Bayliss, N.J., 2009, Deconvolving tectono-climatic signals in deep-marine siliciclastics, Eocene Ainsa basin, Spanish Pyrenees: Seesaw tectonics versus eustasy: Geology, v. 37(3), p. 203–206.

Pickering, K.T., and Cantalejo, B., 2015, Deep-marine environments of the middle Eocene upper Hecho Group, Spanish Pyrenees: Introduction: Earth-Science Reviews, v. 144, p. 1–9.

Pickering, K.T., and Corregidor, J., 2000, 3D Reservoir-Scale Study of Eocene Confined Submarine Fans, South-Central Spanish Pyrenees: Gulf Coast Section SEPM Foundation 20th Annual Research Conference, Deep-Water Reservoirs of the World, p. 776–781.

Pickering, K.T., and Corregidor, J., 2005, Mass transport complexes and tectonic control on confined basin-floor submarine fans, Middle Eocene, south Spanish Pyrenees, *in* Hodgson, D.M., and Flint, S.S., eds., Submarine Slope Systems: Processes and Product: Geological Society of London, Special Publication 244, p. 51–74.

Pickering, K.T., Hodgson, D.M., Platzman, E., Clark, J.D., and Stephens, C., 2001, A new type of bedform produced by backfilling processes in a submarine channel, Late Miocene, Tabernas-Sorbas basin, SE Spain: Journal of Sedimentary Research, v. 71(5), p. 692–704.

Pirmez, C., Beaubouef, R.T., Friedmann, S.J., and Mohrig, D.C., 2000, Equilibrium Profile and Baselevel in Submarine Channels: Examples from Late Pleistocene Systems and Implications for the Architecture of Deepwater Reservoirs: Gulf Coast Section SEPM Foundation 20th Annual Research Conference, Deep-Water Reservoirs of the World, p. 782–805.

Posamentier, H.W., 2003, Depositional elements associated with a basin floor channel-levee system: Case study from the Gulf of Mexico: Marine and Petroleum Geology, v. 20(6–8), p. 677–690.

Posamentier, H.W., and Kolla, V., 2003, Seismic geomorphology and stratigraphy of depositional elements in deep-water settings: Journal of Sedimentary Research, v. 73(3), p. 367–388.

Posamentier, H.W. and Martinsen, O.J., 2011, The character and genesis of submarine mass-transport deposits: Insights from outcrop and 3D seismic data, *in* Shipp, R.C., Weimer, P., and Posamentier, H.W., eds., Mass-Transport Deposits in Deepwater Settings: SEPM (Society for Sedimentary Geology), Special Publication 96, p. 39–66.

Postma, G., and Cartigny, M.J.B., 2014, Supercritical and subcritical turbidity currents and their deposits--A synthesis: Geology, v. 42(11), p. 987–990.

Poyatos-Moré, M., 2014, Physical Stratigraphy and Facies Analysis of the Castissent Tecto-Sedimentary Unit (South-Central Pyrenees, Spain) [PhD Thesis]: Universidad Autónoma de Barcelona, 282 p.

Prather, B.E., 2003, Controls on reservoir distribution, architecture and stratigraphic trapping in slope settings: Marine and Petroleum Geology, v. 20(6–8), p. 529–545.

Prather, B.E., Booth, J.R., Steffens, G.S., and Craig, P.A., 1998, Classification, Lithologic Calibration, and Stratigraphic Succession of Seismic Facies of Intraslope Basins, Deep-Water Gulf of Mexico: American Association of Petroleum Geologists, Bulletin, v. 82(5A), p. 701–728.

Prather, B.E., O'Byrne, C., Pirmez, C., and Sylvester, Z., 2017, Sediment partitioning, continental slopes and base-of-slope systems: Basin Research, v. 29(3), p. 394–416.

Prélat, A., Covault, J.A., Hodgson, D.M., Fildani, A., and Flint, S.S., 2010, Intrinsic controls on the range of volumes, morphologies, and dimensions of submarine lobes: Sedimentary Geology, v. 232(1–2), p. 66–76.

Puigdefàbregas, C., and Souquet, P., 1986, Tectono-sedimentary cycles and depositional sequences of the Mesozoic and Tertiary from the Pyrenees: Tectonophysics, v. 129, p. 173–203.

Qin, Y., Alves, T. M., Constantine, J., and Gamboa, D., 2017, The role of mass wasting in the progressive development of submarine channels (Espirito Santo Basin, SE Brazil): Journal of Sedimentary Research, v. 87, p. 500–516.

Remacha, E., and Fernández, L.P., 2003, High-resolution correlation patterns in the turbidite systems of the Hecho Group (South-Central Pyrenees, Spain): Marine and Petroleum Geology, v. 20(6–8), p. 711–726.

Remacha, E., Fernandez, L.P., and Maestro, E., 2005, The transition between sheet-like lobe and basin-plain turbidites in the Hecho Basin (South-Central Pyrenees, Spain): Journal of Sedimentary Research, v. 75(5), p. 798–819.

Schultz, M.R., Fildani, A., Cope, T.D., and Graham, S.A., 2005, Deposition and stratigraphic architecture of an outcropping ancient slope system: Tres Pasos Formation, Magallanes Basin, southern Chile, *in* Hodgson, D.M., and Flint, S.S., eds., Submarine Slope Systems: Processes and Product: Geological Society of London, Special Publication 244, p. 27-50

Schwenk, T., Spieß, V., Breitzke, M., and Hübscher, C., 2005, The architecture and evolution of the Middle Bengal Fan in vicinity of the active channel-levee system imaged by high-resolution seismic data: Marine and Petroleum Geology, v. 22(5), p. 637–656.

Scotchman, J.I., Bown, P., Pickering, K.T., Boudagher-fadel, M., Bayliss, N.J., and Robinson, S.A., 2015, A new age model for the middle Eocene deep-marine Ainsa Basin, Spanish Pyrenees: Earth-Science Reviews, v. 144, p. 10–22.

Séguret, M., 1972, Étude tectonique des nappes et series décollées de la partie centrale du versant sud der Pyrénées [Ph.D. Thesis]: Publications de l'Universite de Sciences et Techniques de Languedoc, serie Geologie Structurale, v. 2, Montpellier, 188 p.

Sgavetti, R., 1991, Photostratigraphy of ancient turbidite systems, *in* Weimer, P., and M.H., Link, eds., Seismic facies and sedimentary process of submarine fans and turbidite systems: New York, Springer, p. 107–125.

Sharman, G.R., Graham, S.A., Masalimova, L.U., Shumaker, L.E., and King, P.R., 2015, Spatial patterns of deformation and paleoslope estimation within the marginal and central portions of a basin-floor mass-transport deposit, Taranaki Basin, New Zealand: Geosphere, v. 11(2), p. 266–306.

Soler-Sampere, M., and Garrido-Megías, A., 1970, La terminación occidental del manto de Cotiella: Pirineos, v. 98, p. 5–12.

Soutter, E.L., Kane, I.A., and Huuse, M., 2018, Giant submarine landslide triggered by Paleocene mantle plume activity in the North Atlantic: Geology, v. 46(6), p. 511–514.

Sprague, A.R.G., Garfield, T.R., Goulding, F.J., Beaubouef, R.T., Sullivan, M.D., Rossen, C., Campion, K.M., Sickafoose, D.K., Abreu, V., Schellpeper, M.E., Jensen, G.N., Jennette, D.C., Pirmez, C., Dixon, B.T., Ying, D., Ardill, J., Mohrig, D.C., Porter, M.L., Farrell, M.E., and Mellere, D., 2005, Integrated slope channel depositional models: the key to successful prediction of reservoir presence and quality in offshore West Africa, *in* Colegio de Ingenieros Petroleros de México - E-Exitep 2005, Feb 20-23, 2005, Veracruz, México, p. 1–13.

Stevenson, C.J., Talling, P.J., Wynn, R.B., Masson, D.G., Hunt, J.E., Frenz, M., Akhmetzhanhov, A., and Cronin, B.T., 2013, The flows that left no trace: Very large-volume turbidity currents that bypassed sediment through submarine channels without eroding the sea floor: Marine and Petroleum Geology, v. 41, p. 186–205.

Stevenson, C.J., Jackson, C.A., Hodgson, D.M., Hubbard, S.M., and Eggenhuisen, J.T., 2015, Deep-water sediment bypass: Journal of Sedimentary Research, v. 85(9), p. 1058–1081.

Stevenson, C.J., Feldens, P., Georgiopoulou, A., Schönke, M., Krastel, S., Piper, D.J.W., Lindhorst, K., and Mosher, D., 2018, Reconstructing the sediment concentration of a giant submarine gravity flow: Nature Communications, v. 9(2616), p. 1–7.

Stow, D.A.V., and Shanmugam, G., 1980, Sequence of structures in fine-grained turbidites: Comparison of recent deep-sea and ancient flysch sediments: Sedimentary Geology, v. 25(1–2), p. 23–42.

Talling, P.J., Wynn, R.B., Masson, D.G., Frenz, M., Cronin, B.T., Schiebel, R., Akhmetzhanov, A.M., Dallmeier-Tiessen, S., Benetti, S., Weaver, P.P.E., Georgiopoulou, A., Zühlsdorff, C., and Amy, L.A., 2007, Onset of submarine debris flow deposition far from original giant landslide: Nature, v. 450, p. 541–544.

Talling, P.J., Masson, D.G., Sumner, E.J., and Malgesini, G., 2012, Subaqueous sediment density flows: Depositional processes and deposit types: Sedimentology, v. 59(7), p. 1937–2003.

Tinterri, R., 2011, Combined flow sedimentary structures and the genetic link between sigmoidal- and hummocky-cross stratification: GeoActa, v. 10, p. 1–43.

Vail, P.R., Mitchum, R.M., and Thompson, S., 1977, Seismic Stratigraphy and Global Changes of Sea Level, Part 3: Relative Changes of Sea Level from Coastal Onlap, *in* Payton, C.E., ed., Seismic Stratigraphy - Applications to Hydrocarbon Exploration: American Association of Petroleum Geologists, Memoir 26, p. 63–81.

Van Lunsen, H., 1970, Geology of the Ara-Cinca region, Spanish Pyrenees: Geologica Ultraiectina, v. 16, 119 p.

Vendettuoli, D., Clare, M.A., Hughes Clarke, J.E., Vellinga, A., Hizzet, J., Hage, S., Cartigny, M.J.B., Talling, P.J., Waltham, D., Hubbard, S.M., Stacey, C., and Lintern, D.G., 2019, Daily bathymetric surveys document how stratigraphy is built and its extreme incompleteness in submarine channels: Earth and Planetary Science Letters, v. 515, p. 231–247.

Ward, N.I.P., Alves, T.M., and Blenkinsop, T.G., 2018, Submarine sediment routing over a blocky mass-transport deposit in the Espírito Santo Basin, SE Brazil: Basin Research, v. 30(4), p. 816–834.

Wynn, R.B., Cronin, B.T., and Peakall, J., 2007, Sinuous deep-water channels: Genesis, geometry and architecture: Marine and Petroleum Geology, v. 24(6–9), p. 341–387.

Xu, J.P., Barry, J.P., and Paull, C.K., 2013, Small-scale turbidity currents in a big submarine canyon: Geology, v. 41(2), p. 143–146.

Zavala, C., Arcuri, M., Di Meglio, M., Gamero Diaz, H., and Contreras, C., 2011, A Genetic Facies Tract for the Analysis of Sustained Hyperpycnal Flow Deposits, *in* Slatt, R.M., and Zavala, C., eds., Sediment Transfer

from Shelf to Deep Water—Revisiting the Delivery System: American Association of Petroleum Geologists, Studies in Geology, p. 31–52.